Investigating the Proliferation-Quiescence Decision in Tissues and in Cancer Cells

by

Ajai Joseph Pulianmackal

A dissertation submitted in partial fulfillment
of the requirements for the degree of
Doctor of Philosophy
(Molecular, Cellular, and Developmental Biology)
in the University of Michigan
2022

Doctoral Committee:

Associate Professor Laura Buttitta, Chair
Professor Kenneth Cadigan
Associate Professor Ajit Joglekar
Associate Professor Ann Miller

Ajai Joseph Pulianmackal

ajai@umich.edu

ORCID iD: 0000-0001-6429-1650

Dedication

To Achachan and Amma for getting me hooked on books.

Acknowledgements

A lot of people have helped me during my PhD journey. I thank my mentors, teachers, family and friends, without whom I could not have finished my PhD.

First and foremost, I extend my deepest gratitude to my PhD mentor Laura Buttitta for guiding me through my PhD. I appreciate your inputs and encouragement for pursue new techniques and ideas in the lab. You guided me to be passionate, independent scientist and encouraged me to think critically.

I would like to thank my committee, Kenneth Cadigan, Ann Miller and Ajit Joglekar for all the constructive comments and advice during my grad school. I thank Ken for all the interesting conversation we had about science, culture, and movies. My grad school experience would not have been this rich if you were not in the neighboring lab. Many thanks to Ann Miller, whose lab I did my first rotation. I thank her for the encouragement and support she had given me then and now. I thank Ajit for giving me constructive comments during committee meeting and encouraging me to pursue a career to help fight climate change.

I express my gratitude to Buttitta lab members, present and past for creating a great work environment for doing science. I thank Rosaline, Kerry, Yiqin and Shyama for guiding me with different techniques in the lab and inputs in research. I thank the ‘prostate and cancerish stuff group’ Meha, Tom, Allison and Jaimian for all informative and exciting discussion we had about science and life. I thank Elli, Liz, Deena and

Emily for being great colleagues. I thank Cheng-Yu Lee and his lab especially Hide and Arjun for lively discussions during our biweekly lab meetings.

Many faculty and staff in MCDB were crucial during my grad school. I did my second rotation in Cathy Collins' lab. I learnt a lot about fly genetics and microdissections. I thank Torey Arnold and Yan Hao for giving me valuable guidance during my rotation. I thank Gregg, Diane, Stella and Mary for all the helps they provided. I thank my collaborators in and outside UofM for helping me with my thesis.

My grad school experience was vastly molded by the interactions and friendships I have had here. I thank my cohort for their friendship and support. I express my gratitude to Sara and Justin for helping me while I was taking classes or teaching classes. I thank Abhishek and Erpan for teaching me techniques, letting me borrow reagent and for being great friends. I thank Vik, Victor, Wayne, Lijing, Shri, Hari, Srihari, Richard, Doina, Tristan, Akash, Shreyas, Abhinay, Bikash, Nick, Navid, Hema, Maryknoll and other escherites for their friendship and support.

I sincerely thank all my teachers who helped me in my journey to grad school. I would like to thank my high school teachers Augustine, Susmitha, Sreelekha and Mini who made science exciting and interesting to me.

I would like to thank my first research mentor Gaghavendra Gadagkar, who asked me fascinating questions and piqued my interest in biology. I also like to thank Raghavan Varadarajan and Kana Sureshan for giving me opportunities to do research in your labs. I thank Kalika prasad for giving me an amazing opportunity to do research in your lab for 3 years and having great discussions about biological phenomenon. I thank Kareem VK, Gireesh KK, Manil Mohan and Krishnaprasad for being patient and

teaching me most of the molecular biology techniques that I know and for being good friends.

I want to express my gratitude to my undergrad friends Ajeesh, Vrinda, Jishnu, Jimmy, Sarang, Raja, Sujeesh, Vigneshwar, Sree Ganesh, Krishnanand, Sreenath, Sumedha and Athira for being my support system for me during the grad school. I thank Arunkumar and Mano for calling me every week during the last 6 years of my PhD and helping me see things from different points of view.

I would not be doing my research in University of Michigan if not for the support, guidance and encouragement of Colin Jamora. I thank him for giving me the opportunity to work in his lab and preparing me for grad school. I thank my colleagues in Jamora lab, Tanay, Krithika, Neha, Edris, Isha Rania and Ravindra for all the help with my research and for being great friends.

Last but not least, I like to thank my family for supporting me throughout this journey. I thank Lisa for always being there for me and be a pillar of support. I thank my extended family for all the love and support they showed me. I thank my parents and siblings for encouraging me to pursue research.

Table of Contents

List of Figures

Abstract

Tight regulation of cell division is important for proper development and homeostasis in all multicellular organisms. While most cells in an adult metazoan exit cell cycle and exist in a non-dividing or quiescent state, a subset of cells retain the ability to re-enter cell cycle in response to external stimuli to replace lost cells. A cell needs to receive, interpret, and integrate various stimuli with its internal cell cycle control machinery to maintain the proper balance between proliferation and quiescence. When dysregulation of the proliferation-quiescence decision happens, it can give rise to diseases such as cancer and developmental disorders. Hence, understanding the factors that influence the proliferation-quiescence decision will be important for improving our understanding of developmental biology as well as cancer.

In this thesis, I investigate two contexts of regulation for the proliferation-quiescence decision. In chapter 2, I examine prostate cancer cells in cell culture, which make spontaneous and heterogeneous proliferation-quiescence decisions in the *ex-vivo* cell culture context, which is often used to study cancer cells. I show that these cancer cells often make asynchronous proliferation-quiescence decisions, even in pairs of daughter cells born from the same mitosis. Furthermore, I show that signals associated with cancer dormancy *in-vivo*, increase the frequency of cancer cells entering spontaneous quiescence, which may help cancer cells evade chemotherapy and

contribute to cancer recurrence. In chapter 3, I complement this *in-vitro* work with an *in-vivo* epithelial tissue model, the *Drosophila* wing, to examine how the loss of the Nucleoporins Nup98 and Nup96 can affect the proliferation-quiescence decision in cells. Nup 98 and 96 are commonly mutated in a number of cancers through silencing or chromosomal translocations, but how their loss contributes to the overproliferation in cancer remains unclear. I show that a reduction in Nup98 and 96 function leads to nuclear sequestration of a ribosomal subunit, causing defects in ribosome biogenesis and protein synthesis. This leads to cellular stress signaling via activation of the JNK signaling pathway and bypass of cellular quiescence, which leads to increased cell death. However, when cell death is blocked by additional mutations, as often happens in cancer, the JNK-stress signaling instead leads to overproliferation and tissue overgrowth. This work suggests that defects in protein synthesis may underlie the overproliferation in cancers with Nup98 and 96 mutations and suggests an unexpected route for therapeutic intervention to increase protein synthesis in these cancers.

Altogether, this thesis pushes forward the boundary of our understanding of the factors affecting proliferation or quiescence in cancer.

Chapter 1 Introduction and Literature Review

Cell division is a very important biological process required for life. In a human cell, it involves making a new copy of 6.6 billion basepairs of DNA organized into 46 chromosomes, making all organelles and cellular machinery required for proper survival of a cell and finally, and accurately dividing the copied DNA and cellular content to two new daughter cells, all usually within a span of 24hrs or less. Every step in the process of the cell cycle must happen precisely and with minimal error, for proper development of an organism(Kaldis, 2016).

But a cell does not always divide. It must receive, interpret and incorporate signals and information from within and outside the cell to decide whether or not to enter the cell cycle and divide. Thus, the cell cycle is a tightly regulated process where extracellular cues and intra-cellular checkpoints must coordinate to regulate cell growth and development(Barnum & O'Connell, 2014; Kastan & Bartek, 2004). Organisms across the kingdoms of life have evolved various intricate cellular machineries to respond to the cues from environment and connect them to the cell cycle machinery for proper control of cell proliferation during development and homeostasis(Harashima et al., 2013; Pulianmackal et al., 2014).

At its core, the active progression of the cell cycle is controlled by the oscillation of activity among different cyclin/cyclin dependent kinase (Cdk) complexes. In higher eukaryotes, multiple Cdks partner with specific cyclins during different stages of the cell

cycle to perform sequential phosphorylations required for cell cycle progression. For example, Cdk4 or Cdk6 partner with CycD and Cdk2 pairs with CycE in the G1 phase of the cell cycle to promote progression to S phase. Cdk2 or Cdk1 partnered with CycA promotes the completion of S-phase and entry into G2 phase, while Cdk1 partners with CycB to promote mitotic entry (Ding et al., 2020; Malumbres & Barbacid, 2009; Vermeulen et al., 2003). While Cyclin/CdkS promote cell cycle entry and progression, Cdk inhibitors like p21/p27 can inhibit Cdks to cause cell cycle arrest. Many signals either from environment or the internal cell state, impinge upon the core Cyclin/Cdk network to regulate the cell cycle.

Most cells in metazoans spend a significant portion of their existence in a quiescent/G0 non-cycling state. The G0 state can be quite variable encompassing a range of reversibility: from permanently postmitotic to poised to re-enter the cell cycle. Cells in a reversible G0 state respond to external stimuli, such as wounding or growth factor signaling to re-enter the cell cycle(Coller, 2011; Gérard & Goldbeter, 2012; Sun & Buttitta, 2017; Yao, 2014). Examples include epithelial stem cells and hair follicle stem cells(Cotsarelis, 2006). By contrast, the cells that undergo terminal differentiation during development often enter a state of prolonged or permanent cell cycle arrest, which is often thought to be a non-reversible G0. Examples of this include terminally differentiated neurons, differentiated epithelia and mature blood cells(Y. A. Z. Wang et al., 2011; Zhang & Huang, 2012). Cellular senescence is also thought to be a non-reversible G0 state, although with important differences from the cell cycle exit associated with terminal differentiation. Cellular senescence occurs in response to aging and cellular stresses such as shortening of telomeres, excessive DNA damage or

aberrant oncogenic activity. While these states of G0 differ in their causes and stability, in all of these cases, active molecular signaling systems must somehow receive and transfer information to the Cyclin/Cdk complexes to control the decision to leave the cell cycle and maintain arrest or quiescence (Sun & Buttitta, 2017).

When cell cycle control systems are disrupted, it can give rise to too little or too much cell division. In humans, this results in developmental disorders or cancer. Cancer is often thought of as a disease of overproliferation, but in the past 20 years it has become evident that masses of cells forming solid cancers can have different subpopulations that divide asynchronously and proliferate at vastly different rates(Feitelson et al., 2015; Hanahan & Weinberg, 2011). Some of the cells in a tumor may proliferate very slowly or enter and leave a so-called dormant state, where they do not proliferate at all. This gives rise to small reserves of dormant stem cells that could evade a drug treatment and give rise to cancer relapse(Batlle & Clevers, 2017) as in colon cancer (Dalerba et al., 2007; O'Brien et al., 2006; Ricci-Vitiani et al., 2006), leukemia (Bonnet & Dick, 1997; Lapidot et al., 1994; Uckun et al., 1995), (Uckun et al., 1995)brain cancer (Singh et al., 2004) and prostate cancer (Cackowski & Heath, 2022; H. M. Lam et al., 2014; Ruppender et al., 2013). To understand the underlying reasons for the proliferative heterogeneity observed in cancer, we need to understand how a cell processes external and internal signals to make a proliferation-quiescence decision.

Proliferative heterogeneity plays an important role in cancer progression and relapse in prostate cancer. Prostate cancer is the second most common cancer among men and is usually treatable if detected during the early stages. As the cancer progresses, cells move out of the gland to secondary sites, such as bone marrow.

These metastatic cancer cells evade chemotherapy by remaining quiescent but can later re-enter the cell cycle and proliferate causing a deadly cancer relapse. Recent studies have shown that the niche factors secreted by the bone marrow may contribute to the cancer cell quiescence and hence the cancer relapse (Cackowski & Heath, 2022; H. M. Lam et al., 2014; Ruppender et al., 2013).

While quiescent cells contribute to the deadly cancer phenotype in prostate cancer, overproliferation caused by translocation of Nup98 causes leukemias. Nucleoporin 98 (Nup98) is a major translocation partner in leukemias (Gough et al., 2011; D. H. Lam & Aplan, 2001). Most of the studies looking at the role of Nup98 in cancer progression, study the role of the overexpression of the fusion protein in cell cycle regulation. However, overlooked in these studies is the fact that the translocation events in leukemias affect the original locus of Nup98, reducing its level. Hence the role played by the reduction of Nup98 in the proliferation-quiescence decision is largely unknown.

The factors that affect the proliferation-quiescence decision vastly various from different phyla of life. While a few external factors are instrumental In the decision of a cell to divide in unicellular organisms such as yeast, proper coordination with their neighbors and surrounding is important for cell divisions in metazoans. In this introduction, I outline some of the key factors that determine the proliferation-quiescence decision in different eukaryotes and discuss major signaling pathways that help coordinate cell division in metazoans.

1.1 Proliferation-quiescence decisions in single cells

In a single celled eukaryote like yeast, the signals it must incorporate into deciding whether to proliferate are limited. The decision for a yeast cell to leave quiescence and proliferate is mostly dependent on the cell size and the external nutrient conditions.

A large-scale deletion screen was done on budding yeast, *Saccharomyces cerevisiae,* to determine key components regulating the cell cycle in addition to the core cyclin/Cdk complexes. In the study they found that a newborn yeast cell won't divide unless it reaches a minimum or "critical" size, and most mutants that affect cell division affected the size of the yeast cell. This suggested that cell size is a key factor determining the cell cycle in yeast. In addition, they found that cells lacking Cdk inhibitors spend less time in G1 and interestingly most of the cells that had a prolonged G1 had deletions in the ribosome biosynthesis pathway. But not all ribosomal subunit deletions had a cell cycle delay or cell cycle arrest phenotype. This suggests that some components of the ribosomal biosynthesis relay information about the protein homeostasis of the cell to the cell cycle machinery to regulate the cell cycle (Hoose et al., 2012).

Many of the molecular pathways regulating the core cell cycle machinery are evolutionarily conserved from mammals to yeast. *Saccharomyces cerevisiae*, lacks proteins that exhibit identity with mammalian cell cycle inhibitors like Rb, p53 or Cdk inhibitors like p21/ p27. But they have functional homologs for Rb, p21 and p27 that do similar functions. For example, Whi5 is a functional homolog of Rb in *Saccharomyces cerevisiae.* It binds to the transcription factor SBF (SCB binding factor), similar to Rb

binding to E2F in metazoans. Upon reaching proper cell size, Cln3/Cdc28(Cyclin E/Cdk2) phosphorylates Whi5, driving it out of nucleus, and thereby helping SBF to transcribe genes required for G1-S transition (Cooper, 2006; Crane et al., 2019; P. Li et al., 2021; V. C. Li & Kirschner, 2014; Vergés et al., 2007).

Nutrients regulate the yeast cell cycle by affectingthe Target of Rapamycin(TOR) pathway, Protein kinase A(PKA) signaling and the Phosphate responsive pathway (Pho) . When amino acid starved, TOR kinase is inactivated; it cannot phosphorylate proteins and causes cell cycle arrest, acting via PKA target RIM15 (Greatwall kinase) (Pedruzzi et al., 2003). Yeast sense carbohydrates via PKA. A G protein coupled receptor (GPCR) Gpr1 has been shown to activate PKA in response to carbohydrate starvation (Bisschops et al., 2014; Van Zeebroeck et al., 2021). The active PKA then causes RIM15 activation for cell cycle arrest. Similarly, the Pho pathway that senses phosphate starvation also leads to RIM15 activation (Jiménez et al., 2015; Wanke et al., 2005).

Many nutrient sensing pathways in yeast converges to regulate the activity of RIM15 kinase in yeast. Deletion of RIM15, made yeast cell cycle non-responsive to nutrients such as amino acids, carbohydrates, and phosphates. When nutrients are absent and RIM15 is phosphorylated by Pho85 or TOR or PKA, it is retained in cytoplasm. The active Rim15 is known to phosphorylate and activate proteins required for cell cycle arrest. RNA seq analysis has shown that Rim15 regulates the expression of 179 genes involved with the cell cycle including SBF (E2F homolog) and CLN3 (CycE homolog)(Bisschops et al., 2014; Gallego et al., 1997; Lee et al., 2013; Luo et al., 2011; Moreno-Torres et al., 2015, 2017; Swinnen et al., 2006).

1.2 Approaching multicellularity: Proliferation-quiescence decisions in social amoeba

Social single-celled organisms incorporate signals from the environment as well as their neighbors. *Dictyostelium discoideum* is a social amoeba that grows as individual cells when nutrients are present but becomes a multicellular colony or mount of ~10^5 cells when nutrient deprived. The multicellular mount is made up of *Dictyostelium* that differentiate into two different states, stalk cells and spore cells. The stalk cells cease cell division and support the spore cells, which in turn undergo cell division to make spores, which can be dispersed by a structure called a “fruiting body” to gain a chance at encountering a better environment(G. Chen & Kuspa, 2005).

The cell cycle of *Dictyostelium* is rather interesting. The majority of their cell cycle is spent in G2 phase, with little to no apparent G1 stage. When a synchronous population of the amoeba was collected and allowed to grow in normal growth conditions, 70% of cells segregate into late S phase and 30% into late G2 phase of the cell cycle within 4 generations. Interestingly this asynchrony helps decide the fate of cells when they differentiate into spore and stalk. The 70% of the cells that are in late S will develop into spore cells that have a chance to propagate the genetic material and the 30% in late G2 will differentiate to become stalk cells(Gruenheit et al., 2018a). During the multicellullarization process, the pre-spore cells secrete a chlorinated signal molecule called differentiation inducing factor 1 (DIF1) that act as a growth factor and binds to the prestalk cells to induce stalk differentiation (Gruenheit et al., 2018b; Thompson & Kay, 2000).

1.3 Complex multicellularity: the Metazoan proliferation-quiescence decision

Proper development of metazoans, which most often contain multiple multicellular tissues, requires tighter spatial and temporal coordination of cell division. Checks and balances at different steps of the cell cycle make sure that the previous step is complete before going on to the next stage of the cell cycle. This helps maintain genomic integrity and prevent errors from passing down to the next generation. There are internal restriction points and checkpoints that respond to the internal state of a cell, as well as signaling pathways that transmit signals from external factors to properly coordinate the cell cycle.

1.3.1 The restriction point

Most of the regulatory machinery controlling the proliferation decision collectively acts to regulate the cell cycle at the G1 phase. Hence, most differentiated quiescent cells have G1 DNA content. The restriction point or R point is called “a point of no return” in the cell cycle. For a cell to be released from restriction point, it needs signals from growth factors and external stimuli. But once the cell receives these signals, they can procced through cell cycle.

The E2F/DP transcriptional machinery is a master regulator of cell cycle entry as it helps transcription of over 1000 genes required for cell cycle progression such as cyclins and Cdks. While, Cyclin/Cdk complexes and E2F help in progression of cell cycle forward, retinoblastoma protein family (Rb) and Cyclin dependent kinase inhibitors (CKIs) halt the cell cycle (Fischer & Müller, 2017; Segeren et al., 2020).

For the cell cycle to pass the restriction point, various signals coming from mitogens and external stimuli need to activate E2F and Cdk2/CycE activity. Once a cell

exits from mitosis, they generally have unphosphorylated Retinoblastoma protein (Rb). The Rb binds to E2F and prevents it from dimerizing with DP and transcribing cell cycle genes. Also present are the CKIs p21 and p27 that inhibit Cdk2/Cdk4/6 and p15 and p16 that inhibit Cdk4/6. Various mitogen signals converge to induce CycD production and simultaneously decrease the protein level of CKIs through inducing their degradation. CycD then binds to Cdk4 to phosphorylate Rb to free E2F. Free E2F can dimerize with DP and transcribe genes required for the cell cycle including CycE thereby activating the CycE/Cdk2 complex. CycE/Cdk2 then hyperphosphorylates Rb to mark cell cycle commitment. This leads to full release of E2F and leads to production of other genes required for the progression into S phase. (Ashraf et al., 2019; Blagosklonny & Pardee, 2013; Narasimha et al., 2014)

1.3.2 Cyclin dependent Kinase Inhibitors

p27 and p21 are the Cip/Kip family of CKIs that can bind to all Cdks, whereas p16, and p15 are members of the INK family of CKIs that specifically inhibits Cdk4 and 6.

Upon its activation, CycE/Cdk2 phosphorylates p27 at Thr187. The phosphorylated p27 is then recognized by the SCF/Skp2 complex, gets ubiquitinated (Montagnoli et al., 1999) and degraded(Kossatz et al., 2004). p27 can also be regulated by growth factor signals to indirectly increase Cdk2 activity. When mitogens are present, a signaling cascade detects the signal and cause phosphorylation p27 at Ser10 localizing it to the cytoplasm. p27 localized to the cytoplasm can then be recognized by the SCF/SKP2 complex for degradation (Ishida et al., 2002; Rodier et al., 2001).

Unlike p27, p21 is a CKI that can cause cell cycle arrest in G1 or G2 in response to various stimuli. It can cause G1 arrest by Cdk2 inhibition and G2 arrest by inhibiting Cdk1(Deng et al., 2018). Due to its dual functions in the cell cycle, there are 3 main E3 Ubiquitin ligase complexes that can mediate the destruction of p21 protein. When phosphorylated by Cdk2 at Ser130, p21 is targeted by SCF/Skp2 for degradation in G1(Wang et al., 2005; Yu et al., 1998). During S phase, p21 can bind to PCNA to prevent cell cycle progression. PCNA bound p21 can be ubiquitinated by the E3 ligase CRL4/Cdt2 to mediate cell cycle re-entry for the cell (Abbas et al., 2008). p21 can bind to Cdk1 during prometaphase to arrest the cell cycle. Cdk1 bound p21 can be degraded by APC/C Cdc20 to promote progression of cell cycle (Amador et al., 2007).

1.3.3 DNA damage checkpoint

The DNA damage response is essential for maintaining genomic integrity. Activation of this checkpoint arrests cell cycle progression to allow repair of DNA before proceeding to next stage of cell cycle. The kinases ataxia-telangiectasia mutated (ATM) and ataxia telangiectasia mutated and rad3 related (ATR) sense double and single stranded DNA damage, respectively(Cortez et al., 2001; Perry & Kleckner, 2003).

Double strand breaks activate ATM, which then activates CHK2. CHK2 phosphorylates and inactivates the Cdk2 phosphatase, Cdc25A. Cdc25A is required to remove an inactivating phosphorylation on Cdk2, thus Cdc25a inhibition prevents Cdk2 activation, S phase entry and cell cycle progression. ATM can also phosphorylate and activate P53 which could then induce expression of p21 to inhibit Cdks (Maréchal & Zou, 2013; Perry & Kleckner, 2003).

Single strand DNA damage activates ATR, a kinase which phosphorylates CHK1 kinase, which in turn phosphorylates and inactivates cdc25C. Inactive cdc25C cannot remove an inactivating phosphorylation on Cdk1, thus arresting cells in G2. Similar to ATM, ATR can also affect the cell cycle via p53 (Maréchal & Zou, 2013; Weber & Ryan, 2015).

In addition to these mechanisms, WEE1 kinase can be activated in response to DNA damage, and phosphorylates inactivating sites on both Cdk1 and Cdk2(Smith et al., 2020; Weber & Ryan, 2015).

Together, these checkpoints ensure that the cell cycle is arrested when there is unrepaired DNA damage. This helps provide time for the cell to repair the damage before proceeding through the cell cycle to prevent deleterious mutations from being passed onto the progeny(Cortez et al., 2001; Maréchal & Zou, 2013)

1.3.4 Spindle assembly checkpoint

During mitosis, genome stability is maintained by a spindle assembly checkpoint, which delays cell cycle progression until accurate chromosome segregation is ensured. For proper segregation of chromosomes to happen, they need to be correctly attached to the mitotic microtubule spindle via kinetochores. When the kinetochores are not properly attached to the spindles, the checkpoint is activated, halting the cell cycle. The checkpoint inactivates the E3 ubiquitin ligase anaphase promoting complex/cyclosome (APC/C), which is critical for initiating the completion of mitosis by promoting the metaphase-anaphase transition by degrading Securin, which prevents chromosome separation as well as degrading the mitotic Cyclin, Cyclin B. (Lara-Gonzalez et al., 2012; Liu & Zhang, 2016).

1.3.5 ERK/MAPK signaling

Mitogen activated protein kinase (MAPK) is a crucial signaling pathway that regulates a variety of cellular processes such as proliferation, apoptosis, differentiation and stress responses. MAPK signaling is activated when a ligand/stimulus binds to activate the most upstream kinase of the pathway. This leads to activation of the downstream kinases through a kinase cascade, which finally affects the activity of transcription factors, which promote transcription of genes that induce cellular processes such as proliferation (Guo et al., 2020). There are 4 major MAPK cascades: ERK1/2, JNK, p38 MAPK, and ERK5. As with other key signaling pathways that regulate the cell cycle, MAPK signaling is also altered in many cancers (Lawrence et al., 2008).

Extracellular signal-regulated kinase1/2 (ERK) is one of the MAPK family proteins that plays an important role in transmitting external signals to the cell. Various stimuli such as cytokines, viruses, GPCR Ligands and oncogenes can cause activation of ERK/MAPK(Guo et al., 2020). The ERK/MAPK kinase cascade, once activated, phosphorylates ERK1/2 leading to its nuclear localization. Once in the nucleus, ERK1/2 can phosphorylate and activate transcription factors such as c-FOS, c-Jun, c-Myc, Ets and Elk-1. These factors then transcribe genes required for cell cycle progression (J. Y. Kim et al., 2011)

1.3.6 JNK/MAPK signaling

The c-Jun N-terminal kinases (JNKs), also known as stress activated protein kinases (SAPK) are a subfamily of MAPK signaling pathways. JNK responds to wide

variety of cellular stimuli including growth factors, UV, heat shock, infections, osmotic pressure and DNA damage (Hammouda et al., 2020).

Upon its activation, JNK phosphorylates downstream transcription factors of the Activating protein 1 (AP1) family. The AP1 family of transcription factors acts either as a homodimer with 2 Jun proteins (cJun, JunB, JunD) or heterodimer with Jun and Fos protein (c-Fos, GosB, Fra1 and Fra2) (Gazon et al., 2018; Shaulian & Karin, 2001). The effect of JNK signaling is determined by the combination of AP1 proteins.

While c-Jun activates Cyclin D1 and promotes the cell cycle, JunB suppresses it (Bakiri et al., 2000). Interestingly, JNK could play a role both in proliferation and cell death. It can collaborate with NF-KB and JAK-STAT to promote cell survival. Whereas it can also directly activate pro-apoptotic genes like Bad and Bim and inhibit apoptotic inhibitors like Bcl2 and Bcl-xL to cause cell death (Y. R. Chen & Tan, 2000).

1.3.7 TGFβ signaling

Transforming growth factor beta (TGFβ) superfamily signaling plays an important role in regulation of cell division, development and differentiation. Due to its role in coordinating signals from multiple signaling pathways to regulate the cell cycle, TGFβ signaling is usually altered in cancers. In many cancers, increased TGFβ2 expression is associated with cancer progression and development of metastasis (Bragado et al., 2013; Yeh et al., 2019).

Transforming growth factor β receptor have type I and type II receptors. TGFβ isoforms 1-3, activins, BMP, other growth and differentiation factors bind to these receptors to regulate a diverse array of physiological processes like proliferation, differentiation and growth (Dalton & Howe, 2021; Hanrahan et al., 2013).

TGFβ is translated as an immature pro-protein which is cleaved and dimerized into latent TGFβ binding protein (LTBP). This complex is sequestered in extracellular matrix until signals from matrix metalloproteinase (MMP), plasmin or thrombin dependent cleavage of LTBP happens, leading to release of TGFβ dimers (Huppert & Iwafuchi-Doi, 2019). The dimers then bind to the TGFβ receptors to cause their heterotetramerzation. The activated receptors then phosphorylate Smad proteins (R-SMAD 2 and 3). The phosphorylated Smads forms a heterotrimer with SMAD4, localizes to nuclei and binds to DNA with other binding partners. Depending on the binding partners of Smads, TGFβ signaling can cause a myriad of effects in a cell. They can cause cell cycle exit by expression of p21 and repression of myc, or cell proliferation by inducing the growth factor PDGF (Dalton & Howe, 2021; Hanrahan et al., 2013).

TGFβ can also signal independent of Smads. It can activate the p38/JNK cascade or Src, Rho, PI3K cascades (Hata & Chen, 2016; Miyazawa & Miyazono, 2017).

1.3.8 Hippo signaling

Hippo signaling in an evolutionary conserved signaling cascade that integrates various external and internal cues to control cell proliferation, differentiation, and organ size. When dysregulated, Hippo signaling can cause tumor growth and metastasis (Buttitta & Edgar, 2007; Chang et al., 2020).

Mammalian Ste 20-like kinases (MST1/2) and large tumor suppressor kinase (LATS1/2) are major serine/threonine kinases in hippo signaling. When the Hippo signaling is active, MST1/2 bind to the adaptor protein Salvador(Sav) to phosphorylate

LATS1/2. Activated LATS1/2 phosphorylates Yes associated protein (YAP) at Ser168 which causes it to bind to 14-3-3 protein and causes its degradation/cytoplasmic localization. Hence, the phosphorylated YAP hence cannot associate with the TEAD family of transcription factors to transcribe genes that will help in cell survival and division (Chang et al., 2020; McClatchey & Yap, 2012; Mizuno et al., 2012; Shen & Stanger, 2015).

Hippo signaling is primarily responsible for contact inhibition. When cells get to a high density, more adherens junctions are formed. These junctions sequester α-catenin to the membrane. The α-catenin at the adherens junction binds YAP keeping it in the cytoplasm. This prevents YAP/TEAD mediated transcription of proteins like CycD and FoxM and hence inhibits cell cycle progression (W. Kim et al., 2019; Schlegelmilch et al., 2011). Hippo signaling also responds to increased tension by responding to the increased tension sensed by membrane receptors, actin or focal adhesion kinases (Chang et al., 2020).

The nuclear envelope can also act as a tension sensor for activating hippo signaling. Adherent cells grown in culture detach from the substrate when they are undergoing mitosis. These cells later flatten once they enter G1 and as they proceed through later stages of the cell cycle (J. K. Kim et al., 2017). Thus, there are changes in the mechanical tension involved even with normal cell division. The mechanical tension that is applied to the external part of a cell is translated into the nucleus via cytoskeleton structures such as intermediary filaments (J. K. Kim et al., 2017).

Recent studies have shown that the flattening of the nucleus as the cell proceeds from G1 to S phase is required for the cell cycle progression. In HeLa cells, inhibition of

flattening of the nucleus by mechanical means or by inhibiting the intermediate filaments reduces the percentage of cells that transition from G1 to S phase of cell cycle and thereby proceed through cell cycle. The study shows a previously unknown function of tension and hippo signaling in normal cell division. The flattening of the nucleus as the cell transition from G1-S phase activates hippo signaling which in turn contributes to the cell cycle progression (Aureille et al., 2019).

Of note, the morphology of nucleus is often altered in cancer. So often, the irregular nuclear morphology is often used by pathologist in diagnosing the severity of cancer(Chow et al., 2012; Zink et al., 2004). But the irregular nuclear morphology may not be just a consequence of cancer, but could be causing proliferation by altering hippo signaling.

1.3.9 TOR signaling

Target of Rapamycin (TOR) is an evolutionarily conserved kinase that functions at the heart of nutrient sensing in eukaryotes. The signaling pathway responds to and regulates the metabolism of nutrients (amino acids) and growth factors like insulin to regulate cell growth (Fingar & Blenis, 2004; Shamji et al., 2003).

mTOR signaling is regulated by the presence of amino acids and growth factors. 4 RAG GTPases (RAG A-D) heterodimerize into active forms in the lysosome when there are sufficient amino acids available. This leads to the lysosomal localization of mTOR complex. On another axis, growth factors act through PI3K-Akt kinase pathway to phosphorylate and inactivate TSC2, a TOR inhibitor. When TSC2 is inactivated, it causes the release of Rheb GTPase which can activate the mTOR complex localized

on the lysosome to promote cell cycle (González & Hall, 2017; Neuman & Henske, 2011; Wullschleger et al., 2006).

Together, the PI3K pathway driven by growth factors and TOR driven by nutrients and their crosstalk help cells divide only when there is enough nutrients and energy.

In my thesis I explore two different aspects of proliferation-quiescence decision in cancer. In chapter 2, I examined a clonal cell population of metastatic prostate cancer cell(PC3) that have mutations in tumor suppressor genes such as p53, capicua and Phosphatase and Tensin Homolog deleted on Chromosome 10 (PTEN). P53, capicua and PTEN help in the transfer of information from cellullar stress or external stimuli to enhance cellular quiescence(Carroll et al., 1993; Jividen et al., 2018; Ma et al., 2017; Seim et al., 2017). These mutation can cause overproliferation and hence is found to be mutated in many cancers. I tested whether the cancer cell line that have defects in entry into quiescence could spontaneously enter quiescence in normal growth conditions. I also investigated how the proliferation-quiescence decision is affected when factors that affect tumor dormancy were introduced into cells in culture, where all the cells are subjected to similar conditions. In chapter 3 I explore how loss of Nup98 in *Drosophila* wing affect proliferation-quiescence decision during development.

My studies use mammalian cell culture and *Drosophila melanogaster* to study how cancer cells respond to external niche factors and how an oncogenic mutation affects the proliferation-quiescence decision.

1.4 Bibliography

Abbas, T., Sivaprasad, U., Terai, K., Amador, V., Pagano, M., & Dutta, A. (2008). PCNA-dependent regulation of p21 ubiquitylation and degradation via the CRL4Cdt2 ubiquitin ligase complex. *Genes & Development*, *22*(18), 2496–2506. https://doi.org/10.1101/GAD.1676108

Amador, V., Ge, S., Santamaría, P. G., Guardavaccaro, D., & Pagano, M. (2007). APC/C(Cdc20) controls the ubiquitin-mediated degradation of p21 in prometaphase. *Molecular Cell*, *27*(3), 462–473. https://doi.org/10.1016/J.MOLCEL.2007.06.013

Ashraf, H. M., Moser, J., & Spencer, S. L. (2019). Senescence Evasion in Chemotherapy: A Sweet Spot for p21. *Cell*, *178*(2), 267–269. https://doi.org/10.1016/J.CELL.2019.06.025

Aureille, J., Buffière-Ribot, V., Harvey, B. E., Boyault, C., Pernet, L., Andersen, T., Bacola, G., Balland, M., Fraboulet, S., Landeghem, L. Van, & Guilluy, C. (2019). Nuclear envelope deformation controls cell cycle progression in response to mechanical force. *EMBO Reports*, *20*(9), e48084. https://doi.org/10.15252/EMBR.201948084

Bakiri, L., Lallemand, D., Bossy-Wetzel, E., & Yaniv, M. (2000). Cell cycle-dependent variations in c-Jun and JunB phosphorylation: a role in the control of cyclin D1 expression. *The EMBO Journal*, *19*(9), 2056–2068. https://doi.org/10.1093/EMBOJ/19.9.2056

Barnum, K. J., & O'Connell, M. J. (2014). Cell Cycle Regulation by Checkpoints.

Methods in Molecular Biology (Clifton, N.J.), *1170*, 29. https://doi.org/10.1007/978-1-4939-0888-2_2

Batlle, E., & Clevers, H. (2017). Cancer stem cells revisited. *Nature Medicine 2017 23:10*, *23*(10), 1124–1134. https://doi.org/10.1038/nm.4409

Bisschops, M. M. M., Zwartjens, P., Keuter, S. G. F., Pronk, J. T., & Daran-Lapujade, P. (2014). To divide or not to divide: A key role of Rim15 in calorie-restricted yeast cultures. *Biochimica et Biophysica Acta (BBA) - Molecular Cell Research*, *1843*(5), 1020–1030. https://doi.org/10.1016/J.BBAMCR.2014.01.026

Blagosklonny, M. V., & Pardee, A. B. (2013). *The Restriction Point of the Cell Cycle*. https://www.ncbi.nlm.nih.gov/books/NBK6318/

Bonnet, D., & Dick, J. E. (1997). Human acute myeloid leukemia is organized as a hierarchy that originates from a primitive hematopoietic cell. *Nature Medicine 1997 3:7*, *3*(7), 730–737. https://doi.org/10.1038/NM0797-730

Bragado, P., Estrada, Y., Parikh, F., Krause, S., Capobianco, C., Farina, H. G., Schewe, D. M., & Aguirre-Ghiso, J. A. (2013). TGF-β2 dictates disseminated tumour cell fate in target organs through TGF-β-RIII and p38α/β signalling. *Nature Cell Biology*, *15*(11), 1351–1361. https://doi.org/10.1038/NCB2861

Buttitta, L. A., & Edgar, B. A. (2007). How size is controlled: from Hippos to Yorkies. *Nature Cell Biology*, *9*(11), 1225–1227. https://doi.org/10.1038/NCB1107-1225

Cackowski, F. C., & Heath, E. I. (2022). Prostate cancer dormancy and recurrence. *Cancer Letters*, *524*, 103–108. https://doi.org/10.1016/J.CANLET.2021.09.037

Carroll, A. G., Voeller, H. J., Sugars, L., & Gelmann, E. P. (1993). p53 oncogene mutations in three human prostate cancer cell lines. *The Prostate*, *23*(2), 123–134. https://doi.org/10.1002/PROS.2990230206

Chang, Y. C., Wu, J. W., Wang, C. W., & Jang, A. C. C. (2020). Hippo Signaling-Mediated Mechanotransduction in Cell Movement and Cancer Metastasis. *Frontiers in Molecular Biosciences*, *6*, 157. https://doi.org/10.3389/FMOLB.2019.00157/BIBTEX

Chen, G., & Kuspa, A. (2005). Prespore cell fate bias in G1 phase of the cell cycle in Dictyostelium discoideum. *Eukaryotic Cell*, *4*(10), 1755–1764. https://doi.org/10.1128/EC.4.10.1755-1764.2005/ASSET/1C749A8B-B75C-4828-B63F-767A9EA46FA7/ASSETS/GRAPHIC/ZEK0100525390006.JPEG

Chen, Y. R., & Tan, T. H. (2000). The c-Jun N-terminal kinase pathway and apoptotic signaling (review). *International Journal of Oncology*, *16*(4), 651–662. https://doi.org/10.3892/IJO.16.4.651/HTML

Chow, K. H., Factor, R. E., & Ullman, K. S. (2012). The nuclear envelope environment and its cancer connections. *Nature Reviews. Cancer*, *12*(3), 196–209. https://doi.org/10.1038/NRC3219

Coller, H. A. (2011). The Essence of Quiescence. *Science (New York, N.Y.)*, *334*(6059), 1074. https://doi.org/10.1126/SCIENCE.1216242

Cooper, K. (2006). Rb, whi it's not just for metazoans anymore. *Oncogene 2006 25:38*, *25*(38), 5228–5232. https://doi.org/10.1038/sj.onc.1209630

Cortez, D., Guntuku, S., Qin, J., & Elledge, S. J. (2001). ATR and ATRIP: partners in checkpoint signaling. *Science (New York, N.Y.)*, *294*(5547), 1713–1716. https://doi.org/10.1126/SCIENCE.1065521

Cotsarelis, G. (2006). Epithelial Stem Cells: A Folliculocentric View. *Journal of Investigative Dermatology*, *126*(7), 1459–1468. https://doi.org/10.1038/SJ.JID.5700376

Crane, M. M., Tsuchiya, M., Blue, B. W., Almazan, J. D., Chen, K. L., Duffy, S. R., Golubeva, A., Grimm, A. M., Guard, A. M., Hill, S. A., Huynh, E., Kelly, R. M., Kiflezghi, M., Kim, H. D., Lee, M., Lee, T. I., Li, J., Nguyen, B. M. G., Whalen, R. M., … Kaeberlein, M. (2019). Rb analog Whi5 regulates G1 to S transition and cell size but not replicative lifespan in budding yeast. *Translational Medicine of Aging*, *3*, 104–108. https://doi.org/10.1016/J.TMA.2019.10.002

Dalerba, P., Dylla, S. J., Park, I. K., Liu, R., Wang, X., Cho, R. W., Hoey, T., Gurney, A., Huang, E. H., Simeone, D. M., Shelton, A. A., Parmiani, G., Castelli, C., & Clarke, M. F. (2007). Phenotypic characterization of human colorectal cancer stem cells. *Proceedings of the National Academy of Sciences*, *104*(24), 10158–10163. https://doi.org/10.1073/PNAS.0703478104

Dalton, A. C., & Howe, P. H. (2021). Epithelial to Mesenchymal Transition. *Reference Module in Biomedical Sciences*. https://doi.org/10.1016/B978-0-12-820472-6.00005-0

Deng, T., Yan, G., Song, X., Xie, L., Zhou, Y., Li, J., Hu, X., Li, Z., Hu, J., Zhang, Y., Zhang, H., Sun, Y., Feng, P., Wei, D., Hu, B., Liu, J., Tan, W., & Ye, M. (2018).

Deubiquitylation and stabilization of p21 by USP11 is critical for cell-cycle progression and DNA damage responses. *Proceedings of the National Academy of Sciences of the United States of America*, *115*(18), 4678–4683. https://doi.org/10.1073/PNAS.1714938115/-/DCSUPPLEMENTAL

Ding, L., Cao, J., Lin, W., Chen, H., Xiong, X., Ao, H., Yu, M., Lin, J., & Cui, Q. (2020). The Roles of Cyclin-Dependent Kinases in Cell-Cycle Progression and Therapeutic Strategies in Human Breast Cancer. *International Journal of Molecular Sciences*, *21*(6). https://doi.org/10.3390/IJMS21061960

Feitelson, M. A., Arzumanyan, A., Kulathinal, R. J., Blain, S. W., Holcombe, R. F., Mahajna, J., Marino, M., Martinez-Chantar, M. L., Nawroth, R., Sanchez-Garcia, I., Sharma, D., Saxena, N. K., Singh, N., Vlachostergios, P. J., Guo, S., Honoki, K., Fujii, H., Georgakilas, A. G., Bilsland, A., … Nowsheen, S. (2015). Sustained proliferation in cancer: Mechanisms and novel therapeutic targets. *Seminars in Cancer Biology*, *35*, S25–S54. https://doi.org/10.1016/J.SEMCANCER.2015.02.006

Fingar, D. C., & Blenis, J. (2004). Target of rapamycin (TOR): an integrator of nutrient and growth factor signals and coordinator of cell growth and cell cycle progression. *Oncogene 2004 23:18*, *23*(18), 3151–3171. https://doi.org/10.1038/sj.onc.1207542

Fischer, M., & Müller, G. A. (2017). Cell cycle transcription control: DREAM/MuvB and RB-E2F complexes. *Https://Doi.Org/10.1080/10409238.2017.1360836*, *52*(6), 638–662. https://doi.org/10.1080/10409238.2017.1360836

Gallego, C., Garí, E., Colomina, N., Herrero, E., & Aldea, M. (1997). The Cln3 cyclin is down-regulated by translational repression and degradation during the G 1 arrest

caused by nitrogen deprivation in budding yeast. *The EMBO Journal*, *16*(23), 7196–7206.

Gazon, H., Barbeau, B., Mesnard, J. M., & Peloponese, J. M. (2018). Hijacking of the AP-1 signaling pathway during development of ATL. *Frontiers in Microbiology*, *8*(JAN), 2686. https://doi.org/10.3389/FMICB.2017.02686/BIBTEX

Gérard, C., & Goldbeter, A. (2012). From quiescence to proliferation: Cdk oscillations drive the mammalian cell cycle. *Frontiers in Physiology*, *3 NOV*, 413. https://doi.org/10.3389/FPHYS.2012.00413/BIBTEX

González, A., & Hall, M. N. (2017). Focus: Metabolism: Nutrient sensing and TOR signaling in yeast and mammals. *The EMBO Journal*, *36*(4), 397. https://doi.org/10.15252/EMBJ.201696010

Gough, S. M., Slape, C. I., & Aplan, P. D. (2011). NUP98 gene fusions and hematopoietic malignancies: common themes and new biologic insights. *Blood*, *118*(24), 6247–6257. https://doi.org/10.1182/BLOOD-2011-07-328880

Gruenheit, N., Parkinson, K., Brimson, C. A., Van Zon, W., Cotter, S. L., & Thompson Correspondence, C. R. L. (2018a). Cell Cycle Heterogeneity Can Generate Robust Cell Type Proportioning. *Developmental Cell*, *47*, 494-508.e4. https://doi.org/10.1016/j.devcel.2018.09.023

Gruenheit, N., Parkinson, K., Brimson, C. A., Van Zon, W., Cotter, S. L., & Thompson Correspondence, C. R. L. (2018b). Cell Cycle Heterogeneity Can Generate Robust Cell Type Proportioning. *Developmental Cell*, *47*, 494-508.e4. https://doi.org/10.1016/j.devcel.2018.09.023

Guo, Y., Pan, W., Liu, S., Shen, Z., Xu, Y., & Hu, L. (2020). ERK/MAPK signalling pathway and tumorigenesis (Review). *Experimental and Therapeutic Medicine*, *19*(3), 1997–2007. https://doi.org/10.3892/ETM.2020.8454

Hammouda, M. B., Ford, A. E., Liu, Y., & Zhang, J. Y. (2020). The JNK Signaling Pathway in Inflammatory Skin Disorders and Cancer. *Cells 2020, Vol. 9, Page 857*, *9*(4), 857. https://doi.org/10.3390/CELLS9040857

Hanahan, D., & Weinberg, R. A. (2011). Hallmarks of cancer: The next generation. *Cell*, *144*(5), 646–674. https://doi.org/10.1016/J.CELL.2011.02.013/ATTACHMENT/3F528E16-8B3C-4D8D-8DE5-43E0C98D8475/MMC1.PDF

Hanrahan, A. J., Iyer, G., & Solit, D. B. (2013). Intracellular Signaling. *Abeloff's Clinical Oncology: Fifth Edition*, 22-39.e9. https://doi.org/10.1016/B978-1-4557-2865-7.00002-3

Harashima, H., Dissmeyer, N., & Schnittger, A. (2013). Cell cycle control across the eukaryotic kingdom. *Trends in Cell Biology*, *23*(7), 345–356. https://doi.org/10.1016/J.TCB.2013.03.002

Hata, A., & Chen, Y. G. (2016). TGF-β Signaling from Receptors to Smads. *Cold Spring Harbor Perspectives in Biology*, *8*(9). https://doi.org/10.1101/CSHPERSPECT.A022061

Hoose, S. A., Rawlings, J. A., Kelly, M. M., Leitch, C., Ababneh, Q. O., Robles, J. P., Taylor, D., Hoover, E. M., Hailu, B., McEnery, K. A., Downing, S., Kaushal, D., Chen, Y., Rife, A., Brahmbhatt, K. A., Smith, R., & Polymenis, M. (2012). A

Systematic Analysis of Cell Cycle Regulators in Yeast Reveals That Most Factors Act Independently of Cell Size to Control Initiation of Division. *PLoS Genetics*, *8*(3), 1002590. https://doi.org/10.1371/JOURNAL.PGEN.1002590

Huppert, S. S., & Iwafuchi-Doi, M. (2019). Molecular regulation of mammalian hepatic architecture. *Current Topics in Developmental Biology*, *132*, 91–136. https://doi.org/10.1016/BS.CTDB.2018.12.003

Ishida, N., Hara, T., Kamura, T., Yoshida, M., Nakayama, K., & Nakayama, K. I. (2002). Phosphorylation of p27Kip1 on Serine 10 Is Required for Its Binding to CRM1 and Nuclear Export. *Journal of Biological Chemistry*, *277*(17), 14355–14358. https://doi.org/10.1074/JBC.C100762200

Jiménez, J., Bru, S., Ribeiro, M. P. C., & Clotet, J. (2015). Live fast, die soon: cell cycle progression and lifespan in yeast cells. *Microbial Cell*, *2*(3), 62. https://doi.org/10.15698/MIC2015.03.191

Jividen, K., Kedzierska, K. Z., Yang, C. S., Szlachta, K., Ratan, A., & Paschal, B. M. (2018). Genomic analysis of DNA repair genes and androgen signaling in prostate cancer. *BMC Cancer*, *18*(1), 1–20. https://doi.org/10.1186/S12885-018-4848-X/FIGURES/7

Kaldis, P. (2016). Quo Vadis cell growth and division? *Frontiers in Cell and Developmental Biology*, *4*(AUG), 95. https://doi.org/10.3389/FCELL.2016.00095/BIBTEX

Kastan, M. B., & Bartek, J. (2004). Cell-cycle checkpoints and cancer. *Nature 2004 432:7015*, *432*(7015), 316–323. https://doi.org/10.1038/nature03097

Kim, J. K., Louhghalam, A., Lee, G., Schafer, B. W., Wirtz, D., & Kim, D. H. (2017). Nuclear lamin A/C harnesses the perinuclear apical actin cables to protect nuclear morphology. *Nature Communications*, *8*(1). https://doi.org/10.1038/S41467-017-02217-5

Kim, J. Y., Lee, S. G., Chung, J. Y., Kim, Y. J., Park, J. E., Koh, H., Han, M. S., Park, Y. C., Yoo, Y. H., & Kim, J. M. (2011). Ellipticine induces apoptosis in human endometrial cancer cells: The potential involvement of reactive oxygen species and mitogen-activated protein kinases. *Toxicology*, *289*(2–3), 91–102. https://doi.org/10.1016/J.TOX.2011.07.014

Kim, W., Cho, Y. S., Wang, X., Park, O., Ma, X., Kim, H., Gan, W., Jho, E. hoon, Cha, B., Jeung, Y. ji, Zhang, L., Gao, B., Wei, W., Jiang, J., Chung, K. S., & Yang, Y. (2019). Hippo signaling is intrinsically regulated during cell cycle progression by APC/CCdh1. *Proceedings of the National Academy of Sciences of the United States of America*, *116*(19), 9423–9432. https://doi.org/10.1073/PNAS.1821370116/-/DCSUPPLEMENTAL

Kossatz, U., Dietrich, N., Zender, L., Buer, J., Manns, M. P., & Malek, N. P. (2004). Skp2-dependent degradation of p27kip1 is essential for cell cycle progression. *Genes & Development*, *18*(21), 2602–2607. https://doi.org/10.1101/GAD.321004

Lam, D. H., & Aplan, P. D. (2001). NUP98 gene fusions in hematologic malignancies. *Leukemia 2001 15:11*, *15*(11), 1689–1695. https://doi.org/10.1038/sj.leu.2402269

Lam, H. M., Vessella, R. L., & Morrissey, C. (2014). The Role of the Microenvironment – Dormant Prostate Disseminated Tumor Cells in the Bone Marrow. *Drug Discovery*

Today. Technologies, *11*(1), 41. https://doi.org/10.1016/J.DDTEC.2014.02.002

Lapidot, T., Sirard, C., Vormoor, J., Murdoch, B., Hoang, T., Caceres-Cortes, J., Minden, M., Paterson, B., Caligiuri, M. A., & Dick, J. E. (1994). A cell initiating human acute myeloid leukaemia after transplantation into SCID mice. *Nature 1994 367:6464*, *367*(6464), 645–648. https://doi.org/10.1038/367645A0

Lara-Gonzalez, P., Westhorpe, F. G., & Taylor, S. S. (2012). The Spindle Assembly Checkpoint. *Current Biology*, *22*(22), R966–R980. https://doi.org/10.1016/J.CUB.2012.10.006

Lawrence, M. C., Jivan, A., Shao, C., Duan, L., Goad, D., Zaganjor, E., Osborne, J., McGlynn, K., Stippec, S., Earnest, S., Chen, W., & Cobb, M. H. (2008). The roles of MAPKs in disease. *Cell Research 2008 18:4*, *18*(4), 436–442. https://doi.org/10.1038/cr.2008.37

Lee, P., Kim, M. S., Paik, S. M., Choi, S. H., Cho, B. R., & Hahn, J. S. (2013). Rim15-dependent activation of Hsf1 and Msn2/4 transcription factors by direct phosphorylation in Saccharomyces cerevisiae. *FEBS Letters*, *587*(22), 3648–3655. https://doi.org/10.1016/J.FEBSLET.2013.10.004

Li, P., Hao, Z., & Zeng, F. (2021). Tumor suppressor stars in yeast G1/S transition. In *Current Genetics* (Vol. 67, Issue 2, pp. 207–212). Springer Science and Business Media Deutschland GmbH. https://doi.org/10.1007/s00294-020-01126-3

Li, V. C., & Kirschner, M. W. (2014). Molecular ties between the cell cycle and differentiation in embryonic stem cells. *Proceedings of the National Academy of Sciences of the United States of America*, *111*(26), 9503–9508.

https://doi.org/10.1073/PNAS.1408638111/-/DCSUPPLEMENTAL

Liu, S.-T., & Zhang, H. (2016). The mitotic checkpoint complex (MCC): looking back and forth after 15 years. *AIMS Molecular Science*, *3*(4), 597. https://doi.org/10.3934/MOLSCI.2016.4.597

Luo, X., Talarek, N., & De Virgilio, C. (2011). Initiation of the yeast G0 program requires Igo1 and Igo2, which antagonize activation of decapping of specific nutrient-regulated mRNAs. *RNA Biology*, *8*(1). https://doi.org/10.4161/RNA.8.1.13483

Ma, Y., Miao, Y., Peng, Z., Sandgren, J., Díaz De Ståhl, T., Lennartsson, L., Nilsson, S., & Li, C. (2017). *Identification of Mutations, Expression Alterations and Fusion Transcripts by Next Generation RNAseq in Castration-Resistant Prostate Cancer Cell lines with Possible Clinical Relevance*. https://doi.org/10.4172/2469-9853.1000149

Malumbres, M., & Barbacid, M. (2009). Cell cycle, CDKs and cancer: a changing paradigm. *Nature Reviews Cancer 2009 9:3*, *9*(3), 153–166. https://doi.org/10.1038/nrc2602

Maréchal, A., & Zou, L. (2013). DNA Damage Sensing by the ATM and ATR Kinases. *Cold Spring Harbor Perspectives in Biology*, *5*(9). https://doi.org/10.1101/CSHPERSPECT.A012716

McClatchey, A. I., & Yap, A. S. (2012). Contact inhibition (of proliferation) redux. *Current Opinion in Cell Biology*, *24*(5), 685–694. https://doi.org/10.1016/J.CEB.2012.06.009

Miyazawa, K., & Miyazono, K. (2017). Regulation of TGF-β Family Signaling by

Inhibitory Smads. *Cold Spring Harbor Perspectives in Biology*, *9*(3). https://doi.org/10.1101/CSHPERSPECT.A022095

Mizuno, T., Murakami, H., Fujii, M., Ishiguro, F., Tanaka, I., Kondo, Y., Akatsuka, S., Toyokuni, S., Yokoi, K., Osada, H., & Sekido, Y. (2012). YAP induces malignant mesothelioma cell proliferation by upregulating transcription of cell cycle-promoting genes. *Oncogene 2012 31:49*, *31*(49), 5117–5122. https://doi.org/10.1038/onc.2012.5

Montagnoli, A., Fiore, F., Eytan, E., Carrano, A. C., Draetta, G. F., Hershko, A., & Pagano, M. (1999). *Ubiquitination of p27 is regulated by Cdk-dependent phosphorylation and trimeric complex formation*. www.genesdev.org

Moreno-Torres, M., Jaquenoud, M., & De Virgilio, C. (2015). TORC1 controls G1–S cell cycle transition in yeast via Mpk1 and the greatwall kinase pathway. *Nature Communications 2015 6:1*, *6*(1), 1–10. https://doi.org/10.1038/ncomms9256

Moreno-Torres, M., Jaquenoud, M., Péli-Gulli, M. P., Nicastro, R., & De Virgilio, C. (2017). TORC1 coordinates the conversion of Sic1 from a target to an inhibitor of cyclin-CDK-Cks1. *Cell Discovery 2017 3:1*, *3*(1), 1–12. https://doi.org/10.1038/celldisc.2017.12

Narasimha, A. M., Kaulich, M., Shapiro, G. S., Choi, Y. J., Sicinski, P., & Dowdy, S. F. (2014). Cyclin D activates the Rb tumor suppressor by mono-phosphorylation. *ELife*, *2014*(3). https://doi.org/10.7554/ELIFE.02872.001

Neuman, N. A., & Henske, E. P. (2011). Non-canonical functions of the tuberous sclerosis complex-Rheb signalling axis. *EMBO Molecular Medicine*, *3*(4), 189.

https://doi.org/10.1002/EMMM.201100131

O'Brien, C. A., Pollett, A., Gallinger, S., & Dick, J. E. (2006). A human colon cancer cell capable of initiating tumour growth in immunodeficient mice. *Nature 2006 445:7123*, *445*(7123), 106–110. https://doi.org/10.1038/NATURE05372

Pedruzzi, I., Dubouloz, F., Cameroni, E., Wanke, V., Roosen, J., Winderickx, J., & De Virgilio, C. (2003). TOR and PKA Signaling Pathways Converge on the Protein Kinase Rim15 to Control Entry into G0. *Molecular Cell*, *12*(6), 1607–1613. https://doi.org/10.1016/S1097-2765(03)00485-4

Perry, J., & Kleckner, N. (2003). The ATRs, ATMs, and TORs are giant HEAT repeat proteins. *Cell*, *112*(2), 151–155. https://doi.org/10.1016/S0092-8674(03)00033-3

Pulianmackal, A. J., Kareem, A. V. K., Durgaprasad, K., Trivedi, Z. B., & Prasad, K. (2014). Competence and regulatory interactions during regeneration in plants. *Frontiers in Plant Science*, *5*(APR). https://doi.org/10.3389/fpls.2014.00142

Ricci-Vitiani, L., Lombardi, D. G., Pilozzi, E., Biffoni, M., Todaro, M., Peschle, C., & De Maria, R. (2006). Identification and expansion of human colon-cancer-initiating cells. *Nature 2006 445:7123*, *445*(7123), 111–115. https://doi.org/10.1038/NATURE05384

Rodier, G., Montagnoli, A., Di Marcotullio, L., Coulombe, P., Draetta, G. F., Pagano, M., & Meloche, S. (2001). p27 cytoplasmic localization is regulated by phosphorylation on Ser10 and is not a prerequisite for its proteolysis. *EMBO Journal*, *20*(23), 6672–6682. https://doi.org/10.1093/EMBOJ/20.23.6672

Ruppender, N. S., Morrissey, C., Lange, P. H., & Vessella, R. L. (2013). Dormancy in solid Tumors: Implications for Prostate Cancer. *Cancer Metastasis Reviews*, *32*(0), 501–509. https://doi.org/10.1007/S10555-013-9422-Z

Schlegelmilch, K., Mohseni, M., Kirak, O., Pruszak, J., Rodriguez, J. R., Zhou, D., Kreger, B. T., Vasioukhin, V., Avruch, J., Brummelkamp, T. R., & Camargo, F. D. (2011). Yap1 Acts Downstream of α-Catenin to Control Epidermal Proliferation. *Cell*, *144*(5), 782–795. https://doi.org/10.1016/J.CELL.2011.02.031

Segeren, H. A., Van Rijnberk, L. M., Moreno, E., Wubbolts, R., De Bruin, A., & Westendorp, B. (2020). *Excessive E2F Transcription in Single Cancer Cells Precludes Transient Cell-Cycle Exit after DNA Damage*. https://doi.org/10.1016/j.celrep.2020.108449

Seim, I., Jeffery, P. L., Thomas, P. B., Nelson, C. C., & Chopin, L. K. (2017). Whole-genome sequence of the metastatic PC3 and LNCaP human prostate cancer cell lines. *G3: Genes, Genomes, Genetics*, *7*(6), 1731–1741. https://doi.org/10.1534/G3.117.039909/-/DC1

Shamji, A. F., Nghiem, P., & Schreiber, S. L. (2003). Integration of Growth Factor and Nutrient Signaling: Implications for Cancer Biology. *Molecular Cell*, *12*(2), 271–280. https://doi.org/10.1016/J.MOLCEL.2003.08.016

Shaulian, E., & Karin, M. (2001). AP-1 in cell proliferation and survival. *Oncogene 2001 20:19*, *20*(19), 2390–2400. https://doi.org/10.1038/sj.onc.1204383

Shen, Z., & Stanger, B. Z. (2015). YAP Regulates S-Phase Entry in Endothelial Cells. *PLOS ONE*, *10*(1), e0117522. https://doi.org/10.1371/JOURNAL.PONE.0117522

Singh, S. K., Hawkins, C., Clarke, I. D., Squire, J. A., Bayani, J., Hide, T., Henkelman, R. M., Cusimano, M. D., & Dirks, P. B. (2004). Identification of human brain tumour initiating cells. *Nature 2004 432:7015*, *432*(7015), 396–401. https://doi.org/10.1038/NATURE03128

Smith, H. L., Southgate, H., Tweddle, D. A., & Curtin, N. J. (2020). DNA damage checkpoint kinases in cancer. *Expert Reviews in Molecular Medicine*, *22*. https://doi.org/10.1017/ERM.2020.3

Sun, D., & Buttitta, L. (2017). States of G 0 and the proliferation-quiescence decision in cells, tissues and during development. *The International Journal of Developmental Biology*, *61*(6–7), 357–366. https://doi.org/10.1387/IJDB.160343LB

Swinnen, E., Wanke, V., Roosen, J., Smets, B., Dubouloz, F., Pedruzzi, I., Cameroni, E., De Virgilio, C., & Winderickx, J. (2006). Rim15 and the crossroads of nutrient signalling pathways in Saccharomyces cerevisiae. *Cell Division*, *1*, 3. https://doi.org/10.1186/1747-1028-1-3

Thompson, C. R. L., & Kay, R. R. (2000). Cell-Fate Choice in Dictyostelium: Intrinsic Biases Modulate Sensitivity to DIF Signaling. *Developmental Biology*, *227*(1), 56–64. https://doi.org/10.1006/DBIO.2000.9877

Uckun, F. M., Sather, H., Reaman, G., Shuster, J., Land, V., Trigg, M., Gunther, R., Chelstrom, L., Bleyer, A., Gaynon, P., & Crist, W. (1995). Leukemic cell growth in SCID mice as a predictor of relapse in high- risk B-lineage acute lymphoblastic leukemia. *Blood*, *85*(4), 873–878. https://doi.org/10.1182/BLOOD.V85.4.873.BLOODJOURNAL854873

Van Zeebroeck, G., Demuyser, L., Zhang, Z., Cottignie, I., & Thevelein, J. M. (2021). Nutrient sensing and cAMP signaling in yeast: G-protein coupled receptor versus transceptor activation of PKA. *Microbial Cell*, *8*(1), 17. https://doi.org/10.15698/MIC2021.01.740

Vergés, E., Colomina, N., Garí, E., Gallego, C., & Aldea, M. (2007). Cyclin Cln3 is retained at the ER and released by the J chaperone Ydj1 in late G1 to trigger cell cycle entry. *Molecular Cell*, *26*(5), 649–662. https://doi.org/10.1016/J.MOLCEL.2007.04.023

Vermeulen, K., Van Bockstaele, D. R., & Berneman, Z. N. (2003). The cell cycle: a review of regulation, deregulation and therapeutic targets in cancer. *Cell Proliferation*, *36*(3), 131. https://doi.org/10.1046/J.1365-2184.2003.00266.X

Wang, W., Nacusi, L., Sheaff, R. J., & Liu, X. (2005). Ubiquitination of p21Cip1/WAF1 by SCFSkp2: substrate requirement and ubiquitination site selection. *Biochemistry*, *44*(44), 14553–14564. https://doi.org/10.1021/BI051071J

Wang, Y. A. Z., Plane, J. M., Jiang, P., Zhou, C. J., & Deng, W. (2011). Concise Review: Quiescent and Active States of Endogenous Adult Neural Stem Cells: Identification and Characterization. *Stem Cells (Dayton, Ohio)*, *29*(6), 907. https://doi.org/10.1002/STEM.644

Wanke, V., Pedruzzi, I., Cameroni, E., Dubouloz, F., & De Virgilio, C. (2005). Regulation of G0 entry by the Pho80-Pho85 cyclin-CDK complex. *The EMBO Journal*, *24*(24), 4271–4278. https://doi.org/10.1038/SJ.EMBOJ.7600889

Weber, A. M., & Ryan, A. J. (2015). ATM and ATR as therapeutic targets in cancer.

Pharmacology & Therapeutics, *149*, 124–138. https://doi.org/10.1016/J.PHARMTHERA.2014.12.001

Wullschleger, S., Loewith, R., & Hall, M. N. (2006). TOR Signaling in Growth and Metabolism. *Cell*, *124*(3), 471–484. https://doi.org/10.1016/J.CELL.2006.01.016

Yao, G. (2014). Modelling mammalian cellular quiescence. *Interface Focus*, *4*(3). https://doi.org/10.1098/RSFS.2013.0074

Yeh, H.-W., Lee, S.-S., Chang, C.-Y., Lang, Y.-D., & Jou, Y.-S. (2019). *A New Switch for TGFb in Cancer*. https://doi.org/10.1158/0008-5472.CAN-18-2019

Yu, Z. K., Gervais, J. L. M., & Zhang, H. (1998). Human CUL-1 associates with the SKP1/SKP2 complex and regulates p21CIP1/WAF1 and cyclin D proteins. *Proceedings of the National Academy of Sciences*, *95*(19), 11324–11329. https://doi.org/10.1073/PNAS.95.19.11324

Zhang, M., & Huang, B. (2012). The multi-differentiation potential of peripheral blood mononuclear cells. *Stem Cell Research & Therapy*, *3*(6), 48. https://doi.org/10.1186/SCRT139

Zink, D., Fischer, A. H., & Nickerson, J. A. (2004). Nuclear structure in cancer cells. *Nature Reviews. Cancer*, *4*(9), 677–687. https://doi.org/10.1038/NRC1430

Chapter 2 Monitoring Spontaneous Quiescence and Asynchronous Proliferation-Quiescence Decisions in Prostate Cancer Cells

This chapter was published in:

Ajai J Pulianmackal, Dan Sun, Kenji Yumoto, Zhengda Li, Yu-Chih Chen, Meha V Patel, Yu Wang, Euisik Yoon, Alexander Pearson, Qiong Yang, Russell Taichman, Frank C Cackowski, Laura A Buttitta.

Front. Cell Dev. Biol., 10 December 2021. https://doi.org/10.3389/fcell.2021.728663

A.P. created the results shown in Fig 2 and 3

2.1 Abstract

The proliferation-quiescence decision is a dynamic process that remains incompletely understood. Live-cell imaging with fluorescent cell cycle sensors now allows us to visualize the dynamics of cell cycle transitions and has revealed that proliferation-quiescence decisions can be highly heterogeneous, even among clonal cell lines in culture. Under normal culture conditions, cells often spontaneously enter non-cycling G0 states of varying duration and depth. This also occurs in cancer cells and G0 entry in tumors may underlie tumor dormancy and issues with cancer recurrence. Here we show that a cell cycle indicator previously shown to indicate G0 upon serum starvation, mVenus-p27K-, can also be used to monitor spontaneous quiescence in untransformed and cancer cell lines. We find that the duration of spontaneous quiescence in untransformed and cancer cells is heterogeneous and that a portion of this heterogeneity results from asynchronous proliferation-quiescence decisions in pairs of daughters after mitosis, where one daughter cell enters or remains in temporary quiescence while the other does not. We find that cancer dormancy signals influence

both entry into quiescence and asynchronous proliferation-quiescence decisions after mitosis. Finally, we show that spontaneously quiescent prostate cancer cells exhibit altered expression of components of the Hippo pathway and are enriched for the stem cell markers CD133 and CD44. This suggests a hypothesis that dormancy signals could promote cancer recurrence by increasing the proportion of quiescent tumor cells poised for cell cycle re-entry with stem cell characteristics in cancer.

2.2 Introduction

Cycling cells tend to enter quiescence, a reversible, non-cycling state in response to contact inhibition, reduced levels of mitogens, or under various stress conditions. Quiescent cells retain the ability to re-enter the cycle upon the addition of serum or under favorable conditions (Coller et al., 2006;Yao, 2014). However, studies of mammalian cells in the past few years have found that many cells enter a spontaneous reversible G0-like state in cell culture even in the presence of mitogens and abundant nutrients (Spencer et al., 2013;Overton et al., 2014;Min and Spencer, 2019). This suggests that the proliferation-quiescence decision is constantly regulated - even under optimal growth conditions.

The relative percentage of cells that enter a temporary G0-like state after mitosis varies with cell type and culture conditions, suggesting many signaling inputs influence the proliferation-quiescence decision (Spencer et al., 2013). This is also consistent with findings in several cancer cell lines, where some cells enter a temporary quiescent state while others do not (Dey-Guha et al., 2011). This leads to heterogeneity in cell culture, with a subpopulation of cells entering and leaving temporary quiescent states (Overton et al., 2014). This proliferative heterogeneity may underlie states of dormancy in cancer and has been shown to be related to cancer therapeutic resistance (Recasens and Munoz, 2019;Risson et al., 2020;Nik Nabil et al., 2021). This is particularly relevant in prostate cancer, where it is thought that early spreading of tumor cells to the bone marrow and other tissues may provide signals leading to quiescence and tumor dormancy (Chen et al., 2021). Prostate cancer dormancy in tissues such as the bone are problematic as a percentage of patients will later develop recurrent cancer with

significant metastases from these cells, which are often also resistant to treatment (Lam et al., 2014). Understanding how and why quiescent cancer cells reside in environments such as the bone marrow for long periods of time, and finding ways to eliminate them, is an important ongoing challenge in prostate cancer research and treatment.

The difficulties in monitoring the proliferation-quiescence decision and distinguishing different states and lengths of G0 has limited our ability to understand how signals impact the heterogeneity of quiescence in cell populations. Most assays for cell cycling status use immunostaining of cell cycle phase markers or nucleotide analogue incorporation, both of which assess static conditions in fixed samples (Matson and Cook, 2017). Cell cycle reporters such as the FUCCI system (Fluorescent Ubiquitination-based Cell Cycle Indicator), have become widely used to track cell cycle dynamics live in individual cells (Sakaue-Sawano et al., 2008). The FUCCI system and related systems such as CycleTrak and others including a constitutive nuclear marker are able to differentially label cells in G1, S and G_2/M phases, allowing us to visualize the G_1-M transition, however G0 cannot be distinguished from G1 in these approaches (Ridenour et al., 2012;Chittajallu et al., 2015).

Recent methods to monitor quiescence heterogeneity have used live cell imaging with sensors for Cdk2 activity, Ki-67 expression, and expression of Cdk inhibitors such as p21 and p27 (Spencer et al., 2013;Overton et al., 2014;Stewart-Ornstein and Lahav, 2016;Miller et al., 2018;Zambon et al., 2020). Here we take advantage of the cell cycle indicator, mVenus-p27K$^-$, which was generated to work in combination with the G0/G1 FUCCI reporter mCherry-hCdt1(30/120), to specifically label quiescent cells (Oki et al., 2014). This probe is a fusion protein consisting of a fluorescent protein mVenus and a Cdk binding defective mutant of p27 (p27K-). p27 accumulates during quiescence and is degraded by two ubiquitin ligases: the Kip1 ubiquitination-promoting complex (KPC) at the G0-G1 transition, and the SCF^{Skp2} complex at S/G2/M phases (Kamura et al., 2004). When used in combination with the G0/G1 FUCCI reporter, cells can be tracked from a few hours after mitosis until early S phase with distinct colors. This allows us to examine the dynamics of the proliferation-quiescence transition after mitosis on a single-cell level without artificial synchronization.

Prior work with a Cdk2 sensor and monitoring p21 levels revealed that both non-transformed and cancer cells in culture can enter “spontaneously” quiescent states of variable length, even under optimal growth conditions (Spencer et al., 2013;Overton et al., 2014;Yang et al., 2017;Min and Spencer, 2019). The proportion of spontaneously quiescent cells in a population and their variability in the length of quiescence leads to cell cycle heterogeneity (Overton et al., 2014), which may in part also underlie cell cycle heterogeneity within clonal tumors (Dey-Guha et al., 2011;Dey-Guha et al., 2015). This led us to examine whether we could monitor spontaneous quiescence using the mVenus-p27K$^-$ G0 reporter. Here we show that by tracking the trajectory of this reporter activity, we can monitor spontaneous quiescence in non-transformed mouse fibroblasts and prostate cancer cells. While measuring the heterogeneity of spontaneous quiescence, we also observed that a pair of daughter cells resulting from a single mitosis can make asynchronous proliferation-quiescence decisions. In this type of asynchronous decision, one daughter from a mitosis enters G0, while the other enters G1, further increasing cell cycle heterogeneity within a clonal population (Dey-Guha et al., 2011). We find that signals associated with promoting or releasing tumor dormancy can influence quiescence and asynchronous proliferation-quiescence decisions in prostate cancer cells. Using the mVenus-p27K$^-$ G0 reporter, we isolate populations containing quiescent cancer cells and find they are enriched for a subpopulation expressing stem cell markers and express high levels of Hippo pathway signaling components, but with inactivated YAP, which may indicate a state poised for cell cycle re-entry. Finally, we provide evidence that the expression of immune recognition signals may be decreased in populations containing quiescent cancer cells, suggesting a hypothesis for how these cancer cells may preferentially evade the immune system.

2.3 Results

2.3.1 mVenus-p27K$^-$ based G0/G1 cell cycle indicators track spontaneous quiescence

To characterize the proliferation-quiescence transition at single-cell resolution in mouse 3T3 cells under full serum conditions without synchronization, we used the G0 cell cycle indicator mVenus-p27K$^-$ combined with the G0/G1 reporter from the FUCCI cell cycle system, mCherry-hCdt1(30/120) to distinguish G0 cells from G1 cells as previously described (Oki et al., 2014). We first manually examined movies of asynchronously proliferating 3T3 cells stably expressing these reporters to monitor reporter dynamics (Supp. Movie 1,2). With this combination of cell cycle reporters, mVenus-p27K$^-$ expression begins approximately 2-6h after cytokinesis is complete, followed by mCherry-hCdt1expression approximately 2-6h later. Most cells then exhibit a rapid reduction in mVenus-p27K$^-$ within approximately 3h, signaling G1 entry followed by mCherry-hCdt1 degradation at G1 exit (Fig 2-1 A,B). However, for a fraction of cells (ranging between 20-65% in different movies) we observed both mVenus-p27K$^-$ and mCherry-hCdt1 to both continue to accumulate for up to 14h and beyond, without division or evidence of S/G2/M entry for 20h or more, signaling spontaneous G0 entry (Fig 2-1 C). This progression of reporter expression in order from mVenus-p27K$^-$ positive to mVenus-p27K$^-$ and mCherry-hCdt1 double positive to mCherry-hCdt1 was invariant in the movies, although we did observe some cell to cell variation in reporter expression intensity, despite using a clonal cell line.

To monitor and quantitatively measure the dynamic transitions of cell cycle states—from cytokinesis to S phase entry, we developed an Automated temporal Tracking of Cellular Quiescence (ATCQ) analysis platform. This platform includes a computational framework for automated cell segmentation (identification of individual cells in an image), tracking, cell cycle state identification, and quantification from movies (Supp. Fig 2-1). The cell segmentation and tracking allows us to record the fluorescent reporter intensity changes within individual cells in real-time imaging, without the aid of a constitutive nuclear marker. The single-cell fluorescence changes over time, in turn, are used to obtain cell cycle state identification (G0, G1, or early S phase) and quantification, which allows us to examine the kinetics of the proliferation-quiescence transition. The single-cell traces of fluorescent reporters, mVenus-p27K$^-$ and mCherry-hCdt1, graphed by ATCQ is consistent with trajectories of G0 entry (increasing Venus

and Cherry), G0 exit/G1 entry (degradation of Venus, increasing Cherry), and G1 exit/S-phase progression (degradation of Cherry) we manually observed in movies (Fig 2-1D).

To confirm that the Venus/Cherry- double positive population represents G0 phase, we performed a short-term (24h, 1%FBS) serum starvation treatment followed by 48 h of live imaging. As expected in low serum, the reporter trajectories collapsed into predominantly G0 entry (Fig 1E). When we measure the timing of the reporter trajectories we find that the timing of G0 is heterogeneous compared to G1 entry and G1 exit and becomes further prolonged under low serum (Fig 2-1F,G).

We next examined whether the mVenus-p27K$^-$ / mCherry-hCdt1 double positive population under full serum conditions exhibits molecular markers of G0. To do this, we sorted cells into Venus/Cherry double-positive, Cherry single-positive, and Venus/Cherry double-negative populations and performed western blots for markers of G0 vs. G1 phase. As a positive control for G0, cells cultured under serum deprivation were sorted in a similar manner (Supp. Fig 2-2). We found that Venus/Cherry double-positive cells under full serum conditions exhibited hypo-phosphorylated pocket proteins RB and p130, increased endogenous p27, and reduced phosphorylation of Cdk2 on the activating T-Loop (Jeffrey et al., 1995;Sherr and Roberts, 1999;Tedesco et al., 2002). We also confirmed reduced expression of cell cycle genes, and upregulated expression of genes associated with G0 in the double positive cells in full serum by qRT-PCR on sorted cells (Supp. Fig. 2-2) (Oki et al., 2014). Taken together, our tracking and molecular data suggests that many of the Venus/Cherry double-positive cells under full serum conditions enter a temporary G0 of variable length. We therefore conclude that this reporter combination also captures temporary, spontaneous quiescence in a fraction of asynchronously proliferating cells.

2.3.2 Asymmetry in the proliferation-quiescence decision

In the manual tracking of dividing cells, we noticed several instances where pairs of daughters, born of a single mitosis, make different proliferation-quiescence decisions. In this situation, one daughter will remain G0, while the other daughter born at the same time will degrade the mVenus-p27K$^-$ reporter and enter G1, followed by S/G2 and

mitosis (Fig 2-1H). Under normal culture conditions we observe this in 20-40% of 3T3 cells entering G0, with the differences in the timing of G1 entry between asynchronous daughters varying from 1-15 hours. We also find that daughters can exhibit varying lengths of the Venus/Cherry double-positive state (from 5h – 24h) before one from the pair enters G1. We next examined whether such asynchrony in the cell cycle progression of two daughters born of the same mitosis could be observed in other cell types. We manually examined movies of published live cell imaging and observed instances of cell cycle asynchrony in pairs of daughters in BT549 and MCF10A cells. Cell cycle asynchrony in daughters born of the same mitosis has also been reported in MCF7 and HCT116 cells and referred to as “asymmetric” cell divisions, accompanied by differences in AKT signaling between daughters after telophase (Dey-Guha et al., 2011;Dey-Guha et al., 2015). We suggest that both spontaneous G0 and asynchronous proliferation-quiescence decisions in pairs of daughters after mitosis both contribute to cell cycle heterogeneity in clonal cell populations.

2.3.3 PC3 prostate cancer cells exhibit spontaneous quiescence and asymmetry in the proliferation-quiescence decision

Cellular quiescence in prostate cancer is thought to contribute to tumor dormancy and issues with metastatic cancer recurrence. However, it is not well understood how and why prostate cancer cells enter and exit quiescence. We wondered whether spontaneous quiescence and asynchronous proliferation-quiescence decisions may, in part, underlie cell cycle heterogeneity in prostate cancer cells. To examine this, we transduced the mVenus-p27K$^-$ G0 and mCherry-hCdt1 G1 reporters into PC3 cells. We initially selected pools of transduced cells expressing both reporters under reduced serum conditions by FACS. We found that sorted, pooled cells quickly lost expression of one or the other reporter after a limited number of passages. We therefore isolated clones and selected a clonal PC3 Venus-Cherry cell line, stably expressing both reporters at visible levels with normal cell cycle dynamics (i.e a cell doubling time similar to parental PC3). In this line, we readily observe double positive Venus/Cherry cells under normal full-serum culture conditions (Fig 2-2 A) that are negative for EdU

incorporation, negative for Ki-67 and both reporters are silent in cells that progress through the cell cycle into mitosis (Fig 2-2 B-D). We also confirmed that the reporters exhibited the expected G0/G1 dynamics during serum withdrawal and serum re-addition in PC3 cells (Fig 2-2E).

We next attempted to track the reporter dynamics in PC3 cells with live cell imaging and found that these cancer cells were too motile to be tracked accurately for more than a few hours. We therefore used a microfluidic device we term the “cell hotel,” to capture one or a few cells and trap them in a chamber, to allow for manual tracking of individual cells and their daughters (Cheng et al., 2016). Each cell hotel slide allows simultaneous recording of up to 27 chambers under 10X magnification. We confirmed that the PC3 Venus-Cherry cells in the cell hotel exhibited similar growth and cell doubling times as previously reported for PC3 cells in bulk cell culture. In addition we repeated measurements of 3T3 Venus/Cherry cells in the cell hotel for all comparisons to PC3 (Fig. 2-2 F-J).

Similar to the 3T3 cells, we observed a nearly invariant reporter progression of mVenus-p27K$^-$ expression ~2h after cytokinesis, followed by mCherry-hCdt1expression approximately 2h later. Cells that enter the cell cycle, degrade mVenus-p27K$^-$ within approximately 4h, followed by mCherry-hCdt1 degradation and ultimately cell division (Fig 2-2F). As in 3T3 cells, we observed 20% of cells with stabilized mVenus-p27K$^-$ and mCherry-hCdt1 for 14h and beyond, without division or evidence of S/G2/M entry for 20h or more, suggestive of spontaneous G0 entry in PC3 cells (Fig. 2-2 G,H). Notably, spontaneous quiescence in PC3 cells tends to be more rare and shorter than in 3T3 cells (Fig 2-2 H). This could reflect the important role for p53 signaling in spontaneous quiescence (Arora et al., 2017;Yang et al., 2017), as PC3 cells lack functional p53 (Carroll et al., 1993). We also observed evidence of asynchronous proliferation-quiescence decisions, with 30% of daughters making asynchronous G0/G1 decisions within 1-6 hours of each other (Fig 2-2 I,J). Interestingly, the asynchronous proliferation-quiescence decisions were also rarer and the difference in timing between asynchronous daughters was less dramatic in PC3 cells (Fig. 2-2 J).

2.3.4 Tumor dormancy signals can influence quiescence and asynchronous proliferation-quiescence decisions

Bone is a common site for prostate cancer metastasis and work from our group and others have shown that signals from osteoblasts can influence prostate cancer dormancy and PC3 cell cycle dynamics (Jung et al., 2016;Lee et al., 2016;Yumoto et al., 2016). Our previous work on PC3 cell cycle dynamics used the FUCCI cell cycle reporters, which could not distinguish between G0 and G1 arrest (Jung et al., 2016). We therefore examined whether PC3 Venus-Cherry cells co-cultured with osteoblasts increased entry into G0 quiescence. We found that co-culture with mouse MC3T3-E1 pre-osteoblasts under full serum conditions significantly increased the fraction of double positive PC3 Venus-Cherry cells consistent with increased entry into G0 (Fig. 2-3A,B). We next examined whether Gas6 and TGFß2, signals from osteoblasts we have previously shown to induce a G0/G1 cell cycle arrest (Jung et al., 2016;Lee et al., 2016;Yumoto et al., 2016), induced entry into G0. Indeed, exposure to Gas6 or TGFß2 significantly increased the fraction of double positive PC3 Venus-Cherry cells after 48h, suggesting the G0/G1 arrest we previously observed was indeed arrest in G0 (Fig 2-3C).

In the bone marrow, Gas6 and TGFß2 are thought to promote prostate cancer dormancy (Jung et al., 2012;Taichman et al., 2013;Ruppender et al., 2015;Yumoto et al., 2016) while GM-CSF promotes stem cell release from the bone marrow, which may provide cues for metastatic cancer cells in the bone marrow to exit from dormancy and proliferate (Dai et al., 2010). While some of the role for GM-CSF is thought to be due to indirect effects on the bone marrow stem cell niche, studies of GM-CSF directly added to cultured PC3 cells also show increased S-phase entry, proliferation and clonogenic growth consistent with exit from dormancy (Lang et al., 1994;Savarese et al., 1998). We therefore wanted to test whether GM-CSF impacted the proliferation-quiescence decision in PC3 cells and compare this to the effects of the dormancy associated signals Gas6 and TGFß2 on G0. We used the cell hotel to track cell cycle and mVenus-p27K$^-$ and mCherry-hCdt1 dynamics in PC3 cells 2 hours after the addition of Gas 6, TGFß2 or GM-CSF. In response to Gas6 and TGFß2 we observed a significant

decrease in the number of cells undergoing divisions during the 72h live imaging period, consistent with an increase in G0 entry (Fig 2-3D,E). Unexpectedly, we also observed a similar decrease in cell divisions for cells treated with GM-CSF, and an increase in Venus-Cherry double positive cells, suggesting GM-CSF also promotes G0 entry. For the fraction of cells undergoing divisions during the live imaging, we tracked when these cell divisions occur. We found that control cells asynchronously proliferate throughout the live imaging time course, while most cells treated with Gas6, TGFß2 or GM-CSF divide within the first 24h of imaging (Fig. 2-3F). These data suggest that cells uncommitted to the cell cycle either enter or remain in quiescence in response to Gas6, TGFß2 or GM-CSF. Cells that are past the restriction point when the treatment begins, and therefore committed to cycle, must make a subsequent proliferation-quiescence decision after mitosis that may be tipped toward quiescence. To confirm this, we examined the proliferation-quiescence choices made by pairs of daughters that divide under each treatment, broken down into: synchronous entry into G0, synchronous entry into G1 or asynchronous entry with one daughter entering G1 while the other remains in G0. For Gas6 and TGFß2 treated cells, we observed a significant increase in synchronous entry into G0 at the expense of synchronous entry into G1, with little impact on the proportion of cells that exhibit asynchronous proliferation-quiescence decisions (Fig 2-3G). This suggests that Gas6 and TGFß2 continue to promote quiescence in cells that are already committed to cycle after treatment addition. By contrast, GM-CSF treatment increased the proportion of divisions resulting in synchronous entry into G1, suggesting prolonged GM-CSF exposure may eventually promote cell cycle entry in a subset of the population (Fig 2-3G). Of note the pro-proliferative effects previously reported were seen in experiments performed on much longer timescales of at least 3 to 4 days (Lang et al., 1994;Savarese et al., 1998), suggesting the response to GM-CSF may be complex. Our data suggests GM-CSF treatment initially promotes quiescence entry in cells that are prior to the restriction point, but for a subset of cells past the restriction point it promotes their daughters to preferentially enter G1.

We next tracked pairs of daughters from the dividing cells under treatment and measured how long they spent in a Venus/Cherry double positive G0 state after mitosis

prior to entering a Cherry-only G1 state. The goal was to determine whether each treatment also impacted the heterogeneity of transient quiescence, a feature that may initially promote tumor dormancy, but also lead to later recurrence. We found that only treatment with Gas6 impacted cells that entered transient quiescence, by significantly prolonging the time spent in G0 prior to the next G0-G1 transition (Fig 2-3H). This prolonged G0 occurred whether the pairs of daughters entered into G1 synchronously or asynchronously, and increased the differences in timing of G1 entry between pairs of asynchronous daughters (Fig 2-3I). This suggests that Gas6 promotes quiescence, but also promotes quiescence heterogeneity in cells that retain the ability to re-enter the cell cycle.

2.3.5 Quiescent cancer cells are enriched for stem cell markers and express high levels of Hippo pathway signaling components.

Identifying molecular markers of quiescent cancer cells that could be assayed in patient samples is an attractive approach to identify those at risk for metastasis and recurrence. Toward this goal, we used the PC3 Venus-Cherry cells to isolate populations enriched for quiescent cancer cells by FACS, to examine their cell surface markers and gene expression changes. (Figs. 2-4,5). We first assayed the prostate cancer stem cell markers CD133 and CD44 to determine whether increasing cellular quiescence could increase the fraction of CD133/CD44 double positive potential cancer stem cells (Jung et al., 2016). We cultured PC3 Venus/Cherry cells under normal 10% serum conditions, or reduced 0.5% serum conditions for 72h. We confirmed an increase in the G0 population under reduced serum (Fig 2-4 A, B) and compared the fraction of CD133/CD44 double positive cells in the G0, G1 and S/G2/M populations (Fig 2-4C). We observed the majority of the CD133/CD44 double positive cells to be in the G0 population, with a much smaller fraction in G1 and almost none in the S/G2/M population (Fig 2-4 C,D). This suggests that signals in the tumor environment that increase the quiescent population in prostate cancer may also increase the number of potential cancer stem cells that could underlie recurrence.

We previously established a mouse xenograft model of prostate cancer bone metastasis using Du-145 cells, that recapitulates aspects of dormancy and recurrence

(Cackowski et al., 2017). We attempted to use the PC3 Venus/Cherry cells in a similar xenograft model, but found that the cells quickly silenced the cell cycle reporters *in vivo*. We therefore used the xenograft model with Du-145 cells as a tool to compare gene expression profiles for cells in actively growing bone metastases as assessed by bioluminescence imaging ("involved") vs. bones without imaging detected metastases, but which still contained cancer cells that were fewer in number and presumably more slowly growing ("uninvolved"). Use of this approach of comparing cancer cells from high burden / involved vs. low burden / uninvolved sites was previously used in a breast cancer model and showed that cancer cells from the uninvolved sites had more stem-like properties (Lawson et al., 2015). We isolated cells from mouse marrow under both conditions and performed bulk RNA-seq to compare global gene expression changes in the growing vs. dormant state. Due to the small number of human cells recovered from uninvolved bones, we were only able to accurately assign differences in expression for 117 genes (Supp. Fig. 3). Nonetheless using DAVID and the KEGG database to perform pathway analysis of differentially expressed genes, we found an enrichment of genes involved in extracellular matrix interactions and the TGF-beta signaling pathway, factors known to impact prostate cancer dormancy and dormancy escape (White et al., 2006;Bragado et al., 2013;Ruppender et al., 2015). We noted that several of the genes falling into these enriched categories also interface with Hippo signaling, which is a key regulator of cell cycle exit (Zheng and Pan, 2019). We therefore decided to examine whether components of Hippo signaling may be altered in quiescent prostate cancer cells.

To examine differences in gene expression between G0, G1, and S/G2/M populations, we sorted populations and examined gene expression differences using a Hippo signaling Pathway qRT-PCR array (Fig. 2-5A). In G0 cells, we noted a widespread increase in transcripts for Hippo signaling pathway components (e.g. DCHS1, FAT3, MST1, MOB1A, SAV1), transcriptional regulators (TEAD3, MEIS1) as well as targets (AMOTL1, AMOTL2) (Wang et al., 2018). The increased expression of some transcriptional targets of Hippo signaling is surprising, since these cells are in G0 and therefore would be expected to have Hippo signaling on. Hippo signaling acts via phosphorylation to suppress the activity of the downstream transcriptional effectors

YAP1 and TAZ (encoded by the *WWTR1* gene in humans) (Zheng and Pan, 2019). We therefore examined whether YAP and TAZ are suppressed via phosphorylation in G0 cells through active Hippo signaling. We performed westerns for the inactivating phosphorylations on YAP1 and TAZ in G0, G1 and S/G2/M sorted cells (Fig 2-5B) and found a small increase in phosphorylated YAP, but no effect on TAZ. We hypothesize the increased expression of Hippo pathway components may poise quiescent cells to re-enter the cell cycle upon receipt of a dormancy escape signal, but that during G0, active Hippo signaling restrains YAP transcriptional activity through inhibitory phosphorylation. (Fig 2-5 and Supp. Fig 2-4).

Hippo signaling in cancer has been associated with restraining proliferation (Zheng and Pan, 2019), but also has been shown to alter immune response, with active Hippo signaling suppressing tumor immunogenicity (Moroishi et al., 2016;Yamauchi and Moroishi, 2019). We therefore next examined whether G0 cells exhibited alterations in expression of immune response-associated signals. Using the Qiagen Cancer Immunology array on sorted G0, G1 and S/G2/M PC3 cells vs. the mixed population as a reference, we observed a moderate but widespread decrease in the expression of immune-related genes including signals known to target cancer cells for host immune destruction, such as CXCR3, CXCL8, and HLA-C (Fig 2-5C) in G0 cells. This suggests that spontaneously quiescent cancer cells may exhibit altered immunoreactivity. Interestingly, one pro-inflammatory gene, PTGS2 (Cox-2), was strongly upregulated in G0 cells (Fig 2-5C), consistent with the previous work showing this target to be de-repressed when upstream Hippo signaling is active and YAP/TAZ are suppressed by phosphorylation (Zhang et al., 2018). Taken together, our results suggest the inherent cell cycle heterogeneity of metastatic prostate cancer includes a fraction of spontaneously quiescent cells that are enriched for cells expressing cancer stem cell markers and exhibit gene expression changes consistent with a state poised to re-enter the cell cycle, but potentially less visible to the host immune system.

2.4 Discussion

Several cancers contain heterogeneous populations with varying levels of proliferation (Davis et al., 2019). Some studies suggest that quiescent tumor cells contribute to drug-resistance, by providing a population of non-cycling cells that survive cytotoxic chemotherapy (De Angelis et al., 2019;Talukdar et al., 2019;Hen and Barkan, 2020). Understanding the molecular basis of proliferative heterogeneity therefore may assist in developing better therapeutic approaches for cancer. Here, we show that untransformed 3T3 cells and PC3 prostate cancer cells show spontaneous quiescence and heterogeneous G0 lengths under pro-proliferative culture conditions. We propose that spontaneous quiescence may be related to quiescence in cancer, since quiescent cancer cells must leave the cell cycle in the presence of pro-proliferative growth factor and oncogenic signaling.

Spontaneous quiescence has been shown to underlie clonal cell cycle heterogeneity (Overton et al., 2014) and may in part underlie cell cycle heterogeneity in tumors. Here we show an additional mechanism to create heterogeneity, asynchronous G0/G1 decisions, where one daughter from a mitotic event remains in G0, while the other enters G1. These asynchronous decisions are somewhat surprising, since recent work has suggested the signals that influence the proliferation-quiescence decision are integrated over the previous cell cycle phases prior to mitosis and therefore would be expected to be inherited equally in daughters after mitosis (Yang et al., 2017;Min et al., 2020). The asynchrony in asynchronous PC3 cell divisions is often only a few hours but can extend to over 20h or more in the presence of the dormancy inducing factor, Gas6 (Fig 2-3I). Small differences in asynchronous pairs of daughters may possibly be explained by fluctuations resulting in unequal protein and transcript inheritance at mitosis. However, this is a less satisfying hypothesis for differences in G0 exit between asynchronous daughters longer than 10h. Previous work in MCF7 breast and HCT116 colon cancer cells has shown a population of dormant cells resulting from asymmetric Akt signaling after cell divisions (Dey-Guha et al., 2011). In this example, about 1% of cell divisions exhibit asymmetry, resulting in a daughter with low Akt signaling. Importantly, elimination of Akt prevented proliferative heterogeneity in these lines in cell culture (Dey-Guha et al., 2015), and inhibition of asymmetric Akt signaling reduced

tumor recurrence after treatment in a xenograft model (Alves et al., 2018). It is worth noting that PC3 cells lack functional PTEN (Huang et al., 2001;Dubrovska et al., 2009) and therefore would be expected to have higher endogenous Akt signaling that suppresses some degree of asymmetry. In addition, Gas6 and other TYRO3/AXL/MERTK ligands signal in part through Akt, and therefore may also impact Akt asymmetry (Cosemans et al., 2010;Kasikara et al., 2017). Inhibition of Akt signaling can lead to up regulation of p27 in PC3 cells (van Duijn and Trapman, 2006), while over expression of p27 can also inhibit Akt signaling (Chen et al., 2009). Further work will be needed to determine if asymmetric Akt signaling may be a cause or consequence of asynchronous proliferation-quiescence decisions in prostate cancer.

The relationship of dormancy and cellular quiescence remains unclear. Here we show that dormancy-associated signals in prostate cancer, Gas6 and TGFß2, rapidly within a few hours, induce quiescence entry in prostate cancer cells after mitosis. This is in part because these signals tip the balance of proliferation-quiescence decisions in favor of synchronous G0 entry. By contrast, a presumed pro-proliferative signal for PC3 cells, GM-CSF tips the balance in favor of synchronous divisions into G1 for the cells that divide after initial exposure. Thus, although GM-CSF promotes G0 entry initially, sustained signaling may promote cell cycle re-entry in the longer term. Gas6 also has a complex effect on the proliferation-quiescence decision. In addition to promoting G0 in cells that are uncommitted to the cell cycle, Gas6 also prolongs G0 in cells that retain the ability to eventually re-enter the cell cycle. This suggests that the quiescence response to Gas 6 is not an all or nothing response and it can be graded, resulting in varying lengths of G0 to promote quiescence heterogeneity. While none of the signals we tested significantly altered the frequency of asynchronous cell cycle entry in pairs of daughters after mitosis, Gas6 significantly increased the asynchrony in G0 exit and G1 entry. We suggest this could be another source of quiescence heterogeneity in cancer.

Understanding the gene expression changes in dormant cancer cells will be essential to understanding their biology, but will also be useful tools as molecular markers for identifying them in patient samples. Here we show that quiescent PC3 cells

are enriched for prostate cancer stem cell markers CD133 and 44 and that driving quiescence entry through serum starvation significantly increases the population of CD133/44 double positive cells in the population. Quiescent prostate cancer cells also exhibit increased expression of some Hippo pathway components, while the Hippo pathway remains on to restrain cell cycle entry. This finding in cell culture was also supported by our gene expression analysis in an *in vivo* xenograft model for prostate cancer tumor dormancy (Supp. Fig 3). Interestingly, this is correlated with suppressed levels of mRNA for immune targeting factors, and may suggest a mechanism by which quiescent cancer cells evade host immune attack. Whether there is a direct or indirect relationship between the Hippo signaling status and expression of immune targets in quiescent cells remains to be examined.

2.5 Materials and Methods

2.5.1 Cells and cell culture

The mouse embryonic fibroblast 3T3 cell line containing the G0 and G1 cell cycle reporters were kindly provided by Dr. Toshihiko Oki (University of Tokyo). These cells were grown in Dulbecco's modified Eagle's medium (DMEM; Gibco) supplemented with 10% fetal bovine serum (FBS) and 1% penicillin-streptomycin. Serum levels were reduced as indicated in the figures and text for serum starvation experiments. PC3 prostate cancer cells were cultured in RPMI medium with 10% serum and 1% penicillin-streptomycin and transduced with the G0 and G1 cell cycle reporters as previously described (Takahashi et al., 2019).

2.5.2 Live Cell Imaging

NIH/3T3 cells were cultured at low density (to avoid contact inhibition) on 12-well plates in phenol red-free DMEM/10%FBS or 1%DMEM. Experiments in Fig.1 (and Supplements to Fig 1) were performed using an EVOS FL cell imaging system with a 20X objective lens or an IncuCyte Zoom at 37^{o}C, 5% CO_2. The imaging intervals were 20-30 minutes.

For experiments using the “Cell Hotel” (Figs. 2 and 3), 10,000 PC3 cells in RPMI medium with 10% serum were loaded into the inlet of the microfluidic chamber. The chamber loading was monitored until most of the chambers were occupied with single cells (~5mins). Remaining cells were then removed from the inlet and the outlet and replenished with fresh media. Imaging was performed using a Leica DMI 6000 with a Tokai Hit stage-top environmental chamber at 37ºC, 5% CO_2. TGFß2, Gas6 and GM-CSF (R&D systems) were reconstituted according to the manufacturer's guidelines (R&D systems). For Gas6, TGFß2 and GM-CSF treatments, 10,000 PC3 cells were mixed with media containing the ligand (2mg/mL for Gas6, 20ng/mL for TGFß2 and 1mM for GM-CSF) and introduced into the chamber. Cells were then incubated in media with the indicated ligand for 2h of pre-equilibration prior to imaging every 30 minutes.

2.5.3 Fabrication of the Microfluidic Device for Single-Cell Tracking

The microfluidic device used for single-cell tracking was developed in our previous work (Cheng et al., 2016). The device was built by bonding a PDMS (Polydimethylsiloxane, Sylgard 184, Dow Corning) layer with microfluidic patterns to a glass slide. The PDMS layer was formed by standard soft lithography. The SU-8 mold used for soft-lithography was created by a 3-layer photolithography process with 10 µm, 40 µm, and 100 µm thick SU-8 (Microchem) following the manufacturer’s protocol. PDMS was prepared by mixing with 10 (elastomer): 1(curing agent) (w/w) ratio, poured on SU-8 molds, and cured at 100ºC overnight. Inlet and outlet holes are created by biopsy punch cutting. The PDMS with microfluidic channel structures and the glass slide were treated using oxygen plasma (80W for 60 seconds) and bonded. The devices after bonding were heated at 80ºC for an hour to ensure bonding quality. The microfluidic chips were sanitized using UV radiation and primed using a either a Collagen solution (1.45mL Collagen (Collagen Type 1, 354236, BD Biosciences) or Fibronectin solution, 0.1mL acetic acid in 50mL DI Water) overnight before use.

2.5.4 Flow Cytometry analysis and FACS

For cell sorting and flow cytometry assays in Figs. 2-5, cells were cultured in RPMI supplemented with either 10% FBS or 1% as indicated and subpopulations were

sorted according to the intensity of their fluorescent reporters, using a BD FACS Aria II system. Cells were sorted into SDS-PAGE loading buffer or RLT (Qiagen) for immediate protein extraction or RNA isolation. A minimum of ~10^5 cells were collected for each experiment. Antibodies used for PC3 isolation from osteoblasts co-culture in Fig. 2 were APC/Cy7 anti-human HLA A,B,C antibody (Biolegend #311426).

For Figure 4, we assessed PC3 cells for dual positivity for CD44 and CD133 as we previously described (Shiozawa et al., 2016). PC3 cells were seeded at 10^5 cells per well of six well plates in RPMI with 1% penicillin / streptomycin and either 10% or 0.5% serum, then cultured for three days. Both adherent and floating cells were analyzed for flow cytometry using a four laser BD LSR II instrument and FACSDiva™ software. We plotted G0-Venus vs. G1-Cherry from the single, viable (DAPI negative) population and drilled down from each cell cycle phase group (G0, G1, or S/G/M) to analyze the percent CD133+/CD44+ cells from each population. Antibodies were PE-vio770 conjugated CD133/1, clone AC133 (Miltenyi Biotech #130-113-672) diluted 1:50 and APC conjugated CD44 (BD #559942) diluted 1:5.

2.5.5 Western Blotting:

Cleared cell lysates in SDS loading buffers were separated on 4-20% SDS PAGE gels under reducing conditions and transferred to PVDF membranes. Membranes were blocked with 5% milk in TBST and probed with primary antibodies diluted 1:1000 in 5% BSA TBST; YAP1 phospho-serine 127 (Cell Signaling Technology #4911) and TAZ phospho-serine 89 (Cell Signaling Technology #59971). The secondary antibody was Cell Signaling #7074 diluted 1:1000 in 1% milk TBST. Blots were developed in Pierce Supersignal Pico ECL substrate and visualized with a Biorad Image Doc Touch system. The membranes were subsequently stripped and reprobed for total YAP1 (CST #14074), total TAZ (CST #83669), beta actin (CST #4970), or vinculin (CST #13901) as indicated.

2.5.6 qRT-PCR Arrays:

PC3 Venus/Cherry cells were seeded at 10^5 cells per dish in 10 cm dishes and cultured for 3 days in RPMI media with 1% FCS. Cells were seeded on different days

for biologic triplicate or quadruplicate samples. After three days of culture, cells were released by tripysinization, stained with DAPI for viability and sorted by FACS into either the total (mixed) viable cell population, G0, G1, or S/G2/M phases using the Venus/Cherry markers. 10^5 viable cell events for each population were collected directly into Qiagen RLT buffer containing β-mercaptoethanol. Total RNA was isolated with Qiagen RNeasy kits. The samples were analyzed with the Human Hippo Signaling RT2 Profiler PCR array (Qiagen #PAHS-172ZA) or Human Cancer Inflammation and Immunity Crosstalk array (Qiagen #PAHS-181ZA) using the recommended cDNA synthesis and PCR reagents. Data are presented as biologic quadruplicate or triplicate samples of expression relative to the total viable population sample. Visualization and hierarchical clustering was prepared with Morpheus software (Broad Institute). Additional Methods and details for ATCQ and Supplemental Figures are included in the Supplemental Data file.

Acknowledgements:

This work in the Buttitta Lab was supported by funding from the American Cancer Society (RSG-15-161-01-DDC), and the Dept. of Defense (W81XWH1510413). Work in the Yang Lab is supported by the National Science Foundation (Early CAREER Grant #1553031 and MCB#1817909) and the National Institutes of Health (MIRA GM119688). Work in the Pearson lab is supported by the National Institutes of Health (K08-DE026500 and U01-CA243075). Work in the Yoon Lab was in part supported by the National Institute of Health (R01-CA203810). Work in the Cackowski Lab is supported by a Prostate Cancer Foundation Challenge award, University of Michigan Prostate Cancer S.P.O.R.E. NIH/NCI 5 P50CA18678605, Career Enhancement sub-award to F.C.C. F048931, Prostate Cancer Foundation Young Investigator Award 18YOUN04, Department of Defense Prostate Cancer Research Program Physician Research Award W81XWH2010394, and start-up funds from The University of Michigan and Karmanos Cancer Institute. Work in the Taichman lab was supported by National Institutes of Health (3P01CA093900-06) and the Prostate Cancer Foundation (16CHAL05). We thank Dr. T. Oki for providing the G0-Venus vector and Venus/Cherry labeled 3T3 cell line. We thank Chris A. Edwards, manager of Microscopy & Image-analysis Laboratory (MIL) from University of Michigan for help with live-cell imaging. We thank Abbey

Roelofs (U. Michigan LSA-IT) for help with improving the cell tracking and analysis program. We thank Melissa Coon and the University of Michigan DNA Sequencing Core Facility for preparation of libraries and sequencing for the Du-145 experiment, and Rebecca Tagett of the University of Michigan Bioinformatics Core Facility for quality control, alignment, and differential expression analysis of the Du-145 RNA sequencing data. The Du-145 RNA sequencing data is available in GEO under accession: GSE186061. We thank “The Tribe” (ATCQ) for musical inspiration.

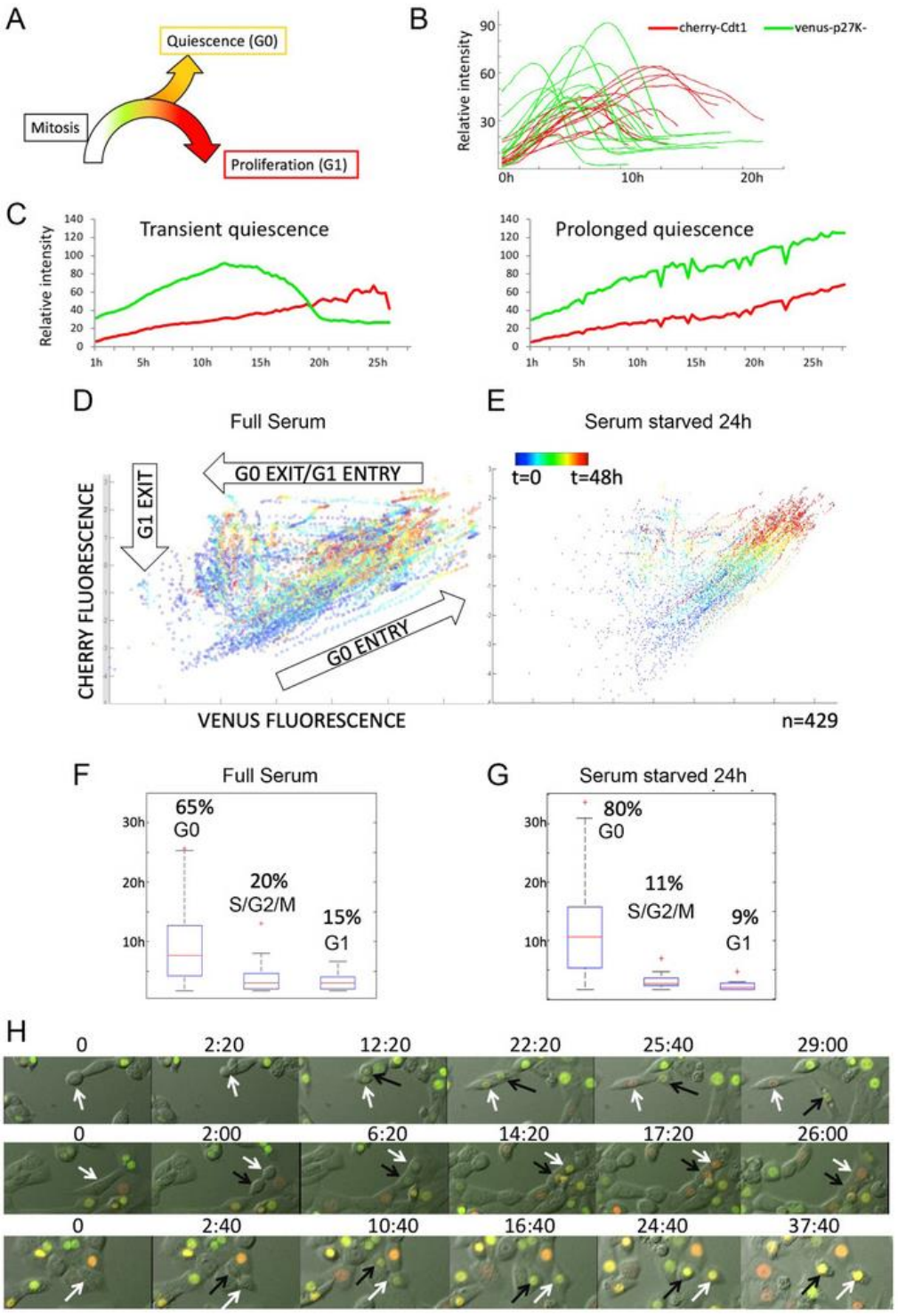

Figure 2-1 The G0 sensor, mVenus-p27K-, can be used to monitor spontaneous quiescence and asynchronous proliferation-quiescence decisions in untransformed cells.

(A) The proliferation-quiescence decision as monitored with the G0 sensor, mVenus-p27K- (G0-Venus) and G1 sensor hCdt1$_{(30\text{-}120)}$ -Cherry (G1-Cherry). For NIH/3T3 cells, on average, 2-4 hours after cytokinesis, G0-Venus expression begins increasing, followed approximately 3-4 hours later by G1-Cherry expression. For cells entering G1, the Venus/Cherry double-positive phase lasts 5-10h. For quantification purposes we define a Venus/Cherry double-positive phase prolonged beyond 14 hours as spontaneous G0. (**B**) Example traces of G0-Venus/G1-Cherry reporter dynamics in cells entering the cell cycle. 0h is relative time, aligned to the start of G0-Venus reporter increase. (**C**) Example traces of G0-Venus/G1-Cherry reporter dynamics in cells under full serum conditions. Left shows a transient spontaneous G0 state of less than 15 hours, while right shows an example of prolonged, spontaneous quiescence lasting over 24 hours. (**D**) Cell trajectories followed over time from several movies show reporter behaviors consistent with G0 entry, G0 exit and G1 entry, and exit from G1 and early S-phase under full serum conditions. (**E**) Under serum starvation for 24h, multiple trajectories collapse into G0 entry. (**F**) Under full serum conditions, time spent in G0 is highly variable. (**G**) Under serum starvation for 24h G0 is prolonged. (**H**) Frames from movies showing examples of mitoses followed by an asynchronous G0/G1 decision (top), synchronous G1 decision (middle) and synchronous G0 decision (bottom).

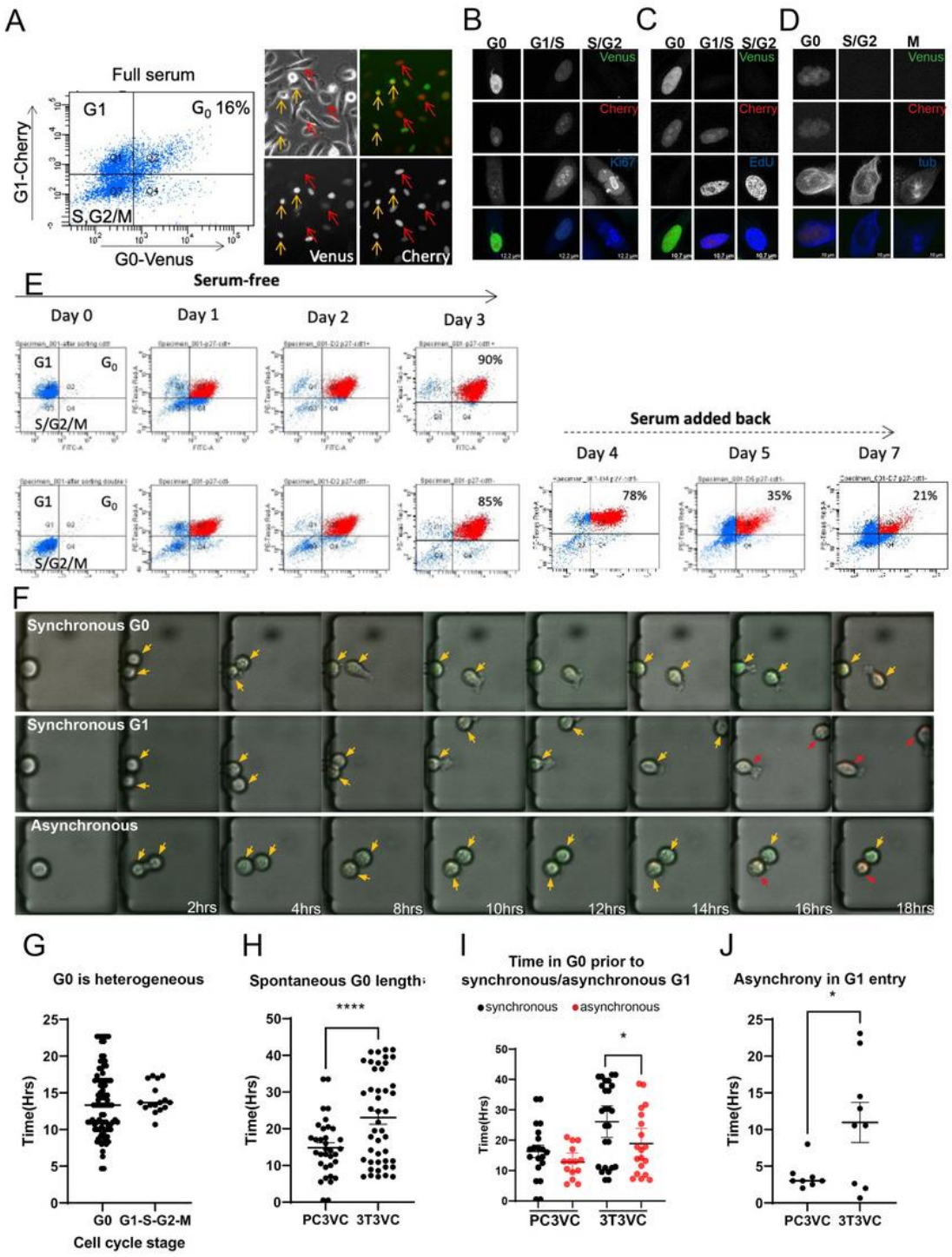

Figure 2-2 Spontaneous quiescence and asynchronous proliferation-quiescence decisions occur in PC3 cells.

(**A**) G0-Venus and G1-Cherry reporters were transduced into PC3 cells and a clone exhibiting normal growth rate and strong, stable reporter expression was isolated. PC3

Venus/Cherry cells exhibit a fraction of cells double positive for G0-Venus/G1-Cherry under full serum conditions. Imaging reveals Venus/Cherry double positive cells (orange arrows), Cherry only positive cells (red arrows) and double negative cells (not indicated). (**B**) PC3 cells double positive for G0-Venus/G1-Cherry are Ki-67 negative, (**C**) EdU negative, (**D**) and cells in mitosis are negative for both reporters. (**E**) G0-Venus and G1-Cherry reporters in PC3 cells respond to serum starvation and re-stimulation as expected. G1 (Cherry-only) cells were isolated by FACS and cultured in serum free media for 3 days. By 3 days, 90% of cells become Venus/Cherry double positive demonstrating that nearly all cells retain the dual reporters. In parallel, double negative late S, G2/M cells were isolated by FACS and cultured in serum free media. By 3 days, 85% of cells become Venus/Cherry double positive, demonstrating that actively proliferating cells retain the dual reporters. Serum was then added back to G0 arrested cells, and within 2-3 days (days 5 and 7 of the entire timecourse) the distribution of G0, G1, S,G2/M cells returns to normal. (**F**) PC3 Venus/Cherry cells were cultured in a microfluidics chamber termed the “cell hotel” for single cell tracking and imaging of daughters. Examples of asynchronous G0/G1 decisions, as well as synchronous spontaneous G0 and synchronous G1 entry are observed in PC3 cells under full serum conditions. Orange arrows indicate cells entering G0 (G0-Venus, G1-Cherry double positive), red arrows indicate cells entering G1 (G1-Cherry only). (**G**) To measure heterogeneity of G0 in PC3 cells under full serum conditions, we quantified time spent in a double-positive Venus/Cherry state for 90 cells. We found G0 length to be highly heterogeneous, compared to the rest of the cell cycle timing for G1, S and G2/M. (**H**) We measured the length of the double Venus/Cherry positive G0 state for ~50 PC3 and 3T3 cells under full serum conditions in the cell hotel. For PC3, we found that most cells transitioned to G1 by 14 hours after the initial rise in G0-Venus fluorescence, with a small number of cells (27.5%) exhibiting longer G0-Venus fluorescence consistent with spontaneous quiescence. By contrast, for 3T3 cells we observed 64.4% of cells to exhibit spontaneous quiescence, a double-positive state lasting more than 14h (dotted line). ($P=0.0005$ by Mann-Whitney test.) (**I**) We also compared the frequency of asynchronous proliferation-quiescence decisions in PC3 vs. 3T3 cells ($P<0.0001$ by Mann-Whitney test) and (**G**) the length of the time difference until G1 entry between

asynchronous daughters in PC3 and 3T3 cells. Lines show the mean and error bars are ± SEM from at least three independent experiments.

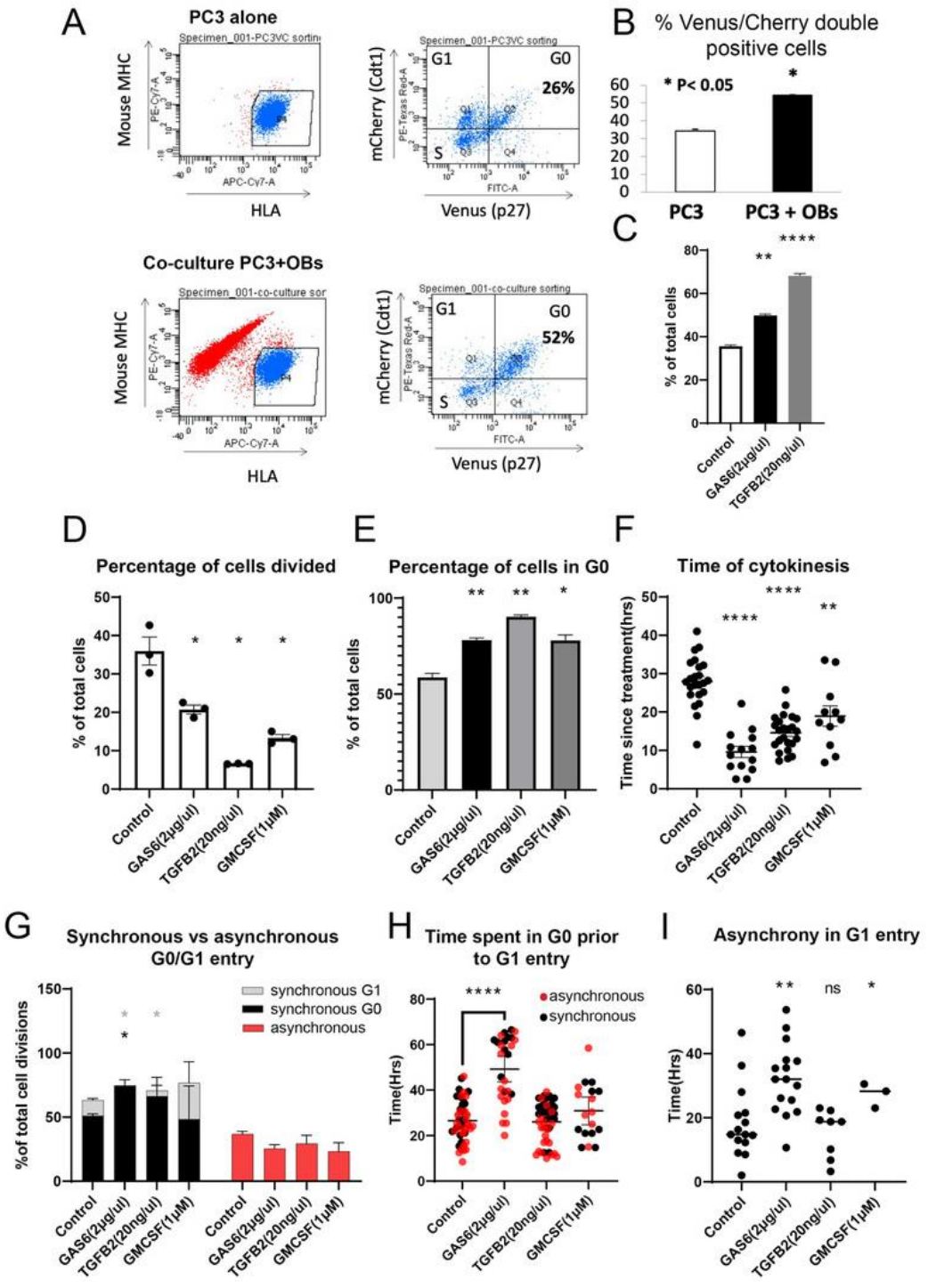

Figure 2-3 Tumor dormancy signals influence quiescence and asynchronous proliferation-quiescence decisions.

(**A**) PC3 Venus/Cherry cells were either cultured alone or co-cultured with mouse osteoblasts, which were excluded from cell cycle analysis by negative human HLA

staining and positive anti-mouse MHC staining. (**B**) PC3 co-culture with osteoblasts induced a significant increase in G0 cells under full serum conditions. (**C**) PC3 cells treated with Gas6 or TGFß2also exhibit a significant increase in G0 cells, measured by flow cytomtery. (**D**) G0-Venus reporter dynamics were tracked using the cell hotel for cells exposed to Gas 6 (n=583), TGFß2 (n=1576) or GM-CSF (n=330) or vehicle only controls (n=336). Experiments were performed at least in triplicate. Gas6, TGFß2 and GM-CSF significantly decreased the percentage of cells that divide. (**E**) We quantified the percent of cells for each treatment that exhibited G0, defined as a Venus/Cherry double positive state for >14h. (**F**) We tracked the timing of asynchronous cell divisions with Gas6, TGFß2 and GM-CSF treatment, and most divisions occurred significantly earlier followed by entry into quiescence. (**G**) Synchronous G0 entry, synchronous G1 entry and asynchronous G0/G1 entry was tracked for cell divisions in Gas 6 (n=121), TGFß2 (n=104), GM-CSF (n=44) or vehicle only controls (n=120). For Gas 6 and TGFß2 we observe a significant increase in synchronous G0 entry, while treatment with GM-CSF increased synchronous entry into G1. (**H**) To measure transient G0, we identified cells that spent more than 4h in G0 prior to G1 entry and measured the length of their G0. Treatment with Gas6 significantly prolonged G0, even in cells that enter transient G0. Cells that enter G1 synchronously are in black, while asynchronous cells are in red. (**I**) For pairs of daughters that enter G1 asynchronously, we measured the difference in time for G1 entry. Gas6 significantly increased the time difference for asynchronous G1 entry. Lines or bars show the mean and error bars are ± SEM. All experiments were performed at least in triplicate and compared to controls with an unpaired t-test, * indicates $P<0.05$, ** indicates $P<0.01$, **** indicates $P<0.001$.

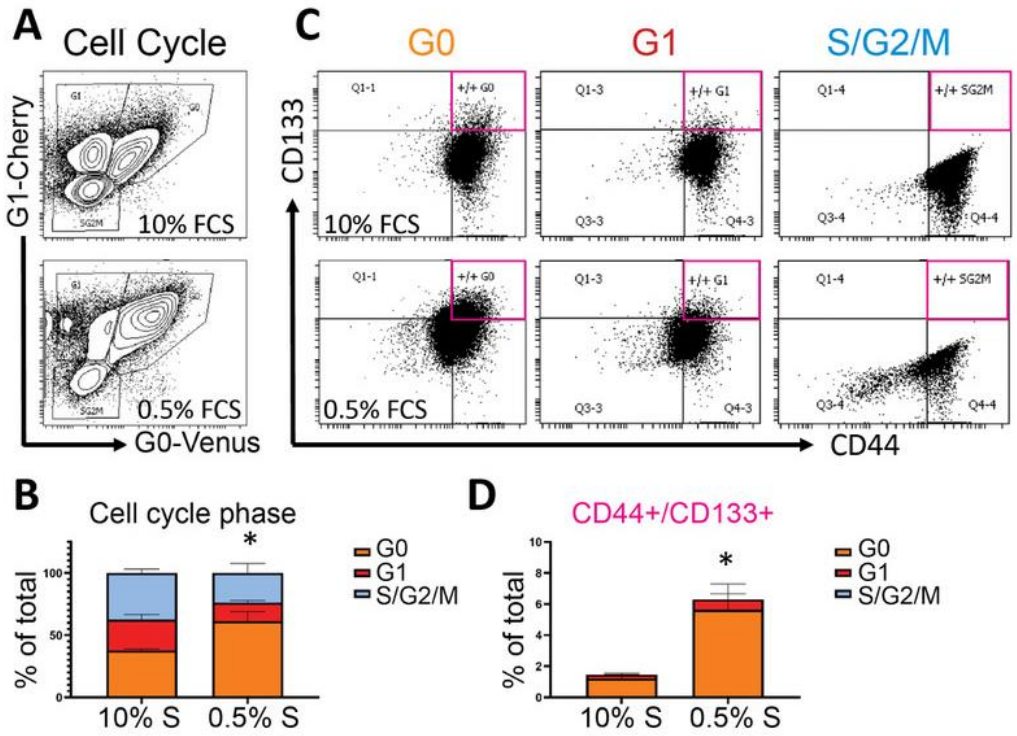

Figure 2-4 Quiescent prostate cancer cells are enriched for a subpopulation of cells that express potential cancer stem cell markers,

(**A**) Flow cytometry plots of cell cycle phase of PC3 Venus-Cherry cells grown with 10% serum (FCS) or 0.5% serum (FCS) for three days (**B**) Quantification of the cell cycle phase data (**C**) Flow cytometry for CD133 and CD44 to assess cancer stem cell marker expression in each of the cell cycle populations. (**D**) CD133/44 double positive cells from each cell cycle phase group, quantified as a percentage of the total events in panel A. Quantified data in panels C and D represent mean ± SEM of three independent experiments. * represents $p < 0.05$ for the G0 population by Student's t-test. Flow cytometry plots in panels A and B show a representative experiment.

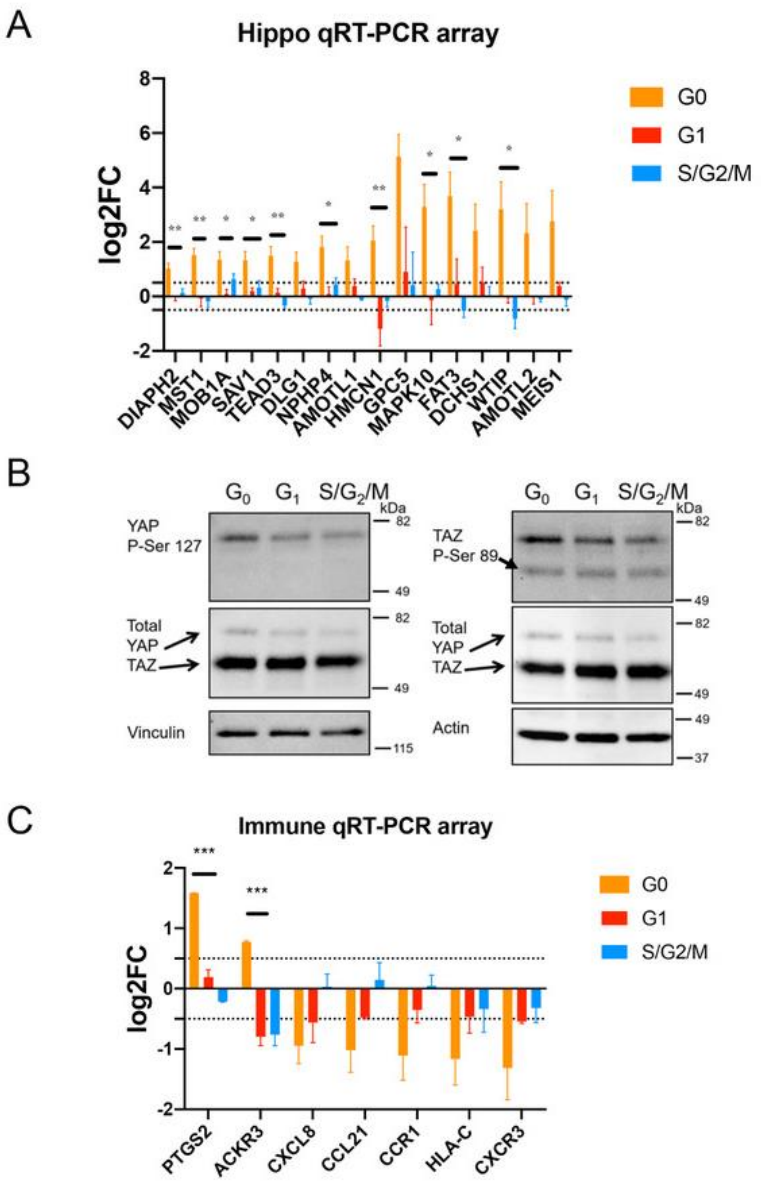

Figure 2-5 Quiescent prostate cancer cells exhibit altered expression of Hippo pathway components and immune-related genes.

(**A, C**) PC3 Venus/Cherry cells were sorted into G0, G1 and S,G2/M fractions for gene expression analysis using Qiagen qRT-PCR arrays. Biological quadruplicates were run on the Hippo Signaling Pathway array and triplicates were run on the Qiagen Cancer Immunology qRT-PCR array. All changes in expression are normalized to asynchronous cells. Selected genes are shown here, the full dataset is shown in the Supp. Fig. 4B. (**A**) G0 cells show a consistent increase in transcripts for Hippo signaling pathway components including positive and negative regulators as well as feedback

targets. (**B**) PC3 Venus/Cherry cells were sorted into G0, G1 and S,G2/M fractions for protein isolation and western blotting. G0 cells exhibit an increase in phosphorylated YAP consistent with active Hippo signaling, but little effect on TAZ (note TAZ protein encoded by WWTR1 gene). (**C**) G0 cells exhibit an altered immune expression profile while G1, S and G2/M cells exhibit few significant changes. CXCL8, CCL21, CCR1, HLA-C and CXCR3 were all significantly different from asynchronous controls by a 2-fold cutoff and t-tests with $P<0.02$. For all gene expression data in A and C, G0 cells were also compared to G1 or S/G2/M cells by unpaired t-tests. * indicates $P<0.05$, ** indicates $P<0.01$, *** indicates $P<0.005$.

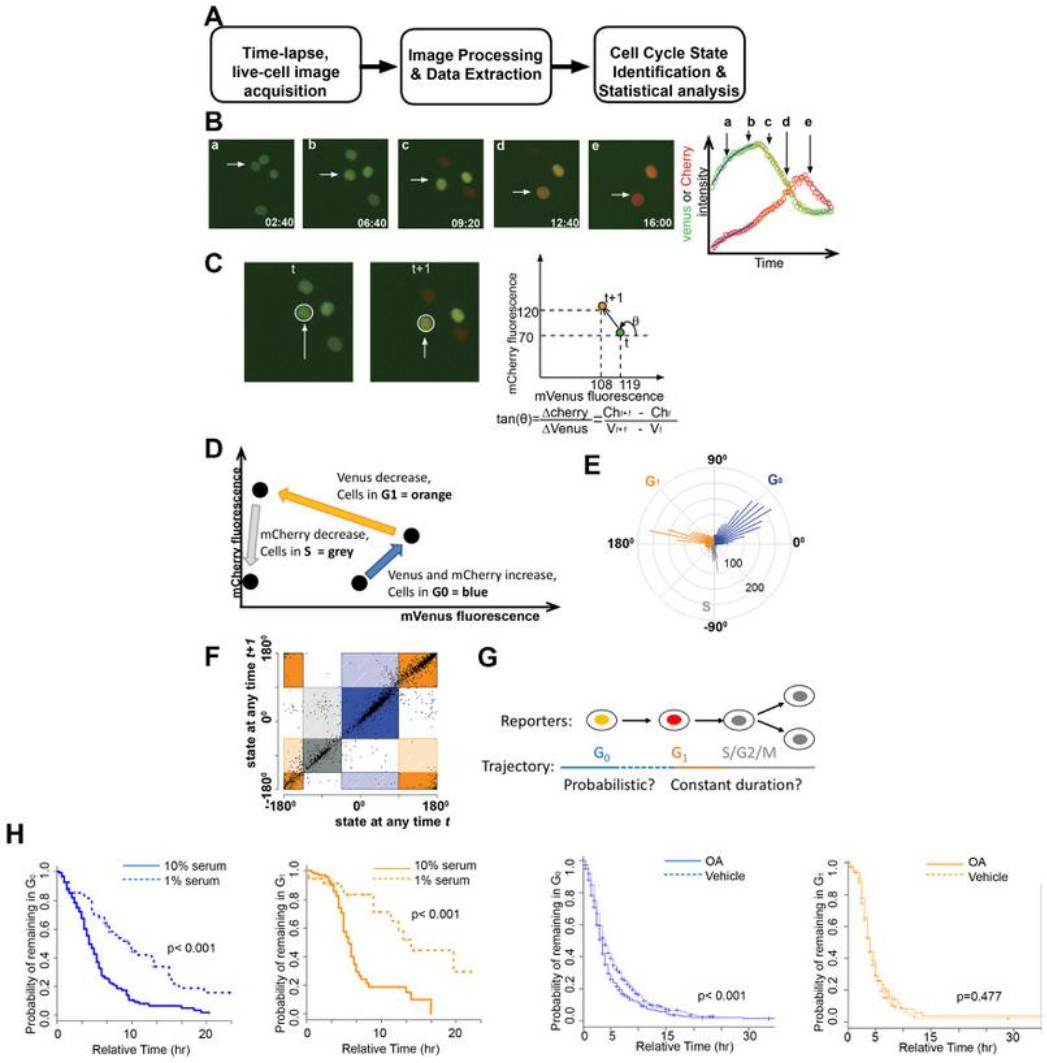

Supplemental Figure 2-1 Automated Tracking of Cellular Quiescence (ATCQ) can be used to quantify and monitor G0 entry and exit in adherent cell culture.

(**A**) A workflow of the ATCQ system. (**B**) (a-e) partitioning images from the single-cell tracking process. White arrow points out the same cell traced at different time points. Representative single-cell trajectory of two fluorescent probes in time-lapse, live-cell imaging. Each circle depicts one fluorescent intensity reading at a given time in either mVenus or mCherry channel. (**C**) Representative images show the same cells traced at two adjacent time frames. The calculation is generated to convert fluorescent intensity readouts to radial readings over time. (**D**) Three distinct cell cycle behaviors in order were observed from G0/G1 cell cycle reporter fluorescent intensity changes in asynchronously growing cells. When cells in state G_0, both mVenus reporter and

mCherry accumulate together, colored in blue. Then cells transit into G_1 when mVenus fluorescent signal decreases while mCherry remains high, colored in orange. The third state is S phase entry, when mCherry signal decreases, colored in grey. (**E**) The radial histogram shows the conversion of the two fluorescent intensity readouts from each time frame to the radian readings over two adjacent time frames. The length of the spikes depicts the frequency of individual cells exhibiting a certain cell cycle behavior at a particular radian. The transition from one state to another is marked by the local minima of the frequency in radial histogram. (**F**) The dot plot shows all the cell-level, post-smoother radian assignment values for temporally adjacent movie frames. In this plot, all the radian values defining cell state can be compared among all cells in any movie frame *t* and the next frame *t+1*. (**G**) A model to explain the variability observed in the G0 state vs other cell cycle states. (**H**) The Kaplan-Meier curves of each state estimates the time cells remaining in each state under either full serum (10%) or low serum (1%) conditions. The analysis shows that cells tend to spend longer times in both G_0 and G_1 states in response to serum starvation (p value<0.001). To test the sensitivity of ATCQ, 50nM Okadaic Acid (OA) was used to inhibit PP2A function for 30min prior to live, time-lapse imaging. Inhibition of PP2A has previously been shown to mildly reduce G0 entry in response to serum starvation by 10%. The Kaplan-Meier curves confirm that cells treated with OA are less likely to enter spontaneous G_0 than cells with vehicle treatment. However, consistent with previous work on PP2A, cells with OA treatment exhibit no significant difference in time spent in G_1. Survival curves were compared using the log-rank test.

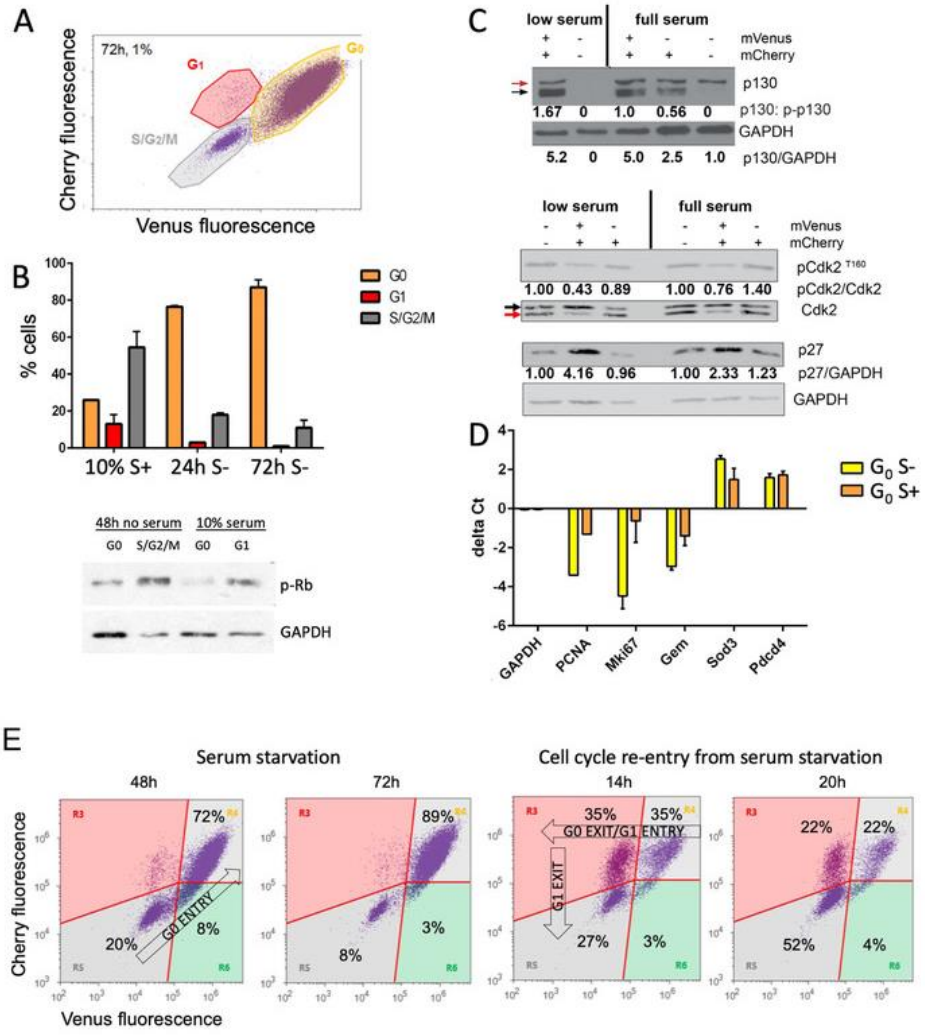

Supplemental Figure 2-2 Cells expressing mVenus-p27K exhibit molecular markers of quiescence.

(**A**) A representative flow cytometry dot plot of NIH3T3 cells expressing mVenus-p27K$^-$ (G0-Venus) and mCherry-hCdt1(30/120) (G1-Cherry), cultured under reduced 1% serum for 72h to induce G0 entry. (**B**) Quantifications of cells in G0, G1 or S,G2/M in full 10% serum, after 24h of reduced (1%) serum (S-) or 72h of reduced (1%) serum. Experiments were performed in triplicate, and averages are plotted with error bars indicating SEM. The sub-population of double positive G0 cells increases as cells are treated with serum starvation. (**C**) Western blots confirm molecular markers of G0 in Venus/Cherry double positive cells under full and low (1%) or no serum conditions. Quantifications confirm an increase in the ratio of un/hypo-phosphorylated to hyper-phosphorylated form p130 in double positive cells. The un/hypo-phosphorylated form

and hyper-phosphorylated form are indicated by the black and red arrows, respectively. The active form of Cdk2, phospho-Cdk2^{T160} , is reduced in Venus/Cherry double positive cells compared to Cherry single positive cells. Endogenous p27 is also highly expressed in double positive cells. Phosphorylation of Rb is also low in G0 Venus/Cherry double-positive cells under serum starvation or full serum compared to single Cherry positive cells (G1) or double negative cells in S/G2/M. (**D**) qRT-PCR on sorted cell populations under normal serum (S+) or 1% serum (S-) conditions shows that active cell cycle regulators PCNA, Ki67 and Geminin are downregulated in G0 Venus/Cherry double positive cells even in spontaneous quiescence (S+), when compared to asynchronously proliferating cells. Conversely, two genes previously associated with G0, Sod3 and Pdcd4 are enriched in spontaneous G0 and low serum G0. Δ CT = log2 of the fold difference from asynchronous unsorted cell samples normalized to Gapdh transcript levels. (**F**) G0-Venus reporter dynamics were tested in a timecourse of serum starvation followed by re-stimulation. By 48h of serum starvation most cells are entering G0, with nearly 90% exhibiting a Venus/Cherry double positive state by 72h. Upon serum addition, cells begin exhibiting significant cell cycle re-entry and G1 entry (Cherry single positive) by 14h. By 20h after serum addition, the majority of cells exhibit S/G2 or M states (double negative).

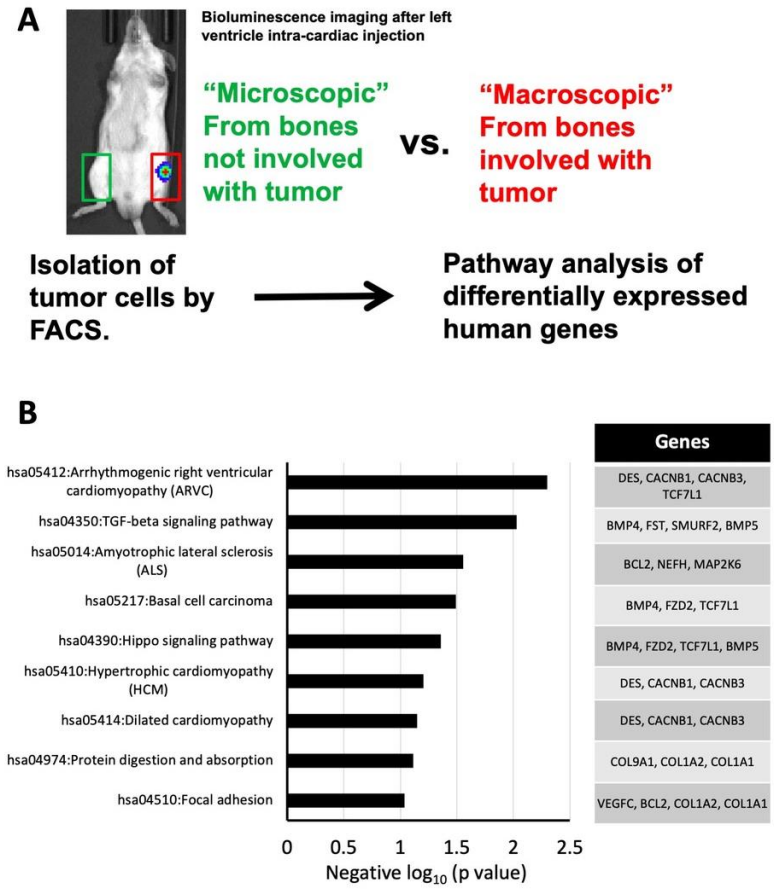

Supplemental Figure 2-3 Identifying differentially expressed genes in growing vs. dormant tumors in the Du-145 mouse xenograft model.

(**A**) Experimental schema. (**B**) Results of pathway analysis of differentially expressed genes in tumor cells from microscopic vs. macroscopic tumors using NIH DAVID software and the KEGG pathway collection. Left; negative log base 10 of the p-value for enrichment in each pathway. Right; Genes responsible for the enrichment in each pathway.

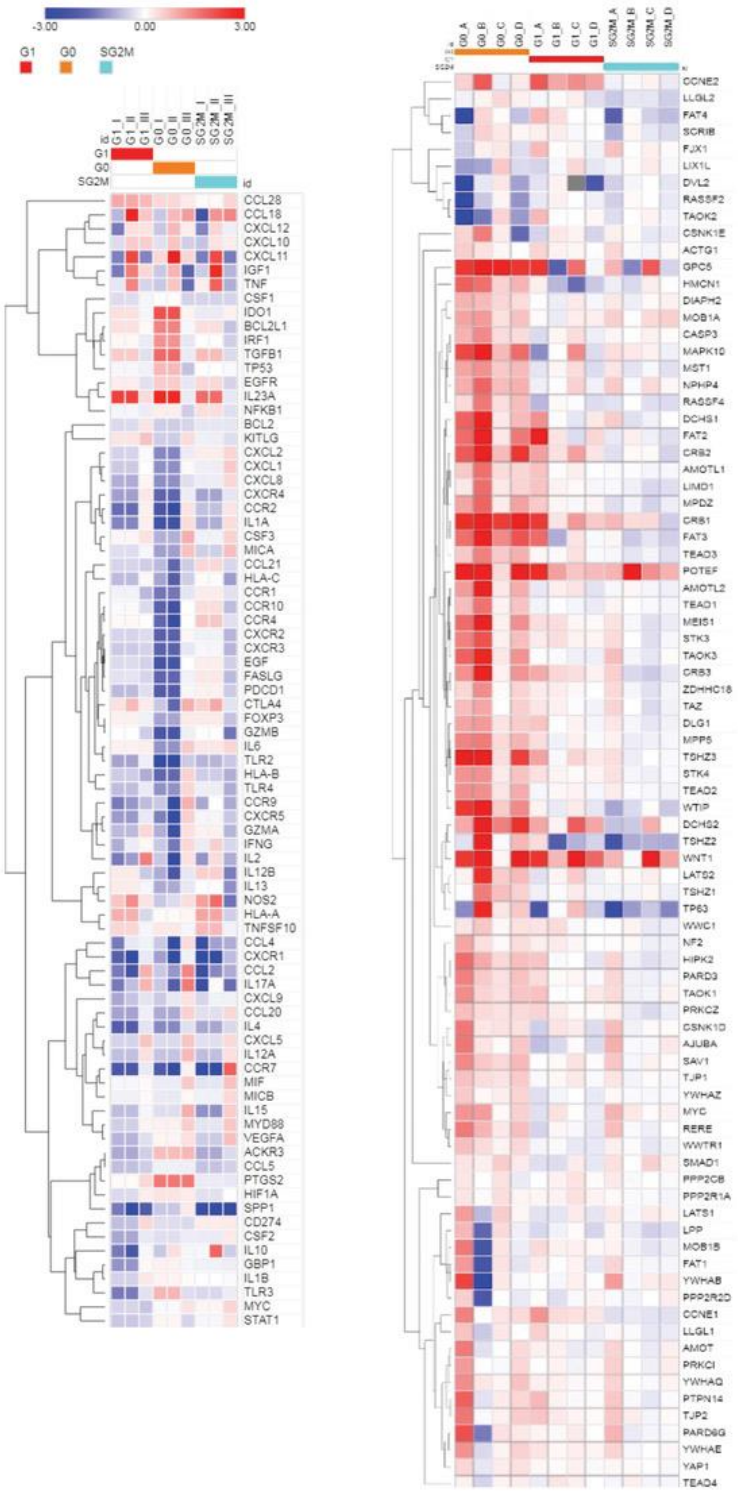
-3.00
0.00
3.00
G1
G0
SG2M
Id
CCL28
CCL18
CXCL12
CXCL10
CXCL11
IGF1
TNF
CSF1
IDO1
BCL2L1
IRF1
TGFB1
TP53
EGFR
IL23A
NFKB1
BCL2
KITLG
CXCL2
CXCL1
CXCL8
CXCR4
CCR2
IL1A
CSF3
MICA
CCL21
HLA-C
CCR1
CCR10
CCR4
CXCR2
CXCR3
EGF
FASLG
PDCD1
CTLA4
FOXP3
GZMB
IL6
TLR2
HLA-B
TLR4
CCR9
CXCR5
GZMA
IFNG
IL2
IL12B
IL13
NOS2
HLA-A
TNFSF10
CCL4
CXCR1
CCL2
IL17A
CXCL9
CCL20
IL4
CXCL5
IL12A
CCR7
MIF
MICB
IL15
MYD88
VEGFA
ACKR3
CCL5
PTGS2
HIF1A
SPP1
CD274
CSF2
IL10
GBP1
IL1B
TLR3
MYC
STAT1
CCNE2
LLGL2
FAT4
SCRIB
FJX1
LIX1L
DVL2
RASSF2
TAOK2
CSNK1E
ACTG1
GPC5
HMCN1
DIAPH2
MOB1A
CASP3
MAPK10
MST1
NPHP4
RASSF4
DCHS1
FAT2
CRB2
AMOTL1
LIMD1
MPDZ
CRB1
FAT3
TEAD3
POTEF
AMOTL2
TEAD1
MEIS1
STK3
TAOK3
CRB3
ZDHHC18
TAZ
DLG1
MPP5
TSHZ3
STK4
TEAD2
WTIP
DCHS2
TSHZ2
WNT1
LATS2
TSHZ1
TP63
WWC1
NF2
HIPK2
PARD3
TAOK1
PRKCZ
CSNK1D
AJUBA
SAV1
TJP1
YWHAZ
MYC
RERE
WWTR1
SMAD1
PPP2CB
PPP2R1A
LATS1
LPP
MOB1B
FAT1
YWHAB
PPP2R2D
CCNE1
LLGL1
AMOT
PRKCI
YWHAQ
PTPN14
TJP2
PARD6G
YWHAE
YAP1
TEAD4

Supplemental Figure 2-4 The complete dataset for qRT-PCR arrays
PC3 Venus/Cherry cells were sorted into G0, G1 and S,G2/M fractions for gene expression analysis using Qiagen qRT-PCR arrays. Biological triplicates were run on the Qiagen Cancer Immunology qRT-PCR array (**A**) and quadruplicates were run on the Hippo Signaling Pathway array (**B**). Changes in expression were normalized to asynchronous cells and represented as a heatmap of the log_2 fold change.

2.6 Bibliography

Alves, C.P., Dey-Guha, I., Kabraji, S., Yeh, A.C., Talele, N.P., Sole, X., Chowdhury, J., Mino-Kenudson, M., Loda, M., Sgroi, D., Borresen-Dale, A.L., Russnes, H.G., Ross, K.N., and Ramaswamy, S. (2018). AKT1(low) Quiescent Cancer Cells Promote Solid Tumor Growth. *Mol Cancer Ther* 17**,** 254-263.

Arora, M., Moser, J., Phadke, H., Basha, A.A., and Spencer, S.L. (2017). Endogenous Replication Stress in Mother Cells Leads to Quiescence of Daughter Cells. *Cell Rep* 19**,** 1351-1364.

Bragado, P., Estrada, Y., Parikh, F., Krause, S., Capobianco, C., Farina, H.G., Schewe, D.M., and Aguirre-Ghiso, J.A. (2013). TGF-beta2 dictates disseminated tumour cell fate in target organs through TGF-beta-RIII and p38alpha/beta signalling. *Nat Cell Biol* 15**,** 1351-1361.

Cackowski, F.C., Eber, M.R., Rhee, J., Decker, A.M., Yumoto, K., Berry, J.E., Lee, E., Shiozawa, Y., Jung, Y., Aguirre-Ghiso, J.A., and Taichman, R.S. (2017). Mer Tyrosine Kinase Regulates Disseminated Prostate Cancer Cellular Dormancy. *J Cell Biochem* 118**,** 891-902.

Carroll, A.G., Voeller, H.J., Sugars, L., and Gelmann, E.P. (1993). p53 oncogene mutations in three human prostate cancer cell lines. *Prostate* 23**,** 123-134.

Chen, F., Han, Y., and Kang, Y. (2021). Bone marrow niches in the regulation of bone metastasis. *Br J Cancer* 124**,** 1912-1920.

Chen, J., Xia, D., Luo, J.D., and Wang, P. (2009). Exogenous p27KIP1 expression induces anti-tumour effects and inhibits the EGFR/PI3K/Akt signalling pathway in PC3 cells. *Asian J Androl* 11**,** 669-677.

Cheng, Y.H., Chen, Y.C., Brien, R., and Yoon, E. (2016). Scaling and automation of a high-throughput single-cell-derived tumor sphere assay chip. *Lab Chip* 16**,** 3708-3717.

Chittajallu, D.R., Florian, S., Kohler, R.H., Iwamoto, Y., Orth, J.D., Weissleder, R., Danuser, G., and Mitchison, T.J. (2015). In vivo cell-cycle profiling in xenograft tumors by quantitative intravital microscopy. *Nat Methods* 12**,** 577-585.

Coller, H.A., Sang, L., and Roberts, J.M. (2006). A new description of cellular quiescence. *PLoS Biol* 4**,** e83.

Cosemans, J.M., Van Kruchten, R., Olieslagers, S., Schurgers, L.J., Verheyen, F.K., Munnix, I.C., Waltenberger, J., Angelillo-Scherrer, A., Hoylaerts, M.F., Carmeliet, P., and Heemskerk, J.W. (2010). Potentiating role of Gas6 and Tyro3, Axl and Mer (TAM) receptors in human and murine platelet activation and thrombus stabilization. *J Thromb Haemost* 8**,** 1797-1808.

Dai, J., Lu, Y., Yu, C., Keller, J.M., Mizokami, A., Zhang, J., and Keller, E.T. (2010). Reversal of chemotherapy-induced leukopenia using granulocyte macrophage colony-stimulating factor promotes bone metastasis that can be blocked with osteoclast inhibitors. *Cancer Res* 70**,** 5014-5023.

Davis, J.E., Jr., Kirk, J., Ji, Y., and Tang, D.G. (2019). Tumor Dormancy and Slow-Cycling Cancer Cells. *Adv Exp Med Biol* 1164**,** 199-206.

De Angelis, M.L., Francescangeli, F., La Torre, F., and Zeuner, A. (2019). Stem Cell Plasticity and Dormancy in the Development of Cancer Therapy Resistance. *Front Oncol* 9**,** 626.

Dey-Guha, I., Alves, C.P., Yeh, A.C., Salony, Sole, X., Darp, R., and Ramaswamy, S. (2015). A mechanism for asymmetric cell division resulting in proliferative asynchronicity. *Mol Cancer Res* 13**,** 223-230.

Dey-Guha, I., Wolfer, A., Yeh, A.C., J, G.A., Darp, R., Leon, E., Wulfkuhle, J., Petricoin, E.F., 3rd, Wittner, B.S., and Ramaswamy, S. (2011). Asymmetric cancer cell division regulated by AKT. *Proc Natl Acad Sci U S A* 108**,** 12845-12850.

Dubrovska, A., Kim, S., Salamone, R.J., Walker, J.R., Maira, S.M., Garcia-Echeverria, C., Schultz, P.G., and Reddy, V.A. (2009). The role of PTEN/Akt/PI3K signaling in the maintenance and viability of prostate cancer stem-like cell populations. *Proc Natl Acad Sci U S A* 106**,** 268-273.

Hen, O., and Barkan, D. (2020). Dormant disseminated tumor cells and cancer stem/progenitor-like cells: Similarities and opportunities. *Semin Cancer Biol* 60**,** 157-165.

Huang, H., Cheville, J.C., Pan, Y., Roche, P.C., Schmidt, L.J., and Tindall, D.J. (2001). PTEN induces chemosensitivity in PTEN-mutated prostate cancer cells by suppression of Bcl-2 expression. *J Biol Chem* 276**,** 38830-38836.

Jeffrey, P.D., Russo, A.A., Polyak, K., Gibbs, E., Hurwitz, J., Massague, J., and Pavletich, N.P. (1995). Mechanism of CDK activation revealed by the structure of a cyclinA-CDK2 complex. *Nature* 376**,** 313-320.

Jung, Y., Decker, A.M., Wang, J., Lee, E., Kana, L.A., Yumoto, K., Cackowski, F.C., Rhee, J., Carmeliet, P., Buttitta, L., Morgan, T.M., and Taichman, R.S. (2016). Endogenous GAS6 and Mer receptor signaling regulate prostate cancer stem cells in bone marrow. *Oncotarget*.

Jung, Y., Shiozawa, Y., Wang, J., Mcgregor, N., Dai, J., Park, S.I., Berry, J.E., Havens, A.M., Joseph, J., Kim, J.K., Patel, L., Carmeliet, P., Daignault, S., Keller, E.T., Mccauley, L.K., Pienta, K.J., and Taichman, R.S. (2012). Prevalence of prostate cancer metastases after intravenous inoculation provides clues into the molecular basis of dormancy in the bone marrow microenvironment. *Neoplasia* 14**,** 429-439.

Kamura, T., Hara, T., Matsumoto, M., Ishida, N., Okumura, F., Hatakeyama, S., Yoshida, M., Nakayama, K., and Nakayama, K.I. (2004). Cytoplasmic ubiquitin ligase KPC regulates proteolysis of p27(Kip1) at G1 phase. *Nat Cell Biol* 6**,** 1229-1235.

Kasikara, C., Kumar, S., Kimani, S., Tsou, W.I., Geng, K., Davra, V., Sriram, G., Devoe, C., Nguyen, K.N., Antes, A., Krantz, A., Rymarczyk, G., Wilczynski, A., Empig, C., Freimark, B., Gray, M., Schlunegger, K., Hutchins, J., Kotenko, S.V., and Birge, R.B. (2017). Phosphatidylserine Sensing by TAM Receptors Regulates AKT-Dependent Chemoresistance and PD-L1 Expression. *Mol Cancer Res* 15**,** 753-764.

Lam, H.M., Vessella, R.L., and Morrissey, C. (2014). The role of the microenvironment-dormant prostate disseminated tumor cells in the bone marrow. *Drug Discov Today Technol* 11**,** 41-47.

Lang, S.H., Miller, W.R., Duncan, W., and Habib, F.K. (1994). Production and response of human prostate cancer cell lines to granulocyte macrophage-colony stimulating factor. *Int J Cancer* 59**,** 235-241.

Lawson, D.A., Bhakta, N.R., Kessenbrock, K., Prummel, K.D., Yu, Y., Takai, K., Zhou, A., Eyob, H., Balakrishnan, S., Wang, C.Y., Yaswen, P., Goga, A., and Werb, Z. (2015). Single-cell analysis reveals a stem-cell program in human metastatic breast cancer cells. *Nature* 526**,** 131-135.

Lee, E., Decker, A.M., Cackowski, F.C., Kana, L.A., Yumoto, K., Jung, Y., Wang, J., Buttitta, L., Morgan, T.M., and Taichman, R.S. (2016). Growth Arrest-Specific 6 (GAS6) Promotes Prostate Cancer Survival by G Arrest/S Phase Delay and Inhibition of Apoptotic Pathway During Chemotherapy in Bone Marrow. *J Cell Biochem*.

Matson, J.P., and Cook, J.G. (2017). Cell cycle proliferation decisions: the impact of single cell analyses. *FEBS J* 284**,** 362-375.

Miller, I., Min, M., Yang, C., Tian, C., Gookin, S., Carter, D., and Spencer, S.L. (2018). Ki67 is a Graded Rather than a Binary Marker of Proliferation versus Quiescence. *Cell Rep* 24**,** 1105-1112 e1105.

Min, M., Rong, Y., Tian, C., and Spencer, S.L. (2020). Temporal integration of mitogen history in mother cells controls proliferation of daughter cells. *Science* 368**,** 1261-1265.

Min, M., and Spencer, S.L. (2019). Spontaneously slow-cycling subpopulations of human cells originate from activation of stress-response pathways. *PLoS Biol* 17**,** e3000178.

Moroishi, T., Hayashi, T., Pan, W.W., Fujita, Y., Holt, M.V., Qin, J., Carson, D.A., and Guan, K.L. (2016). The Hippo Pathway Kinases LATS1/2 Suppress Cancer Immunity. *Cell* 167**,** 1525-1539 e1517.

Nik Nabil, W.N., Xi, Z., Song, Z., Jin, L., Zhang, X.D., Zhou, H., De Souza, P., Dong, Q., and Xu, H. (2021). Towards a Framework for Better Understanding of Quiescent Cancer Cells. *Cells* 10.

Oki, T., Nishimura, K., Kitaura, J., Togami, K., Maehara, A., Izawa, K., Sakaue-Sawano, A., Niida, A., Miyano, S., Aburatani, H., Kiyonari, H., Miyawaki, A., and Kitamura, T. (2014). A novel cell-cycle-indicator, mVenus-p27K-, identifies quiescent cells and visualizes G0-G1 transition. *Sci Rep* 4**,** 4012.

Overton, K.W., Spencer, S.L., Noderer, W.L., Meyer, T., and Wang, C.L. (2014). Basal p21 controls population heterogeneity in cycling and quiescent cell cycle states. *Proc Natl Acad Sci U S A* 111**,** E4386-4393.

Recasens, A., and Munoz, L. (2019). Targeting Cancer Cell Dormancy. *Trends Pharmacol Sci* 40**,** 128-141.

Ridenour, D.A., Mckinney, M.C., Bailey, C.M., and Kulesa, P.M. (2012). CycleTrak: a novel system for the semi-automated analysis of cell cycle dynamics. *Dev Biol* 365**,** 189-195.

Risson, E., Nobre, A.R., Maguer-Satta, V., and Aguirre-Ghiso, J.A. (2020). The current paradigm and challenges ahead for the dormancy of disseminated tumor cells. *Nat Cancer* 1**,** 672-680.

Ruppender, N., Larson, S., Lakely, B., Kollath, L., Brown, L., Coleman, I., Coleman, R., Nguyen, H., Nelson, P.S., Corey, E., Snyder, L.A., Vessella, R.L., Morrissey, C., and Lam, H.M. (2015). Cellular Adhesion Promotes Prostate Cancer Cells Escape from Dormancy. *PLoS One* 10**,** e0130565.

Sakaue-Sawano, A., Kurokawa, H., Morimura, T., Hanyu, A., Hama, H., Osawa, H., Kashiwagi, S., Fukami, K., Miyata, T., Miyoshi, H., Imamura, T., Ogawa, M., Masai, H., and Miyawaki, A. (2008). Visualizing spatiotemporal dynamics of multicellular cell-cycle progression. *Cell* 132**,** 487-498.

Savarese, D.M., Valinski, H., Quesenberry, P., and Savarese, T. (1998). Expression and function of colony-stimulating factors and their receptors in human prostate carcinoma cell lines. *Prostate* 34**,** 80-91.

Sherr, C.J., and Roberts, J.M. (1999). CDK inhibitors: positive and negative regulators of G1-phase progression. *Genes Dev* 13**,** 1501-1512.

Shiozawa, Y., Berry, J.E., Eber, M.R., Jung, Y., Yumoto, K., Cackowski, F.C., Yoon, H.J., Parsana, P., Mehra, R., Wang, J., Mcgee, S., Lee, E., Nagrath, S., Pienta, K.J., and Taichman, R.S. (2016). The marrow niche controls the cancer stem cell phenotype of disseminated prostate cancer. *Oncotarget*.

Spencer, S.L., Cappell, S.D., Tsai, F.C., Overton, K.W., Wang, C.L., and Meyer, T. (2013). The proliferation-quiescence decision is controlled by a bifurcation in CDK2 activity at mitotic exit. *Cell* 155**,** 369-383.

Stewart-Ornstein, J., and Lahav, G. (2016). Dynamics of CDKN1A in Single Cells Defined by an Endogenous Fluorescent Tagging Toolkit. *Cell Rep* 14**,** 1800-1811.

Taichman, R.S., Patel, L.R., Bedenis, R., Wang, J., Weidner, S., Schumann, T., Yumoto, K., Berry, J.E., Shiozawa, Y., and Pienta, K.J. (2013). GAS6 receptor status is associated with dormancy and bone metastatic tumor formation. *PLoS One* 8**,** e61873.

Takahashi, H., Yumoto, K., Yasuhara, K., Nadres, E.T., Kikuchi, Y., Buttitta, L., Taichman, R.S., and Kuroda, K. (2019). Anticancer polymers designed for killing dormant prostate cancer cells. *Sci Rep* 9**,** 1096.

Talukdar, S., Bhoopathi, P., Emdad, L., Das, S., Sarkar, D., and Fisher, P.B. (2019). Dormancy and cancer stem cells: An enigma for cancer therapeutic targeting. *Adv Cancer Res* 141**,** 43-84.

Tedesco, D., Lukas, J., and Reed, S.I. (2002). The pRb-related protein p130 is regulated by phosphorylation-dependent proteolysis via the protein-ubiquitin ligase SCF(Skp2). *Genes Dev* 16**,** 2946-2957.

Van Duijn, P.W., and Trapman, J. (2006). PI3K/Akt signaling regulates p27(kip1) expression via Skp2 in PC3 and DU145 prostate cancer cells, but is not a major factor in p27(kip1) regulation in LNCaP and PC346 cells. *Prostate* 66**,** 749-760.

Wang, Y., Xu, X., Maglic, D., Dill, M.T., Mojumdar, K., Ng, P.K., Jeong, K.J., Tsang, Y.H., Moreno, D., Bhavana, V.H., Peng, X., Ge, Z., Chen, H., Li, J., Chen, Z., Zhang, H., Han, L., Du, D., Creighton, C.J., Mills, G.B., Cancer Genome Atlas Research, N., Camargo, F., and Liang, H. (2018). Comprehensive Molecular

Characterization of the Hippo Signaling Pathway in Cancer. *Cell Rep* 25**,** 1304-1317 e1305.

White, D.E., Rayment, J.H., and Muller, W.J. (2006). Addressing the role of cell adhesion in tumor cell dormancy. *Cell Cycle* 5**,** 1756-1759.

Yamauchi, T., and Moroishi, T. (2019). Hippo Pathway in Mammalian Adaptive Immune System. *Cells* 8.

Yang, H.W., Chung, M., Kudo, T., and Meyer, T. (2017). Competing memories of mitogen and p53 signalling control cell-cycle entry. *Nature* 549**,** 404-408.

Yao, G. (2014). Modelling mammalian cellular quiescence. *Interface Focus* 4**,** 20130074.

Yumoto, K., Eber, M.R., Wang, J., Cackowski, F.C., Decker, A.M., Lee, E., Nobre, A.R., Aguirre-Ghiso, J.A., Jung, Y., and Taichman, R.S. (2016). Axl is required for TGF-beta2-induced dormancy of prostate cancer cells in the bone marrow. *Sci Rep* 6**,** 36520.

Zambon, A.C., Hsu, T., Kim, S.E., Klinck, M., Stowe, J., Henderson, L.M., Singer, D., Patam, L., Lim, C., Mcculloch, A.D., Hu, B., and Hickerson, A.I. (2020). Methods and sensors for functional genomic studies of cell-cycle transitions in single cells. *Physiol Genomics* 52**,** 468-477.

Zhang, Q., Han, X., Chen, J., Xie, X., Xu, J., Zhao, Y., Shen, J., Hu, L., Xu, P., Song, H., Zhang, L., Zhao, B., Wang, Y.J., and Xia, Z. (2018). Yes-associated protein (YAP) and transcriptional coactivator with PDZ-binding motif (TAZ) mediate cell density-dependent proinflammatory responses. *J Biol Chem* 293**,** 18071-18085.

Zheng, Y., and Pan, D. (2019). The Hippo Signaling Pathway in Development and Disease. *Dev Cell* 50**,** 264-282.

Chapter 3 Misregulation of the Nucleoporins 98 and 96 Lead to Defects in Protein Synthesis That Promote Hallmarks of Tumorigenesis.

This chapter was published in:

Ajai J. Pulianmackal, Kiriaki Kanakousaki, Kerry A. Flegel, Olga G. Grushko, Ella Gourley, Emily Rozich and Laura A. Buttitta

Dis Model Mech (2022) 15 (3): dmm049234.

https://doi.org/10.1242/dmm.049234

3.1 Abstract

The Nucleoporin 98KD (Nup98) is a promiscuous translocation partner in hematological malignancies. Most disease models of Nup98 translocations involve ectopic expression of the fusion protein under study, leaving the endogenous *Nup98* loci unperturbed. Overlooked in these approaches is the loss of one copy of normal Nup98 in addition to the loss of Nup96 – a second Nucleoporin encoded within the same mRNA and reading frame as Nup98, in translocations. Nup98 and 96 are also mutated in a number of other cancers, suggesting their disruption is not limited to blood cancers. We found that reducing Nup98-96 function in *Drosophila melanogaster* (where the Nup98-96 shared mRNA and reading frame is conserved) de-regulates the cell cycle. We find evidence of over-proliferation in tissues with reduced Nup98-96, counteracted by elevated apoptosis and aberrant signaling associated with chronic wounding. Reducing Nup98-96 function leads to defects in protein synthesis that trigger JNK signaling and contributes to hallmarks of tumorigenesis when apoptosis is

inhibited. We suggest partial loss of Nup98-96 function in translocations could de-regulate protein synthesis leading to signaling that cooperates with other mutations to promote tumorigenesis.

3.2 Introduction

Communication between the nucleus and cytoplasm occurs through nuclear pore complexes (NPCs), which are composed of highly conserved proteins termed Nucleoporins (Nups). Mutations in several Nups are associated with cancer, including loss-of-function mutations and translocations (Simon and Rout, 2014). Of the Nups associated with translocations, Nup98 is the most promiscuous (Lam and Aplan, 2001; Simon and Rout, 2014).

Nup98 function has been difficult to examine because the gene locus for Nup98 encodes for two essential Nucleoporins, Nup98 and Nup96, which derive from an autocatalytic cleavage of a larger Nup98-96 polypeptide with Nup98 located at the amino terminus (Fontoura et al., 1999; Rosenblum and Blobel, 1999). However, a shorter Nup98 only transcript is also produced by the locus via alternative splicing (Fontoura et al., 1999). Nup98 is a peripheral Nup, found both in nuclear pores and in the nucleoplasm (Griffis et al., 2002). It contains FG (Phenylalanine-Glycine) and GLFG repeats in its N-terminal region that allow Nup98 to interact with different nuclear transport receptors (Bachi et al., 2000; Moroianu et al., 1995) during nucleocytoplasmic shuttling, and it has a role in regulating gene transcription (Capelson et al., 2010; Kalverda et al., 2010). In contrast, Nup96 is a core scaffold protein; it is stably localized at NPC and is part of the core Nup107-160 complex (Walther et al., 2003).

All Nup98 chromosomal translocations that have been observed have a breakpoint in the 3’ end of the Nup98 portion, disrupting the Nup98 coding region located upstream of Nup96 (Xu and Powers, 2009). Thus, Nup98 translocations result in fusions of the N-terminal region of Nup98 with the C-terminal region of a partner

gene, which varies (Simon and Rout, 2014). This almost certainly disrupts the expression of Nup96 as well, which requires Nup98-dependent autocatalytic processing from the Nup98-96 precursor protein to be properly localized and functional (Fontoura et al., 1999; Rosenblum and Blobel, 1999).

While most of the attention on Nup98 translocations in cancer has focused on overexpressing the fusion partners, there is increasing evidence that the disruption of endogenous Nup98 and/or Nup96 may contribute to enhanced proliferation that could cooperate with other oncogenic mutations. Mice carrying a stop codon knocked into the 3' end of the Nup98 portion of the shared Nup98-96 transcript, have been used to examine loss of Nup96 function in the presence of intact Nup98 protein (Faria et al., 2006). Loss of one copy of Nup96 in the mouse leads to mildly enhanced proliferation of T-cells, supporting a potential role for Nup96 as a haplo-insufficient tumor suppressor (Chakraborty et al., 2008), but Nup96+/- mice do not appear to exhibit cell cycle deregulation in other tissues, nor develop cancer (Faria et al., 2006). Conversely, an engineered allele generating loss of one copy of Nup98 in the mouse, but with Nup96 protein expression remaining intact, cooperates with loss of the nuclear export cofactor Rae1 to increase aneuploidy (Jeganathan et al., 2005), but Nup98+/- mice have not been reported to develop cancer, nor to exhibit cell cycle de-regulation on their own (Wu et al., 2001). Studies of Nup98 and Nup96 homozygous mutants have been severely limited by the very early embryonic lethality caused the by loss of each Nup (Faria et al., 2006; Wu et al., 2001), and compound mutants have not been reported. Using a small interfering RNA (siRNA) knockdown approach to selectively target Nup98 in human cells, revealed a role for Nup98 in p53-dependent induction of the Cdk inhibitor p21 in

response to DNA damage, consistent with a tumor-suppressor function for Nup98 (Singer et al., 2012).

Work in *Drosophila* revealed an unexpected off-pore role for Nup98 in modulating the expression of several cell cycle genes (Capelson et al., 2010; Kalverda et al., 2010). Loss of Nup98-96 function in *Drosophila* is lethal and pleiotropic. Flies homozygous for an allele with a stop codon predicted to generate a truncated Nup98 and eliminate Nup96, die prior to metamorphosis (Parrott et al., 2011; Presgraves et al., 2003). A Nup98-96 allele disrupted by a transposon insertion in the fourth exon of Nup98, predicted to disrupt splicing, exhibits germline-specific defects in stem cell proliferation and differentiation (Parrott et al., 2011). Low-level constitutive depletion of Nup98-96 by RNAi in adult flies impacts expression of anti-viral genes (Panda et al., 2014), while acute inhibition of Nup98-96 in imaginal discs leads to misregulation of Hox gene expression (Pascual-Garcia et al., 2014). Consistent with pleiotropic effects, the knockdown of Nup98-96 by RNAi has emerged in a number of screens in *Drosophila*, revealing roles in nuclear translocation of specific proteins (Dopie et al., 2015; Kristo et al., 2017), and blood progenitor proliferation and differentiation (Mondal et al., 2014).

Human *NUP98-96* is located near a known imprinted tumor-suppressor region in the genome (Joyce and Schofield, 1998), which could be significant as loss of heterozygosity via mutation or epigenetic modifications for the remaining Nup98-96 locus may occur in cancers exhibiting translocations. We are not aware of any information reported to date about the expression levels from the non-translocated *NUP98-96* gene in these diseases. We simultaneously inhibited Nup98 and 96 in *Drosophila* using an *in vivo* RNAi knockdown approach and observed cell cycle de-

regulation and cooperation with oncogenic mutations, consistent with a tumor suppressor function for Nup98 and/or 96. Transgenes encoding Nup98 or Nup96 individually do not rescue this phenotype, while expression of a transgene encoding both does – suggesting Nup98 and Nup96 play non-overlapping and potentially synergistic roles in cell cycle regulation.

Here we show that that reducing Nup98-96 function via an RNAi approach in *Drosophila melanogaster* (where the Nup98-96 shared mRNA and reading frame gene structure is conserved) de-regulates the cell cycle. We find evidence of overproliferation in Nup98-96 deficient tissues, counteracted by elevated apoptosis and aberrant JNK signaling associated with wound healing. When the knockdown of Nup98-96 is combined with inhibition of apoptosis, we see synergism leading to overgrowth consistent with a tumor-suppressor function for endogenous Nup98 and/or 96. We suggest that the loss of normal Nup98 and Nup96 function may de-regulate the cell cycle to cooperate with other mutations in cancer.

3.3 Results

3.3.1 Loss of Nup98-96 disrupts G1 arrests and causes cell cycle de-regulation

We previously described an RNAi screen to identify genes that promote proper cell cycle exit in the *Drosophila* eye (Flegel et al., 2016; Sun and Buttitta, 2015). Our initial screen used UAS-RNAi constructs from the Harvard TRiP RNAi collection, driven by the

Glass Multimer Repeats (*GMR*) promoter-Gal4 with an E2F-responsive *PCNA-white* reporter transgene, which provides adult eye color as a readout of E2F and cell cycle activity (Bandura et al., 2013). This screen successfully identified genes that delay proper cell cycle exit by promoting a delay or bypass of G1 arrest, which directly or indirectly impacts E2F activity (Flegel et al., 2016; Sun and Buttitta, 2015). In this screen, we identified an RNAi line targeting the bi-cistronic Nup98-96 transcript as a potential novel regulator of cell cycle exit in the *Drosophila* eye.

Cell cycle exit in the eye is normally completed by 24 hours after puparium formation (APF). To confirm whether knockdown of *Nup98-96* delayed cell cycle exit in the pupa eye, we performed S-phase labeling via 5-ethynyl-2'-deoxyuridine (EdU) incorporation and examined an E2F transcriptional activity reporter *PCNA-GFP* in pupal eyes several hours after normal cell cycle exit. We confirmed that knockdown of *Nup98-96* delayed proper cell cycle exit in the pupa eye to between 28-36h APF (Supp Fig. 1A). We also confirmed that the RNAi line identified in the screen knocked down endogenous Nup98-96 protein tagged with GFP and that re-expression of both exogenous *Nup98* and *Nup96* were required to rescue phenotypes due to *Nup98-96* bi-cistronic transcript knockdown (Supp Fig. 3-1 B,C). Neither exogenous *Nup98* or *Nup96* alone were sufficient to rescue *Nup98-96* RNAi phenotypes, suggesting both Nups contribute to the cell cycle exit defect.

We next examined whether knockdown of *Nup98-96* in the posterior wing using the driver *engrailed-Gal4* (*en-Gal4*) with a temperature sensitive Gal80 (en^{TS}) could delay cell cycle exit in the pupal wing, which also completes the final cell cycle by 24h APF. We used $Gal80^{TS}$ to limit expression of the RNAi to pupal stages to avoid

developmental delays and lethality and an RNAi to the eye pigment gene *white* (*white*^{RNAi}), which has no effect on cell cycle exit served as a negative control (Flegel et al., 2016). Labeling S-phases with EdU incorporation from 26-28h APF and mitoses using anti-phosphorylated Ser10-Histone H3 (PH3) antibody revealed that knockdown of *Nup98-96* delayed cell cycle exit in the wing until 28-30h APF (Fig 3-1A-D).

We have shown that delays in cell cycle exit accompanied with high E2F activity can result from slowing the final cell cycle, or by causing additional cell cycles (Flegel et al., 2016; Sun and Buttitta, 2015). To determine which is the case with knockdown of *Nup98-96*, we expressed *Nup98-96* RNAi in the eye, using a sensitized background with the *GMR*-Gal4 driver driving the G1-S Cyclin, Cyclin E (*CycE*) and the apoptosis inhibitor *P35* (Hay et al., 1994). This sensitized background causes enlarged eyes and 1-3 extra cell cycles in the pupa eye prior to a robust cell cycle exit (Sun and Buttitta, 2015). The enlarged eyes of this sensitized background are visibly suppressed by factors that delay the cell cycle and enhanced by manipulations that cause extra cell cycles (Sun and Buttitta, 2015). Knockdown of *Nup98-96* effectively enhanced the eye overgrowth of this sensitized background and resulted in extra cone cells and extra interommatidial cells in the pupal eye, confirming that the delay of cell cycle exit was caused by additional cell cycles (Fig.3-1 E-H).

We next examined proliferating larval wing discs, to determine whether the effects of *Nup98-96* knockdown were specific to the pupa or also impacted earlier cell cycles. We used *en-Gal4/Gal80*^{TS} to express *Nup98-96* RNAi in the posterior wing disc, labeled with GFP, for 72h prior to dissection and detected mitoses with PH3 or performed 5-10 min of EdU labeling for S-phase immediately prior to fixation. We

observed an increase in mitoses when *Nup98-96* was knocked down, accompanied by an increase in S-phase labeling (Fig. 3-1 I-L, Supp. Fig 3-1G). Consistent with knockdown of *Nup98-96* leading to a bypass of a G1 cell cycle arrest, we also observed abundant S-phases in the posterior zone of non-proliferating cells (ZNC, yellow arrowhead), which are normally quiescent at this stage (Johnston and Edgar, 1998). Similar effects on larval wing disc proliferation were also observed using two independent *Nup98-96* RNAi lines from the VDRC collection (Supp. Fig.3-1D).

Increased EdU and PH3 labeling at fixed timepoints can be due to increased proliferation or increased time spent in S and M phases respectively. To examine whether S to M progression is slowed when *Nup98-96* is knocked down, we performed an EdU pulse/chase assay combined with PH3 labeling in L3 larval wing discs. We fed larvae with food containing EdU for 1 hour followed by a chase without EdU for 7h. At the end of the chase, we fixed larval wing discs and stained for PH3 and scored the number of mitotic cells double positive for EdU and PH3 in the posterior vs. anterior wing pouch for *white* RNAi vs. *Nup98-96* RNAi discs. The posterior to anterior ratio of double-positive cells that transition from S to M-phase in control *white* RNAi discs is approximately 1, indicating similar cell cycle timing in the posterior and anterior wing disc of late L3 larvae (Mesquita et al., 2010). By contrast, the fraction of EdU-positive mitoses in the posterior compared to the anterior disc was increased when *Nup98-96* was knocked down in the posterior, suggesting that these cells are progressing from S to M without significant delay (Fig. 3-1 M-O). An increased posterior to anterior ratio could indicate either an increase in proliferation rate in the posterior disc, or a non-autonomous decrease in the anterior (Mesquita et al., 2010). Indeed, the increased ratio

of EdU-positive mitoses in the *Nup98-96* RNAi domain is in part due to a non-autonomous effect resulting in fewer S-M transitions in 7hr in the anterior compartment (Supp. Fig 3-1). However, when we compared the fraction of EdU-positive mitoses in *Nup98-96* RNAi posterior discs to posterior *white* RNAi wings (an external control), we observe a ~20% increase although it is not statistically significant. Altogether this indicates Nup98-96 knockdown cells proliferate faster than their neighbors and proliferate at rates similar to or slightly faster than control cells.

3.3.2 Nup98-96 knockdown results in apoptosis and activation of JNK signaling

Despite the increased rate of proliferation and disruption of G1 arrest in the larval and pupal tissues, we noted that the posterior wing expressing *Nup98-96* RNAi was consistently smaller than normal suggesting an increase in cell death (Supp. Fig, 3-1C). Indeed, knockdown of *Nup98-96* for 72h dramatically increased apoptosis in the posterior wing disc, as measured by anti-cleaved Caspase 3 and anti-DCP1 staining (Fig. 3-2 A-B, Supp. Fig. 3-2). The increased apoptosis and reduced size in the posterior disc could be fully rescued by exogenous expression of both *Nup98* and *96* in the presence of *Nup98-96* RNAi (Supp. Fig. 3-1C , Supp. Fig 3-2C,D). Expression of *Nup98-96* RNAi in the dorsal wing disc using *apterous-Gal4,Gal80^{TS}* (*ap^{TS}*) for 72h also induced robust apoptosis, indicating that the effect was not specific to the posterior disc (Supp. Fig. 3-2E). We knocked down the initiator caspase Dronc or effector caspase Drice in attempt to rescue the apoptotic cells, but neither fully suppressed the apoptotic response to *Nup98-96* knockdown (Fig.3- 2 C,D), nor did co-expression of a dominant negative form of p53 (not shown, Brodsky et al., 2000). We next co-expressed the

baculoviral caspase inhibitor P35 with *Nup98-96* RNAi, which suppressed apoptosis (Supp Fig 2) and resulted in dramatic wing disc overgrowth phenotypes, including folding of the epithelium and occasional duplication of wings (Fig. 3-2 E,F). The overgrowth and duplication of wing tissues was reminiscent of a phenotype observed during wing damage and regeneration when JNK signaling is activated (Perez-Garijo et al., 2009; Schuster and Smith-Bolton, 2015; Verghese and Su, 2017; Worley et al., 2018). We therefore examined whether *Nup98-96* knockdown resulted in activation of JNK signaling by staining for phospho-JNK (Fig.3- 2G,H) and induction of the JNK signaling transcriptional target *puckered* (using a *puc-LacZ* expression reporter, Supp. Fig. 3-2I). Knockdown of *Nup98-96* for 72h led to high levels of compartment-autonomous JNK signaling in the wing disc.

High JNK signaling can paradoxically lead to both proliferation and cell death in *Drosophila* tissues (Fogarty and Bergmann, 2017). We next tested whether inhibition of JNK signaling via dominant negative form of the *Drosophila* JNK, Basket (Bsk^{DN}) could suppress the apoptotic and proliferative response to knockdown of *Nup98-96*. Co-expression of Bsk^{DN} with *Nup98-96* RNAi had a complex effect on apoptosis in the wing, enhancing levels of apoptosis in some samples, while suppressing in others (Fig.3- 2 I-J,M). Unexpectedly, co-expression of Bsk^{DN} with *Nup98-96* RNAi did not suppress the increased mitoses observed in posterior wings expressing *Nup98-96* RNAi, and even mildly enhanced the differences in mitotic labeling between anterior and posterior compartments (Fig. 3-2K-L, N). Although, we noted an overall decrease in PH3 labeling across both compartments when Bsk^{DN} was co-expressed in the posterior wing disc (Supp. Fig 3-2J), suggesting blocking JNK signaling reduced compensatory proliferation

both autonomously and non-autonomously. The few adult wings that could be recovered with both *Nup98-96* RNAi and *Bsk^{DN}* expression exhibited a more severely reduced posterior compartment than *Nup98-96* RNAi alone (Fig. 3-2O). This suggests activation of JNK signaling provides compensatory proliferation and may partially increase survival when *Nup98-96* is knocked down, consistent with previously described roles in wing damage and regeneration (Bergantinos et al., 2010; Herrera et al., 2013).

3.3.3 Nup98-96 knockdown leads to mis-patterning and gene expression resembling a wound healing and loser phenotype.

The JNK signaling and overgrowth phenotypes caused by suppressing apoptosis during *Nup98-96* knockdown, are reminiscent of a phenomenon called apoptosis-induced compensatory proliferation (AIP) (Fogarty and Bergmann, 2017), which can impact tissue patterning. As previously described for other JNK-driven *Drosophila* tumor models, we observed dramatic tissue folding and invasion behaviors at both the A-P and D-V compartment boundaries when *Nup98-96* was inhibited in the presence of *P35* expression, (Supp. Fig3- 3A-C) (Muzzopappa et al., 2017). Therefore, we next investigated whether wing disc patterning is disrupted by *Nup98-96* knockdown as previously shown in AIP.

We first examined Wg levels in discs expressing Nup98-96 RNAi, since AIP and wing duplications have been associated with ectopic Wg (Baonza et al., 2000; Perez-Garijo et al., 2009; Verghese and Su, 2017; Worley et al., 2018). We found that knockdown of *Nup98-96* resulted in ectopic Wg in the dorsal wing hinge and this effect was amplified in in the presence of P35 (Fig. 3-3 A-D). We also observed ectopic

phosphorylation of the transcription factor Mad (Supp. Fig. 3-3D), consistent with the previously described effect of AIP on Dpp signaling (Perez-Garijo et al., 2009; Pinal et al., 2018).

Both Wg and Notch have been implicated in the G1 arrest in the posterior ZNC (Duman-Scheel et al., 2004; Herranz et al., 2008). We therefore next examined the expression of two targets of Notch and Wg signaling; Cut, which is expressed in G1 arrested cells at the Dorso-Ventral (D-V) boundary, and Vestigial (Vg), which is expressed in a broader domain of the pouch induced by longer-range Wg signaling (de Celis et al., 1996; Kim et al., 1996; Neumann and Cohen, 1997). We found that Cut expression at the D-V boundary was nearly eliminated when *Nup98-96* was knocked down, both with and without *P35* (Fig. 3-3 E-G). This suggests Notch signaling at the D-V boundary is compromised when *Nup98-96* function is reduced. Vg, an important wing identity and growth regulator (Halder et al., 1998; Williams et al., 1991; Williams et al., 1993; Zecca and Struhl, 2010), was also dramatically reduced in the pouch upon *Nup98-96* knockdown (Fig.3-3H) suggesting Wg released from the D-V boundary is also compromised. Notch and Wg have been suggested to regulate the ZNC cell cycle arrest via repression of dMyc expression, but we did not observe any effects of *Nup98-96* knockdown on dMyc levels in the ZNC (not shown). Interestingly, the downregulation of Vg was also observed in regenerating discs (Smith-Bolton et al., 2009), potentially due to the replacement of dying pouch cells with cells from the neighboring areas of the wing (Zecca and Struhl, 2010). Taken together, these data demonstrate that reduction of Nup98-96 function in the presence of P35 leads to AIP and wing mis-patterning and cell identity changes associated with a chronic wounding and regeneration response.

While high JNK signaling and apoptosis-induced compensatory proliferation can explain many of the phenotypes we observe with *Nup98-96* knockdown, this does not reveal the proximal defect caused by loss of Nup98-96 function. To determine additional effects of *Nup98-96* knockdown on gene expression in the wing, we performed comparative gene expression analysis via RNAseq to identify mRNAs increased or decreased upon *Nup98-96* RNAi compared to the control *white* RNAi for 72h in late L3 wing discs (Supplemental Table 1). We observed the strong upregulation of many genes directly associated with JNK signaling (e.g. *puc, mmp1, Ets21C*) (Kulshammer et al., 2015; McEwen and Peifer, 2005; Uhlirova and Bohmann, 2006), Jak/STAT signaling (*upd, upd2, Socs36E*) (Amoyel et al., 2014) and developmental delays associated with wing damage and regeneration (*chinmo, Ilp8*) (Colombani et al., 2012; Garelli et al., 2012; Katsuyama et al., 2015; Narbonne-Reveau and Maurange, 2019). Consistent with the wing overgrowth phenotypes, several genes of the genes listed above have been shown to act in combination to promote tumorigenic overgrowth in flies (Toggweiler et al., 2016), and we see a striking overlap of about one third of the genes changed upon *Nup98-96* RNAi with gene expression changes observed in a well-established invasive fly tumor model (507 out of 1774 genes, Supplemental Table 1) (Kulshammer et al., 2015).

Consistent with increased cell cycle progression, we also observed the upregulation of several DNA damage and replication genes regulated by E2F activity (*Orc1*, multiple DNA Polymerases, *SpnE*, *Rnr-L*, *RfC4*) (Buttitta et al., 2010; Dimova et al., 2003). However, we did not observe strong upregulation of other G1-S promoting genes such as *dMyc* (1.52-fold change), *bantam*, *cycE* or *cycD*. When we compared

gene expression signatures globally, we found a strong overlap (2.63-fold more genes than expected by chance) with a wounding and regeneration gene expression signature (Khan et al., 2017, Supplemental Table 2). We also noted upregulation of several genes associated with proteotoxic and oxidative stress (*Xrp1*, multiple Glutathione S transferases, *Aox1,* and specific DNA damage response genes) (Baumgartner et al., 2021). We found the strongest overlap of the *Nup98-96* knockdown signature with a cell competition “loser” gene expression signature (5.67-fold more genes than expected by chance, 316/443 genes, Supplemental Table 3), which is also known to activate chronic JNK signaling (Kucinski et al., 2017).

3.3.4 Nup98-96 knockdown leads to defects in proteins synthesis

The strong overlap of the gene expression changes in *Nup98-96* knockdown with the cell competition “loser” signature suggested to us that a proximal effect of Nup98 loss could be on ribosome biogenesis. We further examined a gene expression signature associated with Xrp1, an AT-Hook, bZip transcription factor which mediates signaling downstream of ribosomal protein mutations and proteotoxic stress (Langton et al., 2021; Lee et al., 2018). We found a striking proportion of Xrp1 targets (115 out of 159 overlapping in our dataset, Supplemental Table 4) were upregulated when *Nup98-96* was knocked down (Ji et al., 2019). Consistent with a defect in ribosome function, we observed a decrease in protein synthesis when *Nup98-96* was knocked down in wings, as measured by a puromycin labeling assay (Deliu et al., 2017), (Fig. 3-4 A,B). We did not observe downregulation of any ribosomal proteins in our RNAseq dataset, with the exception of a 2-fold decrease in *RpS19b*, which is a non-minute, duplicated ribosomal

protein gene with tissue-specific expression (Marygold et al., 2007). Any effects on *RpS19b* levels are likely buffered by its paralog *RpS19a,* which exhibits much stronger expression in larval wings and was unchanged by *Nup98-96* knockdown (Brown et al., 2014).

Nups play a key role in the nuclear export of ribosomal subunits in cooperation with the exportin chromosomal region maintenance 1 (CRM1; also known as exportin-1 or XPO1), which binds to nuclear export sequences (NESs) to facilitate export of cargo proteins (Gleizes et al., 2001; Johnson et al., 2002; Moy and Silver, 2002; Oeffinger et al., 2004). We wondered if the proximal defect in *Nup98-96* knockdown tissues might be defects in nuclear export of ribosomal complexes. First, we examined whether our partial knockdown of Nup98-96 function by RNAi was sufficient to disrupt nucleo-cytoplasmic localization, since previous work had suggested knockdown of *Nup98-96* transcripts in *Drosophila* S2 cells did not produce such defects (Sabri et al., 2007). We confirmed that by 52h of knockdown with en^{TS} *in vivo*, we could easily visualize defects in nuclear localization of a ubiquitously expressed RFP with a nuclear localization signal (NLS) and by 72h of knockdown, nuclear localization of NLS-RFP was dramatically reduced (Supp. Fig 3-4 A). We next confirmed that knockdown of an essential component of the nuclear export machinery for ribosome subunits, *Nmd3* (Ma et al., 2017) also effectively reduced protein synthesis (Fig. 3-4 C). As a positive control we also knocked down *CG4364*, the fly homolog of the pre-rRNA processing component Pescadillo (Lapik et al., 2004) (Fig. 3-4 D-E). Inhibition of ribosome export machinery and pre-rRNA processing were both sufficient to induce strong phosphorylation of JNK (Fig. 3-4 F-G) in the wing disc.

Ribosome large and small complexes are exported from the nucleus separately as assembled pre-ribosomal particles and must associate with cytoplasmic maturation factors to exchange specific components to form mature functional ribosomes (Lo et al., 2010). We screened through collections of endogenously tagged Rp subunits and found RpL10Ab, but not other Rp subunits (RpS20 and RpL5) were mis-localized when *Nup98-96* was knocked down (Fig. 3-4 H-K). Interestingly, the defect in RpL10Ab localization was nuclear retention, the opposite of the effect of Nup98-96 knockdown on NLS-RFP. RpL10Ab (also called L10a or uL1) is required to associate with Nmd3 for efficient pre-60S nuclear export (Musalgaonkar et al., 2019). Normally, RpL10Ab is translated in cytoplasm, localized to the nucleolus for assembly into the pre-60S complex and then exported bound to the Nmd3 adaptor. The nuclear retention of RpL10Ab upon *Nup98-96* knockdown was initially puzzling as the other RpL subunits examined did not exhibit similar localization defects. However recent work has revealed that in mammals RpL10A is associated with a subset of specialized ribosomes and is not found in all 60S complexes (Shi et al., 2017). We suggest that knockdown of *Nup98-96* partially compromises protein synthesis by inhibiting proper cytoplasmic translocation of a subset of pre-60S subunits that are RpL10Ab-associated. Importantly, RpL10Ab is not a Minute gene (Marygold et al., 2007), possibly because it is a sub-stoichiometric ribosome component. Consistent with this, we do not recover significant overlap with the proteasomal stress portion of the “Loser” gene expression signature when Nup98-96 is compromised (Baumgartner et al., 2021), again suggesting protein synthesis is only partially reduced when Nup98-96 function is compromised.

3.3.5 Nup98-96 knockdown in mammalian cells leads to defects in proteins synthesis and JNK activation

As described in the introduction, there is abundant evidence that loss of Nup98-96 function might contribute to tumorigenesis. We wondered whether inhibition of Nup98-96 in mammalian cells would also impact protein synthesis and JNK signaling as we observe in *Drosophila*. Of note, a screen for factors involved in ribosome biogenesis in HeLa cells identified several Nups containing FG repeats, including Nup98 as hits involved in pre-60S export, suggesting Nup98 effects on protein synthesis will be broadly conserved (Wild et al., 2010). We used small-interfering RNA (siRNA) to *Nup98-96* in MCF7 breast cancer cells and PC3 prostate cancer cells for 72 hours and compared effects on Nup98 protein levels, protein synthesis and pJNK to a control scrambled siRNA (ctrl siRNA). We found that siRNA to *Nup98-96* was sufficient to reduce protein synthesis and increase phosphorylation of JNK in both cell types (Fig. 3-5 A-H, Supp. Fig 3-5).

3.3.6 Overexpression of Nup98 leads to defects in proteins synthesis and JNK activation

Most of the attention on Nup98 translocations in cancer has focused on overexpressing Nup98 fusion partners. However when overexpressed, Nup98 has been shown to behave as a dominant negative and disrupt the nuclear envelope and nuclear transport (Fahrenkrog et al., 2016; Mendes et al., 2020), possibly by forming phase-separated aggregates outside of the nuclear pore (Ahn et al., 2021; Schmidt and Gorlich, 2015). We noted that Nup98 overexpression in the posterior wing disc reduced

tissue size, and in severe cases disrupted pattering (Fig. 3-6 A-F). We therefore examined whether Nup98 overexpression in the *Drosophila* wing disc mimicked aspects of Nup98-96 inhibition, as described for other *Drosophila* tissues (Pascual-Garcia et al., 2014). Overexpression of a strong *UAS-Nup98* cDNA construct (2F) reduced nuclear localization of an NLS-tagged RFP, resulting in increased cytoplasmic accumulation and a reduced nuclear:cytoplasmic ratio (Fig. 3-6 G-H). Overexpression of a *UAS-Nup98-96* cDNA construct was also sufficient to increase cell death and activate JNK signaling in the posterior wing disc (Fig. 3-6 I-J), and overexpression of both *UAS-Nup98* and *96* or *UAS-Nup98* alone (2F) reduced protein synthesis levels (Fig. 3-6 K-M). We suggest that Nup98-96 acts as a “goldilocks” gene (Braune and Lendahl, 2016), where too much or too little activity leads to chronic stress signaling and increased cellular turnover, potential hallmarks of tumorigenesis. This complication might explain why this locus is particularly prone to mis-regulation by translocations in cancer, which would reduce Nup98-96 normal functions and simultaneously provide additional Nup98-containing fusion proteins.

3.4 Discussion

3.4.1 Partial Nup98-96 loss of function leads to paradoxical increases in cell cycling and cell death accompanied by reduced protein synthesis

Protein synthesis and the cell cycle are usually coupled by pathways such as insulin and TOR signaling as well as growth and cell cycle checkpoints, which promote or limit cell cycle progression and protein synthesis coordinately (Grewal, 2009; Lockhead et al., 2020; Romero-Pozuelo et al., 2017; Romero-Pozuelo et al., 2020). Here, we describe a seemingly paradoxical situation where protein synthesis and cell cycle are effectively uncoupled. When Nups 98 and 96 are partially compromised, cells with reduced protein synthesis cycle more and even bypass developmentally induced G1 arrests. This is accompanied by high levels of chronic JNK signaling and induction of apoptosis, along with expression of genes involved in tissue regeneration and compensatory proliferation. When apoptosis is blocked using the caspase inhibitor P35, tissue overgrowth and mis-patterning results, reminiscent of tumorigenesis. We propose that mutations or gene expression changes that reduce Nup98 and Nup96 function, in the presence of apoptosis suppression, can contribute to tumorigenesis. This may help explain contexts of Nup98 and/or Nup96 loss that could pre-dispose for cancer (Franks and Hetzer, 2013; Simon and Rout, 2014; Singer et al., 2012).

The phenotype we describe here for *Nup98-96* inhibition is strikingly similar to that recently described for a ribosomal protein mutant, when cell death is blocked (Akai et al., 2021). When we examined the gene expression signature in response to reduced *Nup98-96*, we observed a strong overlap with conditions of reduced protein synthesis caused by stoichiometric imbalances in ribosomal proteins (Kucinski et al., 2017; Lee et al., 2018). We suggest this effect of *Nup98-96* inhibition is due to defects in nucleo-cytoplasmic transport of RpL10A, although we cannot rule out that localization of other ribosomal proteins may also be affected. Because the defect is in RpL10A localization,

rather than levels, we were unable to rescue the *Nup98-96* knockdown phenotypes with RpL10A overexpression. On the contrary, we observed several stress signaling phenotypes when we overexpressed RpL10A itself even in a wild-type background, suggesting RpL10A levels must also be carefully controlled (Chaichanit et al., 2018; Wonglapsuwan et al., 2011). This may be of broader consequence to the *Drosophila* research community since Gal4/*UAS*-driven overexpression of this ribosomal protein is used for translatome profiling through translating ribosome affinity purification (Thomas et al., 2012). Importantly, localization of 40S and 60S subunits are not globally disrupted in our *Nup98-96* knockdown conditions and protein synthesis is only partially reduced. We suggest that this is because RpL10A is a sub-stoichiometric component of ribosomes and that only the subset of ribosomes containing RpL10A are affected. In mammals RpL10A-containing ribosomes have been shown to translate genes required for cell survival and are depleted of those required for cell death (Shi et al., 2017). Whether this is the case for *Drosophila* RpL10A- containing ribosomes remains to be determined, although increasing RpL10A expression in *Drosophila* has been shown to affect E-cadherin and InR levels, suggesting components of these pathways could be regulated by RpL10A levels (Chaichanit et al., 2018).

The effects of reducing *Nup98-96* expression are likely to be pleiotropic, and we cannot rule out the possibility that Nup98 and 96 mis-regulation may also lead to more direct effects on the cell cycle, independent of JNK signaling and reduced protein synthesis. Indeed, when JNK signaling is blocked by a dominant negative, overall compensatory proliferation is significantly reduced, but Nup98-96 reduced tissue still exhibits a slightly higher mitotic index than tissue with normal Nup98-96 levels. This

could be in part the result of a known Nup98 interaction with the APC/C which leads to aneuploidy when Nup98 levels are reduced (Jeganathan et al., 2006; Jeganathan et al., 2005). This interaction with the APC/C may also explain the disruption of terminal cell cycle arrest caused by reduced Nup98-96, as high APC/C activity promotes proper timing of the final cell cycle (Buttitta et al., 2010; Reber et al., 2006; Ruggiero et al., 2012; Tanaka-Matakatsu et al., 2007). We tested for aneuploidy using flow cytometry on wing discs and did not observe obvious accumulation of aneuploidy when *Nup98-96* is knocked down, either with or without apoptosis inhibition. Alternatively, effects on nuclear export of cell cycle factors or their mRNAs may also contribute to the cell cycle phenotypes (Chakraborty et al., 2008), although we did not find obvious changes in protein levels or dynamics of Cyclins A or B. We also examined whether mis-regulation of transcriptional targets of Nup98 regulated through off-pore roles may explain the phenotypes we observe, but we did not find significant overlap of genes altered in our *Nup98-96* knockdown with Nup98-bound targets determined by ChIP-seq in larval brains (Pascual-Garcia et al., 2017) or Nup98 regulated genes identified by RNAseq in S2 cells (Kalverda et al., 2010). We found a mild enrichment (1.43-fold over that expected by chance) in the overlap of genes altered in our *Nup98-96* knockdown with Nup98-ChIP seq targets in S2 cells. (Pascual-Garcia et al., 2017, Supplemental Table 5). Overall, the previously described wounding/regeneration and “loser” gene expression programs explain nearly half (49.7%) of the gene expression changes we observe in wing discs when Nup98-96 is reduced (Fig. 3-3) suggesting these may be the main divers of the phenotypes we observe.

3.4.2 Potential for AIP in Nup98 cancers

apoptosis in cells with inhibited *Nup98-96* leads to phenotypes consistent with sustained apoptosis-induced proliferation (AIP), which is thought to contribute to tumorigenesis in epithelia (Fogarty and Bergmann, 2017). Epithelial tumors exhibit wounding phenotypes, chronic inflammation and cell death (Dvorak, 1986; Karin and Clevers, 2016). Chronic AIP leads to sustained proliferation and results in abnormal, hyperplastic overgrowth (Perez-Garijo et al., 2009; Pinal et al., 2018). AIP therefore could contribute to overproliferation in epithelial cancers with disrupted *Nup98-96* expression (Perez-Garijo, 2018). AIP has been suggested to occur in colorectal cancer and melanoma (Bordonaro et al., 2014; Donato et al., 2014), both of which have been suggested to exhibit Nucleoporin mis-regulation (Roy and Narayan, 2019). How this might relate to aberrant signaling in hematological malignancies related to Nup98 mis-expression is unclear. It is possible effects of Nup98 mis-regulation impact different tissue types through similar pathways, that impinge on distinct downstream target genes in different tissues. For example, expression of a NUP98-HOXA9 fusion in a *Drosophila* model with a normal *Nup98-96* locus leads to hyperplastic over-proliferation in hematopoietic tissues but minimal effects in epithelial tissues (Baril et al., 2017), while loss of *Nup98-96* in larval hematopoietic tissues leads to a loss of progenitors, a phenotype also observed upon inhibition of the ribosomal protein RpS8 (Mondal et al., 2014). Thus *Nup98-96* loss likely has distinct yet overlapping effects in different tissue types. NUP98 mutations in leukemias are associated with mutations affecting apoptosis such as BCR-ABL, NRAS, or KRAS and ICSBP (Gabriele et al., 1999; Gough et al., 2011; Gurevich et al., 2006; Hu et al., 2016; Slape et al., 2008). Mouse models with

Nup98 protein fusions exhibit increased apoptosis (Choi et al., 2008; Lin et al., 2005), and a zebrafish model of NUP98-HOXA9-driven leukemia upregulates Bcl2 to suppress apoptosis (Forrester et al., 2011). In a mouse model of Nup98-HoxD13-driven leukemia, loss of p300 leads to reduced apoptosis and enhanced activation of Jak/Stat signaling, reminiscent of signaling effects we see in AIP (Cheng et al., 2017). In our *Nup98-96* RNAi experiments we reduce Nup98 protein levels to about 50-70% of the normal level, consistent with other studies using this RNAi approach (Pascual-Garcia et al., 2014). Our data suggests that this locus can behave as a dominant negative when the Nup98 portion is overexpressed through translocations as well as a haplo-insufficient tumor suppressor in some contexts. We propose that disruption of the *NUP98-96* locus in cancers with or without *NUP98* translocations may contribute to tumorigenesis through aberrant JNK signaling and AIP, in the presence of additional hits that block cell death.

Acknowledgements: We thank Drs. Cordula Schulz, Sofia Merajver, Catherine Collins, Helena Richardson and Maya Capelson for sharing flies and reagents. We thank the Bloomington (BDSC), Vienna (VDRC) and Kyoto (DGRC) *Drosophila* stock centers for providing stocks critical to this work. We also thank A. Sustar and the former lab of Dr. Gerold Schubiger for sharing Ptc and Vg antibodies originally obtained from the S. Carroll and T. Kornberg Labs. This work in the Buttitta Lab was supported by The American Cancer Society (RSG-15-161-01-DDC), the University of Michigan Rogel Cancer Center Discovery Fund and the NIH (R01GM127367). We thank the U. Michigan Advanced Genomics Core for library preparation and high-throughput

sequencing. We thank the Buttitta Lab members for helpful input on this project. L.A.B. thanks Lynn Taylor for essential childcare support during the writing of this paper.

3.5 Materials and Methods:

3.5.1 Flystocks used:

UAS-Nup98-96 RNAi (TRiP BL28562, VDRC lines, KK100388 and GD6897)

UAS-white RNAi (TRiP BL35573)

UAS-Dronc RNAi (TRiP BL 32963)

UAS-Drice RNAi (TRiP BL 32403)

UAS-Nmd3 RNAi (VDRC105619 and VDRC46166)

UAS-CG4364 RNAi (VDRC27607)

GMR-Gal4, UAS-CycE(I); GMR-P35 from H. Richardson

Nup98-96-GFP (VDRC 318656 FlyFos collection)

UAS-Nup98-96 cDNA(2M), UAS-Nup98 cDNA (3M), UAS-Nup98 cDNA (myc2F), UAS-Nup96 cDNA (myc7M), UAS-Nup96 cDNA (myc8M) all from C. Schulz and M. Capelson.

en^{TS} is w; *en-Gal4,UAS-GFP; tub-Gal80TS/TM6B* from (Buttitta et al., 2007)

ap^{TS} is w; *ap-Gal4,UAS-GFP; tub-Gal80TS/TM6B* from (Buttitta et al., 2007)

en^{TS} RFP is w; *en-Gal4,UAS-*RFP_{NLS}*; tub-Gal80TS/TM6B*

UAS-Bsk^{DN} (on III mutated in kinase domain) and *puc*^{e69}*-LacZ* provided by C. Collins.

UAS-P35 on X (BL6298)

RpS20-GFP (Kyoto 109696 w^{1118}; PBacRpS20^{KM0175} / TM2)

RpL5-GFP (Kyoto 109767 w^{1118}; PBac RpL5^{KM0174} / SM6a and Kyoto 109768 w^{1118}; PBac RpL5^{KM0163})

RpL10Ab-YFP (Kyoto 115462 w^{1118}; PBac RpL10Ab^{CPTI003957})

Ubi-RFP$_{NLS}$: (derived from BL35496)

y,*w*,*hs-flp12* (derived from BL1929)

w; *act>stop>Gal4*, *UAS-GFP*$_{NLS}$*; UAS-P35* from (Neufeld et al., 1998)

3.5.2 Immunofluorescence:

Drosophila samples were fixed in 4% paraformaldehyde/1XPBS solution for 20-30 min., rinsed twice in 1X PBS with 0.1% Triton-X-100 detergent (1XPBST). The samples were then incubated in appropriate dilution of antibodies in PAT (1XPBS + 0.1% Triton X-100 + 1% BSA) for 4 h at room temperature or overnight at 4°C. The samples were then washed three times for 10 mins in 1XPBST and incubated in secondary antibody conjugated with required fluorophore for 4 h in PBT-X + 2% normal goat serum (1XPBS + 0.3% Triton X-100 + 0.1% BSA) at room temperature or overnight at 4°C. DAPI or Hoechsts 33258 was used as a nuclear counter-stain and samples were mounted on glass slides using 5µl of Vectashield mounting medium (Vector Labs). Slides were imaged using a Leica DMI6000 epifluorescence system with subsequent deconvolution or a Leica SP5 confocal microscope.

For PC3 and MCF-7 cells, fixation and washes were performed as described above, except in 12-well dishes or 8-chamber slides, with just 1h of incubation with primary and secondary antibodies at room temperature. Experiments for each siRNA were performed in triplicate.

3.5.3 EdU labeling and pulse-chase assay:

Crosses were flipped every day and kept at room temperature (22°C). For EdU labeling in Fig 1K-L (labeling post-dissection), larvae were dissected inverted and incubated in 10µM EdU prior to fixation and labeling. The post-dissection EdU labeling was performed 3 independent times with EdU labeling intervals of 2 min., 5min., and 10min. Data from the 5 min. labeling is shown. For the EdU pulse-chase assay, vials with embryos were transferred to 29°C after 2 days. Larvae at mid- L3, (~66 hrs after the transfer) were removed from the vials by floating in 30% Sucrose/1XPBS solution. The larvae were transferred to a vial with YG food mixed with 100µM EdU and blue food coloring (to track feeding) at 29°C for 1h. Larvae with blue abdomens were then transferred to fresh non-EdU food (chase) for 6-8h at 29°C (equivalent to 7-9h at 25°C). EdU pulsed-chased wandering L3 larvae were collected, dissected, fixed, and antibody stained for EdU, PH3 and GFP (to mark the anterior-posterior compartment boundary). The EdU labelling was performed using a Click it EdU-555 kit (Cat No C10338, Invitrogen) following the manufacturer's instruction. The slide was then imaged using confocal microscopy and the total number of cells positive for both EdU and PH3 were scored and normalized to the total mitotic index. This experiment was replicated 3

independent times for 6h, 7h and 8h pulse-chase intervals, with at least 5 animals per replicate. Data for the 7h replicate is shown.

3.5.4 Protein synthesis puromycin assay:

L3 larvae were dissected in Ringer's solution (Sullivan, 2000) and inverted larvae heads containing wing discs were incubated with 20µm of OPP (O-Propargyl-Puromycin, Invitrogen) in Ringer's solution for 12 mins. The sample was then fixed with 4% paraformaldehyde/1XPBS solution for 20 min, and labelled using the Click-it OPP kit (Cat No C10457, Invitrogen) following the manufacturer's instruction.

3.5.5 Antibodies used:

Mouse anti-PH3 Cell Signaling 9707 1:1000

Rabbit anti-PH3 Millipore 06-570 1:2000

Rabbit anti-Dcp1 Cell Signaling 9578 1:100

Rabbit anti-pJNK Promega v7931 1:100 (for *Drosophila*, used slightly younger pre-wandering larvae due to high peripodial signal in later larvae)

Rabbit anti-pSmad Cell Signaling 9516 1:50 (dissection must be performed on ice)

Rabbit anti-GFP Invitrogen A11122 1:1000 (for co-labeling GFP with EdU)

Mouse anti-cut DSHB 2B10 1:100

Mouse anti-lamin Dm0 DSHB ADL67.10 1:100

Mouse anti-Wg DSHB 4D4 1:100

Rabbit anti-Vg (1:200) via G. Schubiger, from S. Carroll

mouse anti-Patched (1:200) via G. Schubiger, from T. Kornberg

3.5.6 siRNA in mammalian cells:

MCF7 cells were a gift from S. Merajver lab (U. Michigan). PC3 cells were a stable cell line expressing cell cycle reporters hCdt1-mCherry and p27K-mVenus previously described (Takahashi et al., 2019). The cells were gown to 50-70% confluency in a 12-well plate or 8 well chamber slide. The cells were then transfected with 20nM of Nup98 SiRNA or control siRNA using Lipofectamine RNAi MAX (Invitrogen), following manufacturer's protocol. The cells were incubated with the indicated siRNA for 72 hrs. The cells were then harvested for fixation and staining or lysed for western blot. siRNAs: Silencer Select Negative Control No. 1 (ThermoFisher) siRNA Catalog number: 4390843. Nup98-96 siRNA#1 – Silencer Pre-designed siRNA Cat no: AM16708 (ThermoFisher), Nup98-96 siRNA#2 – Silencer Select Pre-designed siRNA Cat no: 4392420 (ThermoFisher), Nup98-96 siRNA#3 – Nup98 siRNA (Santa Cruz Biotech, Cat no: sc-43436).

3.5.7 Image analysis and quantification:

Image quantification was performed using FIJI. For quantification of Dcp1, PH3 or pJNK labeling in Figs 1 and 2, regions of similar size (ROIs) in the anterior and posterior wing disc were hand-drawn using the nuclear (Dapi or Hoeschsts 33258) staining to indicate tissue boundaries and GFP labeling for compartment boundaries. Integrated density of labeling was normalized to ROI area for *white RNAi* and *Nup98-96*

RNAi under conditions blinded to sample identity. Area-normalized integrated density with subtraction of background ROIs outside of the tissue, was used for EdU, PH3, Nup98 and puromycin quantification. For ratios in the EdU/PH3 pulse chase assay, double-labeled cells were counted in each compartment and the ratio normalized to total mitotic index across wing discs is shown. Each dot in the scatter plot represents an individual wing disc from a different animal (For Figs 1,2, 4) or individual cells from experiments performed in triplicate (Fig 5).

3.5.8 Mounting and imaging of adult wings:

Adult wings were preserved in Ethanol, washed in Methyl salicylate and mounted in Canada Balsam (Sigma) as described (O'Keefe et al., 2012). Adult wings were photographed under brightfield conditions on a Leitz Orthoplan2 at 5× magnification, using a Nikon DS-Vi1 color camera and Nikon NIS Elements software.

***RNAseq*:**

Experimental animals contained the genotype: *UAS-P35/w; ap-Gal4, UAS-GFP/ +; tub-gal80TS/UAS-Nup98-96 RNAi TRiP*

Control animals contained the genotype: *UAS-P35/w; ap-Gal4, UAS-GFP/ +; tub-gal80TS/UAS-white RNAi TRiP*

Crosses were performed at room temperature and embryos were collected within a 12h window to synchronize developmental staging and shifted to 18°C. Animals were reared in uncrowded conditions (70 larvae per vial). On day 4 animals were transferred to 28°C and 72h later 3rd instar wing discs were dissected in sterile 1X PBS. We followed a

Trizol-based RNA preparation protocol with dounce homogenization of 40 wing discs per sample with 3 replicated per genotype, as previously described (Flegel et al., 2016).

Using PolyA selection, the University of Michigan's Sequencing Core generated barcoded libraries for each sample and confirmed the quality via the Bioanalyzer and qPCR. Sequencing was performed with the Illumina HiSeq 2000 platform and high read quality was confirmed using FastQC. Reads were aligned to the BDGP6.82 D. melanogaster genome using Rsubread (v1.21.5), with featureCounts resulting in >77% of the reads being successfully assigned to genes (Liao et al., 2014). Counts per million (cpm) were determined with edgeR (v3.13.4) and transcripts with low expression were identified and removed using the data-based Jaccard similarity index determined with HTSFilter (v1.11.0). The cpm were TMM normalized (calcNormFactors), voom transformed (Law et al., 2014), fit to a linear model (lmFit), then differential gene expression calls were made with eBayes. The full dataset is available on GEO (GSE152679). Differentially expressed genes were defined as having a $\log_2$ fold-change of ± 0.5 (1.42-fold change) and adj. p.value <0.05 (Supplemental Table 1). For significance of overlap in differentially expressed genes with other datasets (Figure 3), hypergeometric probabilities were calculated using the hypergeometric distribution as described (Flegel et al., 2016). For significance of overlap with previously published Nup98 ChIP-seq, our list of differentially expressed genes was compared to lists of genes near Nup98 ChIP-seq peaks and examined for overlap greater than that expected by chance using the hypergeometric distribution.

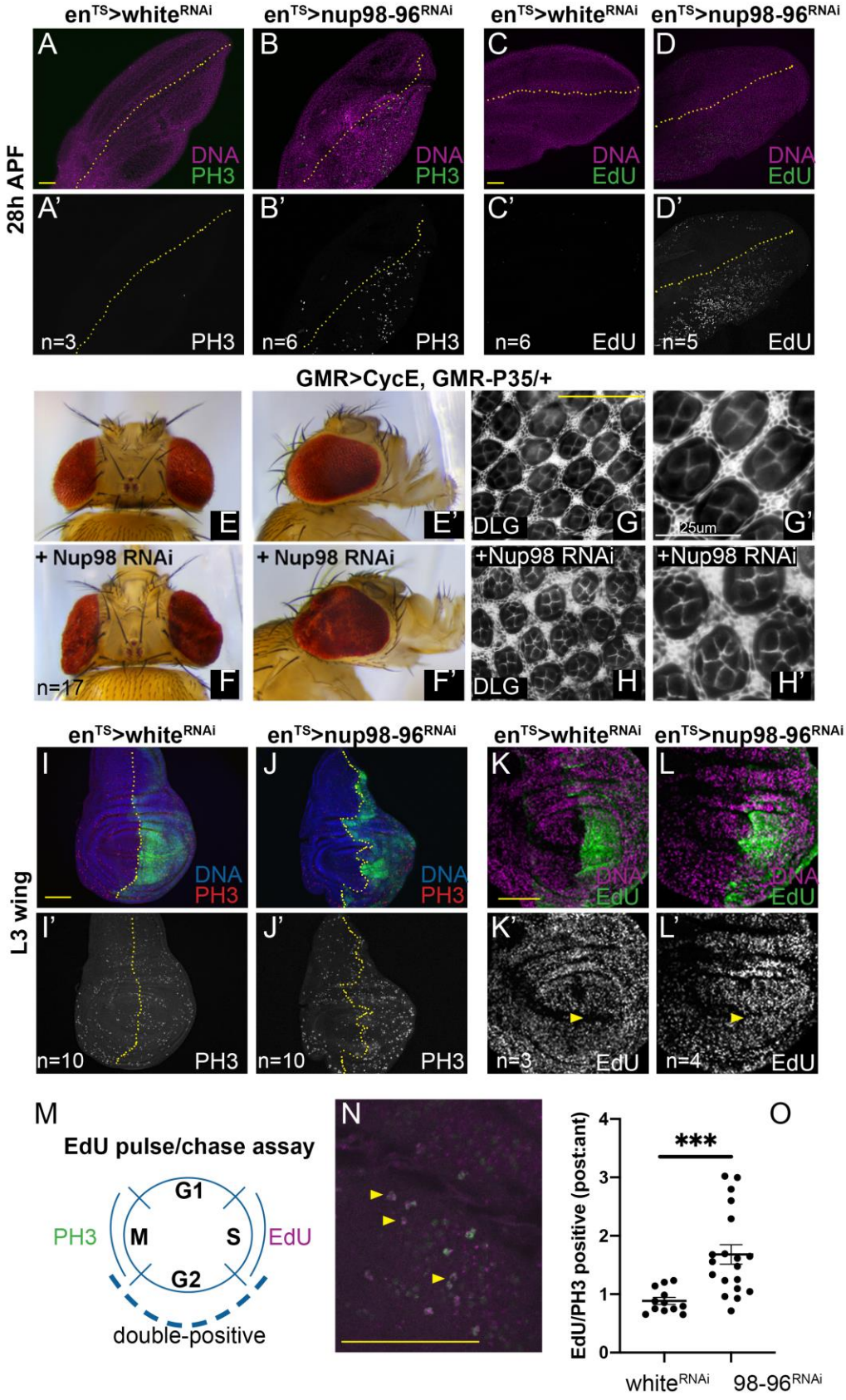
en^TS>white^RNAi
en^TS>nup98-96^RNAi
en^TS>white^RNAi
en^TS>nup98-96^RNAi
28h APF
A
B
C
D
DNA
PH3
DNA
EdU
A'
B'
C'
D'
n=3
PH3
n=6
PH3
n=6
EdU
n=5
EdU
GMR>CycE, GMR-P35/+
E
E'
DLG
G
25um
G'
+ Nup98 RNAi
+ Nup98 RNAi
+Nup98 RNAi
+Nup98 RNAi
n=17
F
F'
DLG
H
H'
en^TS>white^RNAi
en^TS>nup98-96^RNAi
en^TS>white^RNAi
en^TS>nup98-96^RNAi
L3 wing
I
J
K
L
DNA
PH3
DNA
EdU
I'
J'
K'
L'
n=10
PH3
n=10
PH3
n=3
EdU
n=4
EdU
M
EdU pulse/chase assay
G1
PH3
M
S
EdU
G2
double-positive
N
O
EdU/PH3 positive (post:ant)
***
4
3
2
1
0
white^RNAi
98-96^RNAi

Figure 3-1 Inhibition of Nup98-96 leads to G1 bypass and cell cycle de-regulation (A-D) Using *engrailed-Gal4* modified with a temperature sensitive Gal80 (*en*^{TS}), the indicated UAS-RNAis were expressed in the posterior wing disc from mid L3 to 28h after puparium formation (APF) at 28°C. The dotted line indicates the pupal wing anterior/posterior boundary. Nup98-96 inhibition increased the number of mitoses (indicated by phospho-Ser10 histone H3, PH3) and S-phases indicated by 5-ethynyl-2-deoxyuridine (EdU) labeling in the posterior wing, at stages when the wing is normally post-mitotic. (E) Adult eyes from a heterozygous sensitized background expressing *UAS-cyclin E* (*cycE*) under the *GMR-Gal4* promoter and *GMR*-driven *P35* is shown. (F) Adding in *UAS-Nup98-96* RNAi enhanced eye size and folding, (G,H) and increased the number of cone cells and interommatidial cells as shown by staining for the septate junction protein Discs large (Dlg). (I-L) Using *en*^{TS}, the indicated *UAS*-RNAis were expressed in the posterior wing disc for 72h prior to dissection of wandering L3. The dotted line indicates the anterior/posterior boundary. Nup98-96 inhibition increased the number of mitoses and S-phases in the posterior wing disc. The EdU experiment was performed multiple times with 5, 10 or 20 min of EdU labeling. Data and number of replicates from 5 min of EdU labeling is shown. A yellow arrowhead in K'-L' indicates the posterior zone of non-proliferating cells (ZNC) which is normally G1 arrested, but undergoes S-phases when Nup98-96 is knocked down. (M-O) An EdU pulse for 1 h followed by a 7h chase and PH3 staining was used to label mid L3 wing disc cells that progress from S-M phase in ~8h. This experiment was repeated 3 times, with intervals of 6h,7h,and 8h chase. (N) An example of a PH3 (green)/ EdU (magenta) double labeled disc is shown. (O) Quantification of double labeled cells in the posterior: anterior

compartments normalizes for EdU incorporation in each disc and provides an indication of cell cycling speed differences between compartments. RNAi to Nup98-96 increased cycling speed in the posterior wing disc. ($P<0.024$; t-test with Welch's correction). Yellow bar = 50 µm

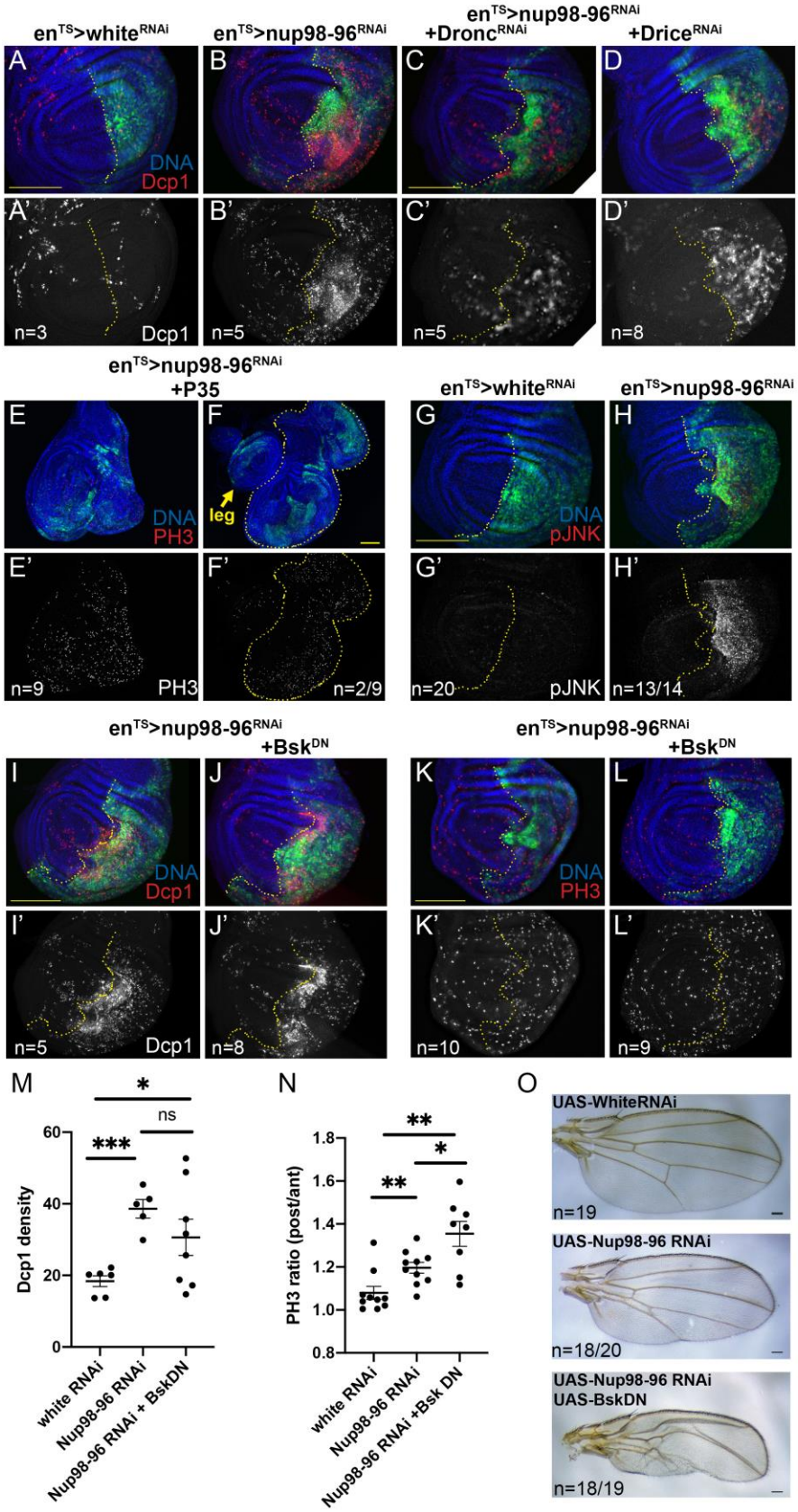
en^TS>white^RNAi
en^TS>nup98-96^RNAi
en^TS>nup98-96^RNAi +Dronc^RNAi
+Dronc^RNAi
en^TS>nup98-96^RNAi +Drice^RNAi
+Drice^RNAi
A
B
C
D
DNA
Dcp1
A'
B'
C'
D'
n=3
Dcp1
n=5
n=5
n=8
en^TS>nup98-96^RNAi +P35
+P35
E
F
G
H
DNA
PH3
leg
DNA
pJNK
E'
F'
G'
H'
n=9
PH3
n=2/9
n=20
pJNK
n=13/14
en^TS>nup98-96^RNAi +Bsk^DN
+Bsk^DN
I
J
K
L
DNA
Dcp1
DNA
PH3
I'
J'
K'
L'
n=5
Dcp1
n=8
n=10
n=9
M
Dcp1 density
60
40
20
0
*
ns
***
white RNAi
Nup98-96 RNAi
Nup98-96 RNAi + BskDN
N
PH3 ratio (post/ant)
1.8
1.6
1.4
1.2
1.0
0.8
**
*
**
white RNAi
Nup98-96 RNAi
Nup98-96 RNAi +Bsk DN
O
UAS-WhiteRNAi
n=19
UAS-Nup98-96 RNAi
n=18/20
UAS-Nup98-96 RNAi
UAS-BskDN
n=18/19

Figure 3-2 Inhibition of Nup98-96 leads to cell death and compensatory proliferation (A-L) Using *en*^{TS}, the indicated *UAS*-RNAis were expressed in the posterior wing disc for 72h prior to dissection of wandering L3 (unless otherwise indicated). The dotted line indicates the anterior/posterior boundary. (A-D) Nup98-96 inhibition increased apoptosis in the posterior disc, as indicated by cleaved Death Caspase-1 (Dcp1). (E-F) Co-expression of *UAS-P35* with *Nup98-96 RNAi* lead to tissue overgrowth (E) and by day 5, wing pouch duplication (F). (G-H) Nup-98-96 knockdown led to activation of JNK signaling as detected by phosphorylated JNK staining (pJNK). (I-N) Co-expression of a dominant negative form of *Drosophila* JNK, *Basket* (*Bsk*^{DN}) had variable effects on Dcp1 staining and increased the ratio of PH3 labeling in posterior:anterior discs, although overall PH3 signal decreased with *Bsk*^{DN} (Supp. Fig. 2). (Welch's t-test comparisons, ns= not significant, *P<0.05, ** P<0.01, ***P<0.005.). Yellow bar = 100µm

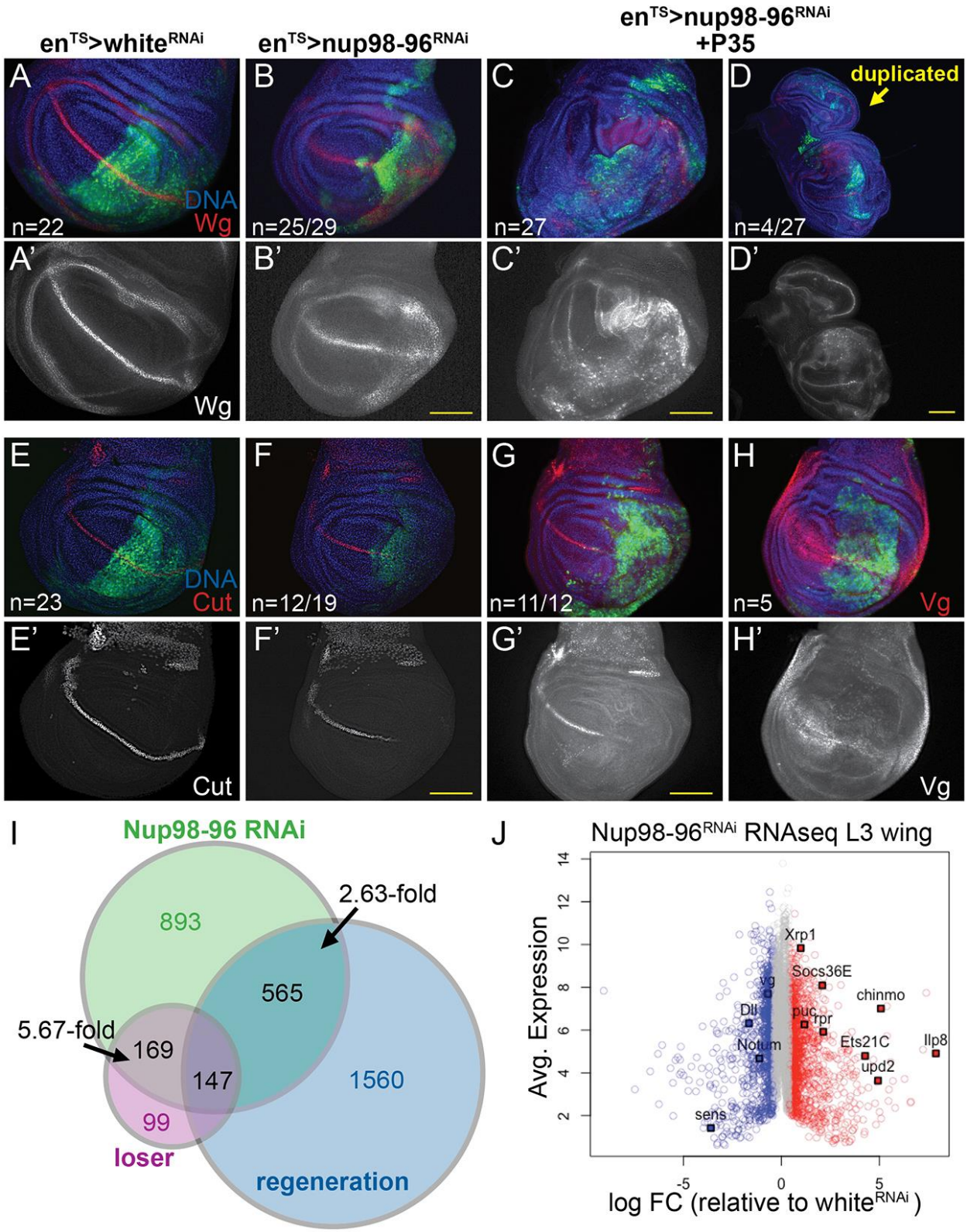
en^TS>white^RNAi
en^TS>nup98-96^RNAi
en^TS>nup98-96^RNAi +P35
A
B
C
D
duplicated
DNA
Wg
n=22
n=25/29
n=27
n=4/27
A'
B'
C'
D'
Wg
E
F
G
H
DNA
Cut
n=23
n=12/19
n=11/12
n=5
Vg
E'
F'
G'
H'
Cut
Vg
I
Nup98-96 RNAi
893
2.63-fold
565
5.67-fold
169
147
1560
99
loser
regeneration
J
Nup98-96^RNAi RNAseq L3 wing
Avg. Expression
log FC (relative to white^RNAi)
Xrp1
Socs36E
vg
chinmo
Dll
puc
rpr
Ets21C
Ilp8
Notum
upd2
sens

Figure 3-3. Inhibition of Nup98-96 leads to mis-patterning and gene expression changes associated with wounding and a “loser” phenotype

(A-H) Using *en*^{TS}, the indicated *UAS*-RNAis were expressed in the posterior wing disc for 72h prior to dissection of wandering L3 (unless otherwise indicated). Discs in C, D, G and H co-express P35 to block apoptosis and allow for tissue overgrowth. Samples in C and D were dissected after 5 days of *Nup98-96 RNAi+P35* expression. (A-D) Wg levels are disrupted at the Dorso-Ventral (DV) margin but increased at the dorsal hinge upon Nup98-96 knockdown. The effect on Wg and wing disc overgrowth is enhanced with P35. (E-G) Cut expression at the DV margin is disrupted by Nup98-96 knockdown, independent of P35 expression. (H) Vestigial (Vg) is reduced when Nup98-96 is knocked down. (I-J) RNAseq was performed on dissected late L3 wing discs expressing UAS-Nup98-96 or white RNAi for 72h, driven by *apterous*-Gal4 with *tub-Gal80*^{TS} *(ap*^{TS}*)*. (I) A comparison of the overlap of genes significantly altered by *Nup98-96 RNAi* (0.5-$\log_2$fold or more) to previously published "wounding" and "loser" gene expression signatures in wings. The fold-enrichment in the overlap of genes, above that expected by chance is shown. (J) An M-A plot of the RNAseq data with significantly increased expression indicated in red, and significantly decreased expression in blue. Genes in grey are not significantly altered. Yellow bar = 100µm.

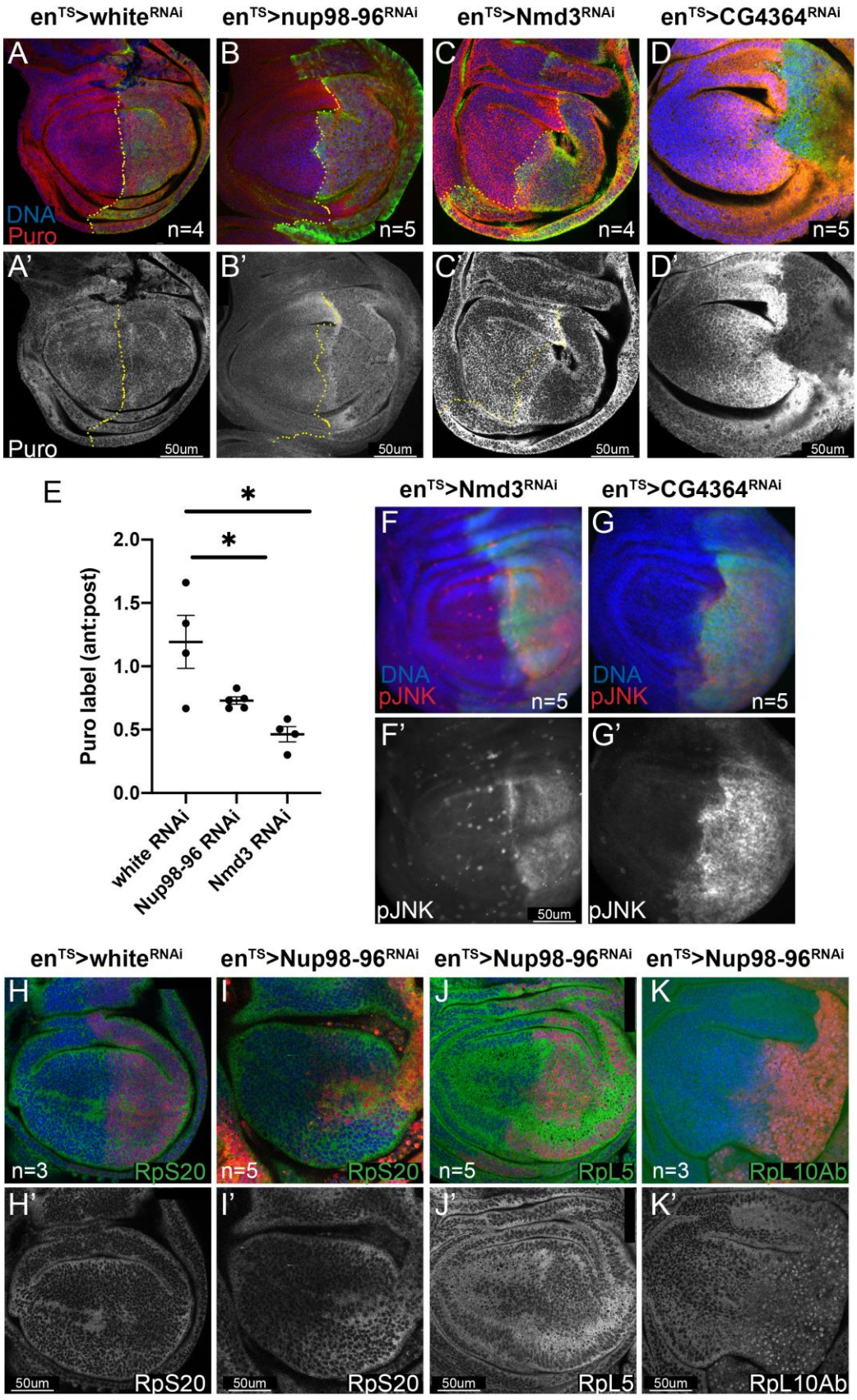
en^TS>white^RNAi
en^TS>nup98-96^RNAi
en^TS>Nmd3^RNAi
en^TS>CG4364^RNAi
A
B
C
D
DNA
Puro
n=4
n=5
n=4
n=5
A'
B'
C'
D'
Puro
50um
50um
50um
50um
E
*
*
2.0
1.5
1.0
0.5
0.0
Puro label (ant:post)
white RNAi
Nup98-96 RNAi
Nmd3 RNAi
en^TS>Nmd3^RNAi
en^TS>CG4364^RNAi
F
G
DNA
pJNK
n=5
n=5
F'
G'
pJNK
50um
pJNK
en^TS>white^RNAi
en^TS>Nup98-96^RNAi
en^TS>Nup98-96^RNAi
en^TS>Nup98-96^RNAi
H
I
J
K
n=3
RpS20
n=5
RpS20
n=5
RpL5
n=3
RpL10Ab
H'
I'
J'
K'
50um
RpS20
50um
RpS20
50um
RpL5
50um
RpL10Ab

Figure 3-4 Knockdown of Nup98-96 leads to ribosomal protein mislocalization and compromised protein synthesis

(A-D) Using *en*^{TS}, the indicated *UAS*-RNAis were expressed in the posterior wing disc for 72h prior to dissection of wandering L3 and labeled for protein synthesis using O-propargyl-puromycin (puro) incorporation. Puro labeling experiments in discs were performed at multiple timepoints (10-20 min), data from one experiment with 12 min. of labeling is shown. (E) The ratio of anterior:posterior puro-labeling is used to normalize for puro incorporation. *Nup98-96* and *Nmd3* knockdown reduced puro labeling (*P<0.05, unpaired t-test). (F-G) Knockdown of *Nmd3* or *CG4364* (Pescadillo homolog) for 48h in the posterior wing disc using *en*^{TS} activated JNK signaling. (H-K) Using *enRFP*^{TS}, the indicated *UAS*-RNAis were expressed for 72h in backgrounds expressing GFP or YFP-protein traps for the indicated Rp subunits. (K) RpL10Ab-YFP shows an aberrant nuclear enrichment when Nup98-96 is knocked down.

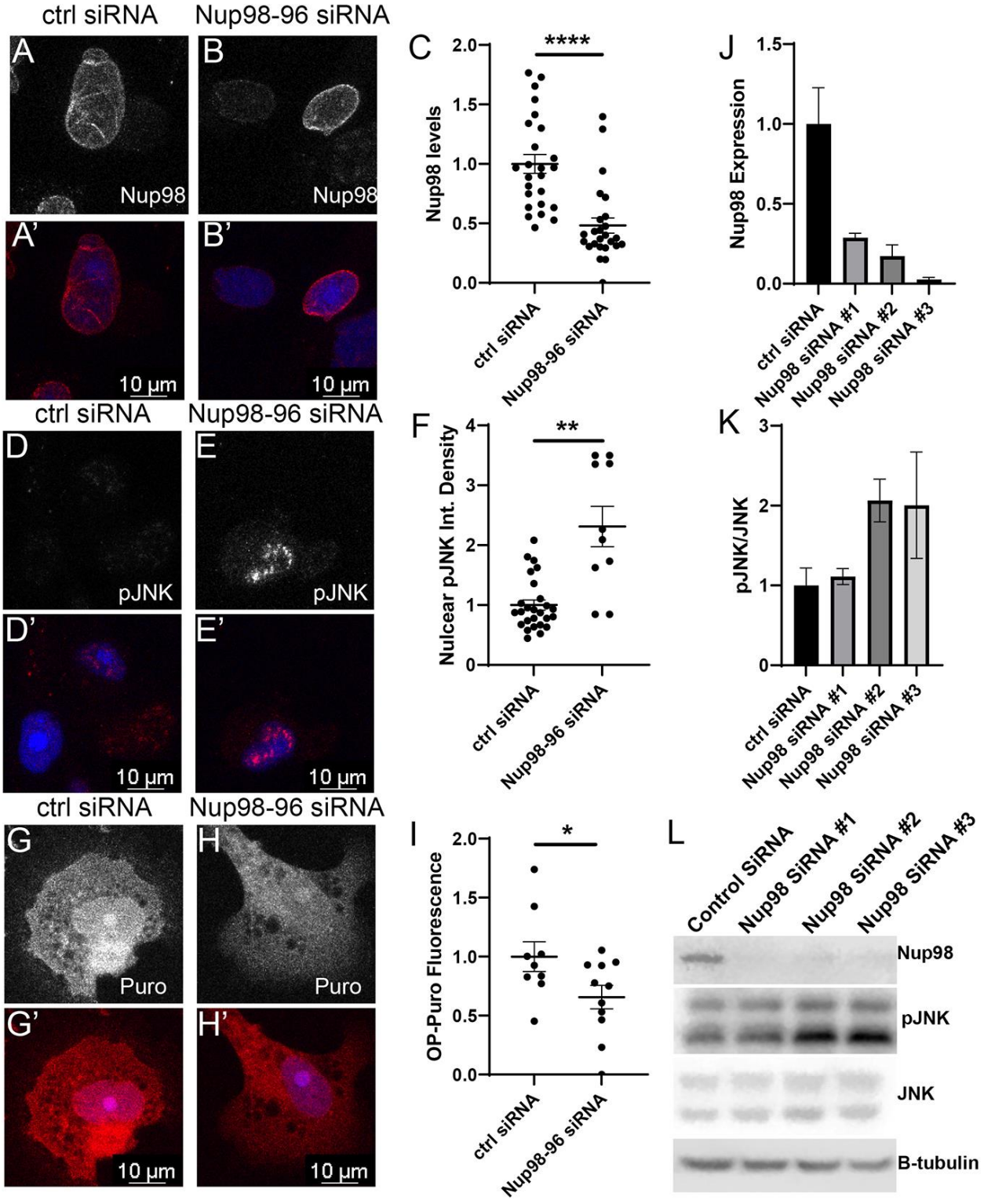

Figure 3-5. Knockdown of Nup98-96 in mammalian cells leads to reduced protein synthesis and JNK signaling

(A-B, D-E, G-H) PC3 cells were treated with small interfering (si) RNAs for 72h and cells were either fixed and stained with anti-Nup98 antibody (A-B), or phospho-JNK (D-E), or labeled with puro for 12 minutes (G-H). Control siRNA (Ctrl) is a scrambled siRNA. Nup98 siRNA reduces Nup98 levels (C) as well as reduced protein synthesis (F) and increases pJNK labeling (I). Western blot analysis on PC3 cells treated with Ctrl and Nup98 siRNAs (L) shows Nup98 siRNAs reduced the protein level of Nup98 (J) as well as increases phosphorylated JNK (K). Quantifications of fluorescence were performed on individual cells from at least two independent experiments. Quantifications for the western were done in triplicates for 3 different sets of siRNAs****P<0.0001, ***P<0.001, **P<0.01, *P<0.05 by unpaired t-tests, (G) uses Welch's correction for unequal sample size.

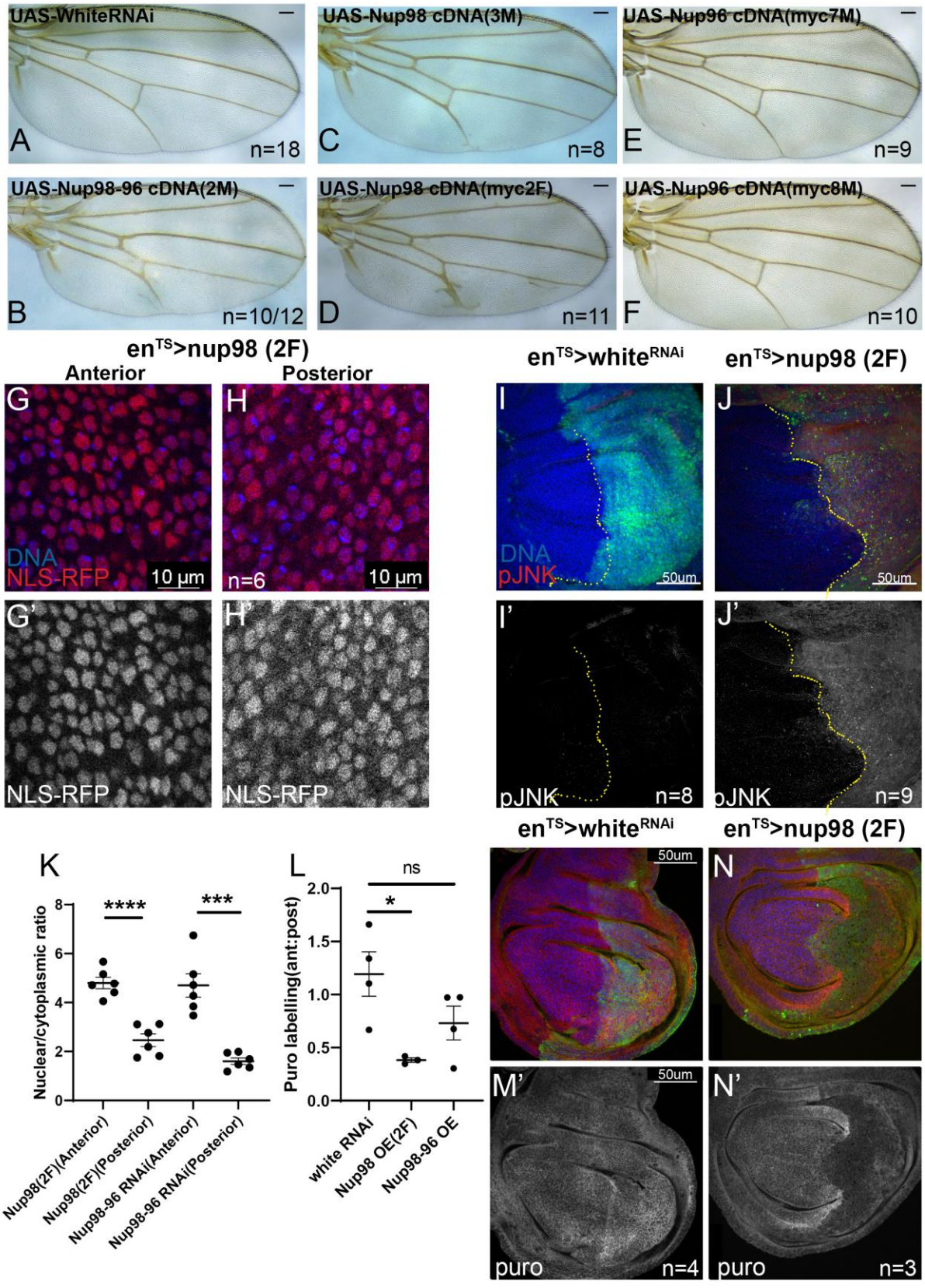
UAS-WhiteRNAi
A
n=18
UAS-Nup98 cDNA(3M)
C
n=8
UAS-Nup96 cDNA(myc7M)
E
n=9
UAS-Nup98-96 cDNA(2M)
B
n=10/12
UAS-Nup98 cDNA(myc2F)
D
n=11
UAS-Nup96 cDNA(myc8M)
F
n=10
en^TS>nup98 (2F)
Anterior
Posterior
G
H
DNA
NLS-RFP
10 µm
n=6
G'
H'
NLS-RFP
en^TS>white^RNAi
en^TS>nup98 (2F)
I
J
DNA
pJNK
50um
I'
J'
pJNK
n=8
n=9
K
Nuclear/cytoplasmic ratio
****
***
Nup98(2F)(Anterior)
Nup98(2F)(Posterior)
Nup98-96 RNAi(Anterior)
Nup98-96 RNAi(Posterior)
L
Puro labelling(ant:post)
ns
*
white RNAi
Nup98 OE(2F)
Nup98-96 OE
en^TS>white^RNAi
en^TS>nup98 (2F)
50um
N
M'
N'
puro
n=4
n=3

Figure 3-6 Overexpression of Nup98 disrupts protein synthesis and activates JNK signaling

(A-F) Using *en*^{TS}, the indicated *UAS*-cDNA constructs were expressed in the posterior wing from mid-L2 and adult wings were mounted. Overexpression of Nup96 had no effect on the posterior wing while overexpression of Nup98 or Nup98-96 reduced posterior wing size and disrupted vein patterning. (G-H) Using *en*^{TS} a ubiquitous-RFP-NLS was expressed with *UAS-Nup98* 2F for 24h. The nuclear:cytoplasmic ratio for RFP-NLS was quantified and shown for the anterior wing disc (no Nup98 expression) and posterior wing disc (Nup98 overexpression). Ratios are also provided for *Nup98-96 RNAi* (from Supp. Fig 4) for comparison. (I-J) Using *en*^{TS}, *Nup98-96* cDNA was expressed in the posterior wing disc for 72h prior to dissection of wandering L3 and labeling with pJNK. UAS-*white* RNAi serves as a negative control showing endogenous pJNK at this stage is very low. (K-M) Using *en*^{TS}, the indicated *UAS*-cDNA or RNAi was expressed for 72h prior to dissection and labeling with puro to measure protein synthesis. Overexpression of Nup98 2F reduced protein synthesis in the posterior disc, which Nup98-96 overexpression had a milder effect. (*P<0.05 by unpaired t-test).

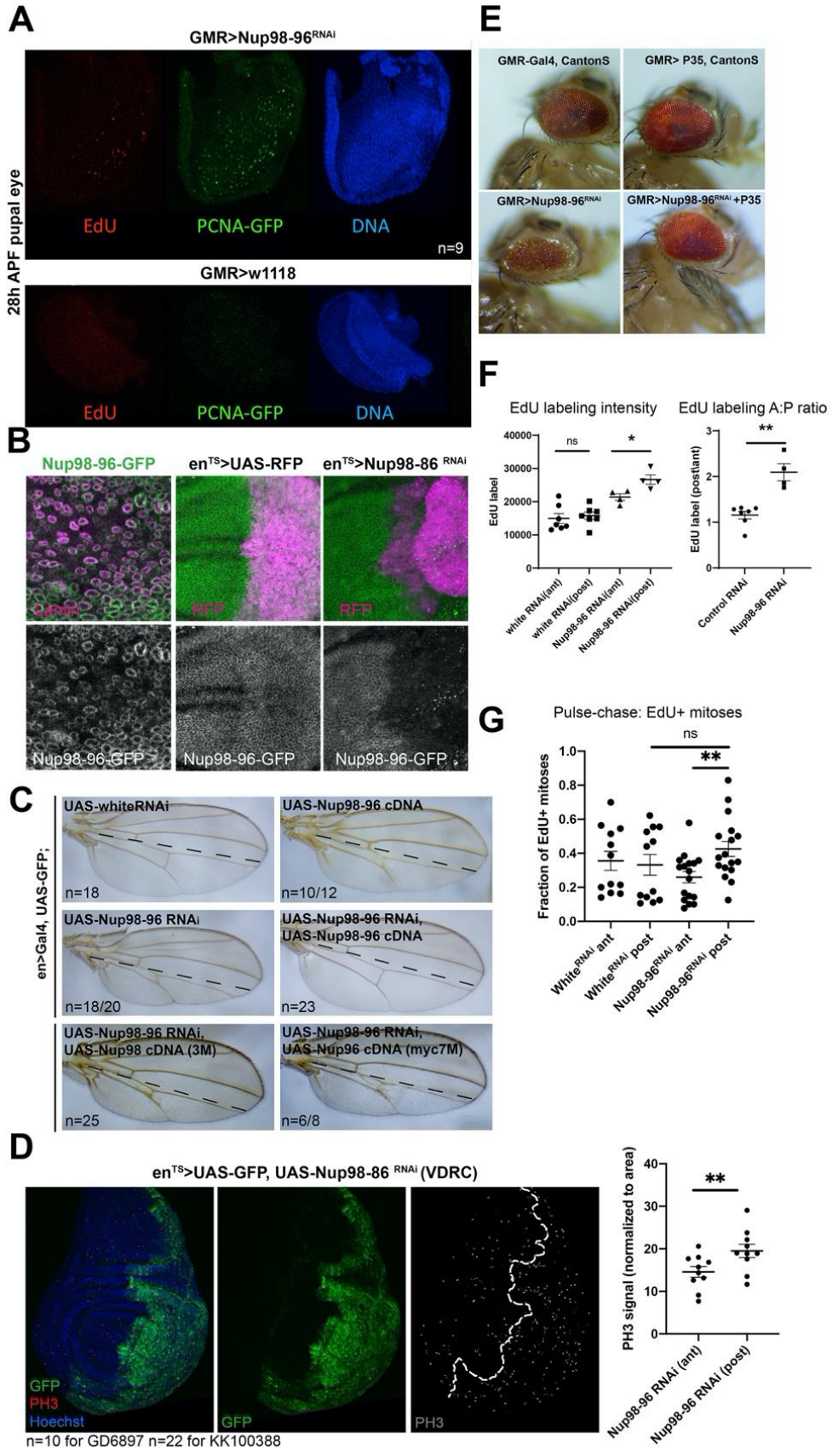
A
GMR>Nup98-96RNAi
28h APF pupal eye
EdU
PCNA-GFP
DNA
n=9
GMR>w1118
EdU
PCNA-GFP
DNA
E
GMR-Gal4, CantonS
GMR> P35, CantonS
GMR>Nup98-96RNAi
GMR>Nup98-96RNAi +P35
F
EdU labeling intensity
EdU label
ns
*
white RNAi(ant)
white RNAi(post)
Nup98-96 RNAi(ant)
Nup98-96 RNAi(post)
EdU labeling A:P ratio
EdU label (post/ant)
**
Control RNAi
Nup98-96 RNAi
B
Nup98-96-GFP
enTS>UAS-RFP
enTS>Nup98-86 RNAi
CamR
RFP
RFP
Nup98-96-GFP
Nup98-96-GFP
Nup98-96-GFP
G
Pulse-chase: EdU+ mitoses
ns
**
Fraction of EdU+ mitoses
WhiteRNAi ant
WhiteRNAi post
Nup98-96RNAi ant
Nup98-96RNAi post
C
en>Gal4, UAS-GFP;
UAS-whiteRNAi
n=18
UAS-Nup98-96 cDNA
n=10/12
UAS-Nup98-96 RNAi
n=18/20
UAS-Nup98-96 RNAi, UAS-Nup98-96 cDNA
n=23
UAS-Nup98-96 RNAi, UAS-Nup98 cDNA (3M)
n=25
UAS-Nup98-96 RNAi, UAS-Nup96 cDNA (myc7M)
n=6/8
D
enTS>UAS-GFP, UAS-Nup98-86 RNAi (VDRC)
GFP
PH3
Hoechst
GFP
PH3
n=10 for GD6897 n=22 for KK100388
PH3 signal (normalized to area)
**
Nup98-96 RNAi (ant)
Nup98-96 RNAi (post)

Supplemental Figure 3-1 Nup98-96 knockdown leads to delay in cell cycle exit and increased proliferation.

(A) 28h APF pupal eyes were labeled for 2h with EdU to detect S-phase and stained for GFP to detect PCNA promoter driven GFP. S-phases and PCNA promoter activity is evident when RNAi to Nup98-96 is driven with GMR-Gal4. GMR-Gal4 without any RNAi (in a w1118 background) serves as a control. Genotypes are: (top) w; GMR-Gal4 /+; UAS-Nup98-96 RNAi (TRiP)/PCNA prom-GFP (bottom) w; GMR-Gal4/+; PCNA prom-GFP/+.

(B) Nup98-96-GFP is from the FlyFos collection containing a Fosmid on II with Nup98-96 coding region plus regulatory DNA and a GFP tag (Sarov et al., 2016) We confirmed this line exhibits the expected ubiquitous nuclear envelop labeling by co-staining with Lamin Dm0. (Right) We co-expressed Nup98-96-GFP in a background with en-Gal4 driving RFP alone or RFP in combination with UAS-Nup98-96 RNAi (TRiP), we confirmed effective knockdown of Nup98-96-GFP in the en-Gal4 expressing domain. Genotypes are: (left) w; Nup98-96-GFP; + (middle) w; Nup98-96-GFP/ enGal4, UAS-RFP; + (right) w; Nup98-96-GFP/ enGal4, UAS-RFP; UAS-Nup98-96 RNAi (TRiP)/+.

(C) cDNA rescue constructs providing UAS-Nup98, UAS-Nup96 or UAS-Nup98-96 were tested for the ability to rescue the wing phenotypes caused by Nup98-96 RNAi. Only expression of both Nup98 and Nup96 (middle right) fully rescued posterior wing size. Note that over-expression of both Nup98 and Nup96 without RNAi also led to reduced posterior wing size (see Fig. 6). Genotypes are: (top left) w; en-Gal4, UAS-GFP/+; UAS-white RNAi (TRiP)/+ (top right) w; en-Gal4, UAS-GFP/+; UAS-Nup98-96 (middle left) w; en-Gal4, UAS-GFP/UAS-Nup98-96 RNAi (VDRC GD); UAS-white RNAi (TRiP)/+ (middle right) w; en-Gal4, UAS-GFP/UAS-Nup98-96 RNAi (VDRC GD); UASNup98-96 cDNA/+ (bottom left) w; en-Gal4, UAS-GFP/UAS-Nup98-96 RNAi (VDRC GD); UAS-Nup98 cDNA 3M/+ (bottom right) w; en-Gal4, UAS-GFP/UAS-Nup98-96 RNAi (VDRC GD); UAS-Nup96 cDNA 7M/+.

(D) Two independent RNAi lines from the VDRC gave similar phenotypes to the TRiP RNAi in the larval wing disc. Line GD6897 is shown at wandering L3 after 72h of expression at 28°C with PH3 labeling for mitoses. Genotype: w; en-Gal4, UAS-GFP; UAS-Nup98-96 RNAi GD6897; Tub-Gal80TS/ +.

(E) Related to EdU pulse-chase experiment in Fig. 1M. Quantification of double-labeled EdU/PH3 cells in posterior wing discs. Genotypes: w; en-Gal4, UAS-GFP/ + ; Tub-Gal80TS/ UAS-white RNAi or w; en-Gal4, UAS-GFP/ + ; Tub-Gal80TS/ UAS-Nup98-96 RNAi.

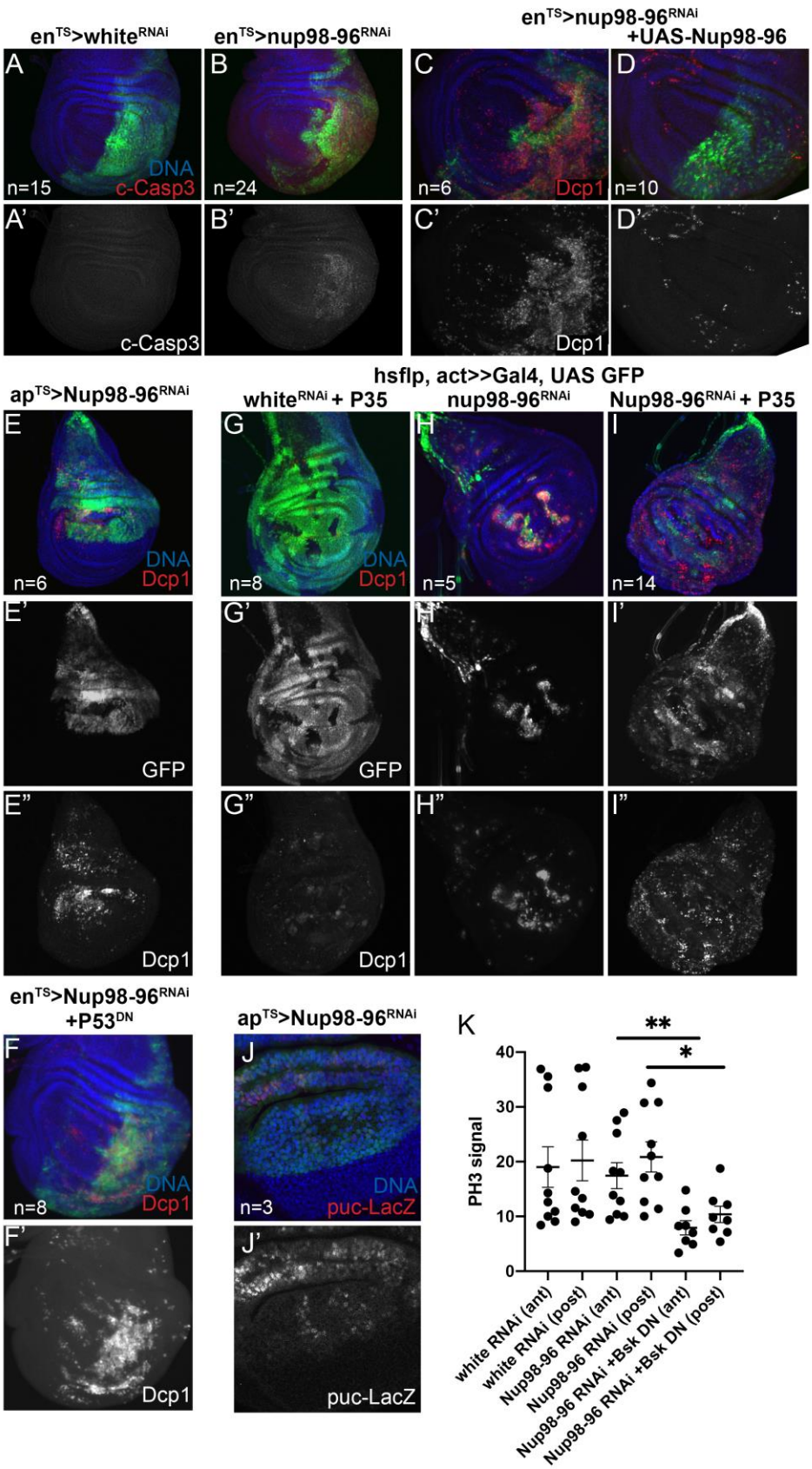
en^TS>white^RNAi
en^TS>nup98-96^RNAi
en^TS>nup98-96^RNAi +UAS-Nup98-96
A
B
C
D
DNA
c-Casp3
n=15
n=24
n=6
Dcp1
n=10
A'
B'
C'
D'
c-Casp3
Dcp1
hsflp, act>>Gal4, UAS GFP
ap^TS>Nup98-96^RNAi
white^RNAi + P35
nup98-96^RNAi
Nup98-96^RNAi + P35
E
G
H
I
DNA
Dcp1
n=6
n=8
n=5
n=14
E'
G'
H'
I'
GFP
E"
G"
H"
I"
Dcp1
en^TS>Nup98-96^RNAi +P53^DN
ap^TS>Nup98-96^RNAi
F
J
DNA
Dcp1
n=8
DNA
puc-LacZ
n=3
F'
J'
Dcp1
puc-LacZ
K
**
*
PH3 signal
40
30
20
10
0
white RNAi (ant)
white RNAi (post)
Nup98-96 RNAi (ant)
Nup98-96 RNAi (post)
Nup98-96 RNAi +Bsk DN (ant)
Nup98-96 RNAi +Bsk DN (post)

Supplemental Figure 3-2 Nup98-96 knockdown leads to apoptosis which is rescued by co-expression of UAS-Nup98-96 cDNA.

The indicated transgenes were driven by *en-Gal4*, with *UAS GFP* for 72h prior to dissection using *Gal80^{TS}*. (A,B) Cleaved caspase 3 labeling indicates apoptosis in the posterior compartment when Nup98-96 is knocked down. (C, D) Co-expression of *Nup98-96* cDNA rescues the apoptosis caused by Nup98-96 knock-down, as assessed with Dcp-1. (E) Expression of *Nup98-96 RNAi* in the dorsal compartment (using *ap-Gal4, UAS-GFP; tub-Gal80^{TS}*) also leads to apoptosis. (F-H) Expression of *Nup98-96 RNAi* in clones throughout the wing pouch (using *hs-flp* with *act>stop>-Gal4, UAS-GFP*) also leads to apoptosis within clones, while co-expression with *P35* (using *hs-flp* with *act>stop>-Gal4, UAS-GFP, UAS-P35*) suppresses apoptosis within clones and leads to apoptosis outside of clones expressing *Nup98-96 RNAi*. (I) Expression of *Nup98-96 RNAi* in the dorsal compartment (using *ap-Gal4, UAS-GFP; tub-Gal80^{TS}*) leads to upegulation of *puc-LacZ* expression (from *puc^{e69}* allele), a hallmark of JNK signaling. (J) Quantifications of PH3 signal broken down by ant/post compartment. *Nup98-96 RNAi* and *Bsk DN* are expressed only in the posterior using *en-Gal4, UAS-GFP; tub-Gal80^{TS}*. Note that overall PH3 labeling is reduced in both compartments when JNK signaling is inhibited with *Bsk DN*.

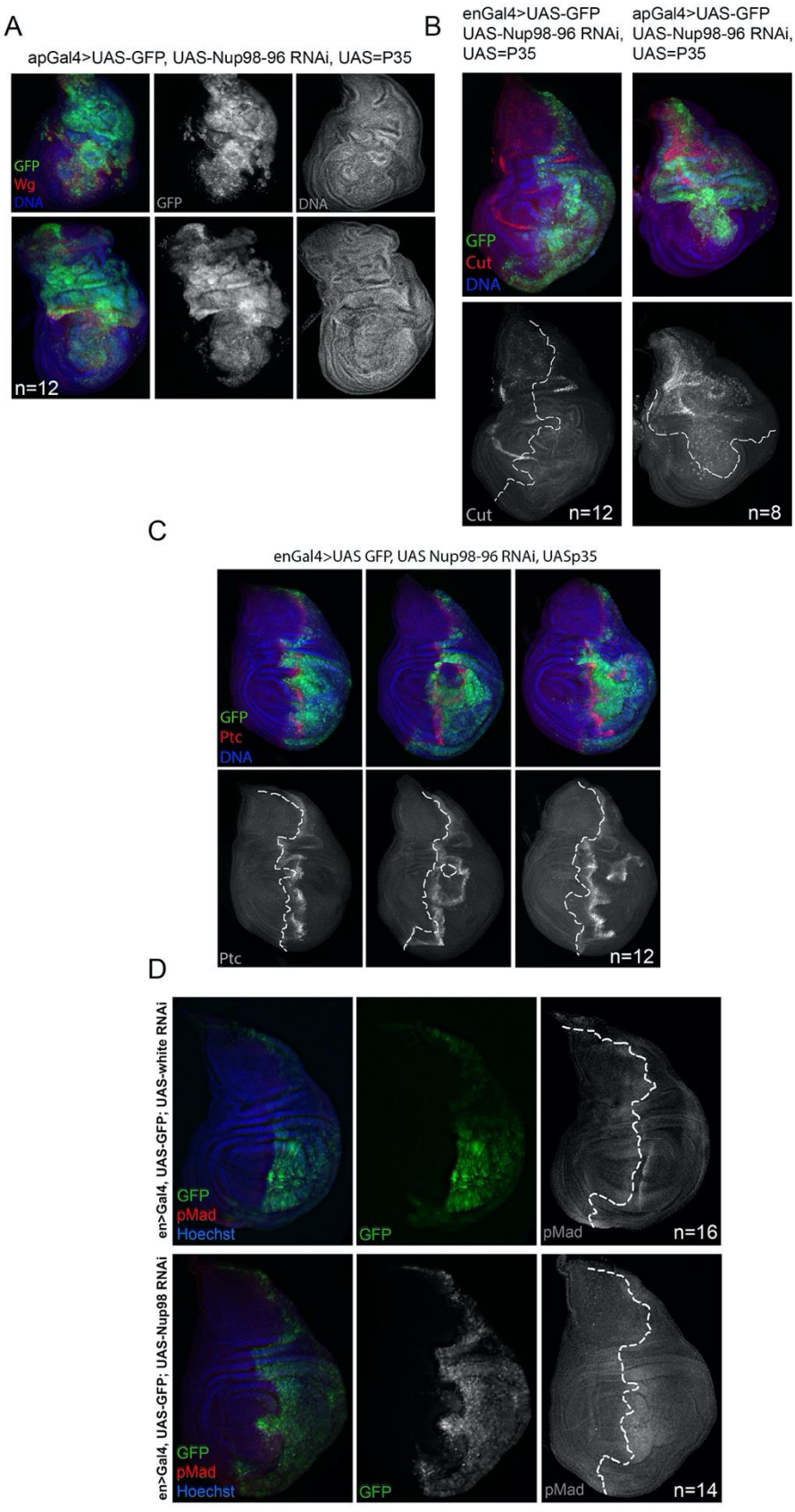
A
apGal4>UAS-GFP, UAS-Nup98-96 RNAi, UAS=P35
GFP
Wg
DNA
GFP
DNA
n=12
B
enGal4>UAS-GFP
UAS-Nup98-96 RNAi,
UAS=P35
apGal4>UAS-GFP
UAS-Nup98-96 RNAi,
UAS=P35
GFP
Cut
DNA
Cut
n=12
n=8
C
enGal4>UAS GFP, UAS Nup98-96 RNAi, UASp35
GFP
Ptc
DNA
Ptc
n=12
D
en>Gal4, UAS-GFP; UAS-white RNAi
GFP
pMad
Hoechst
GFP
pMad
n=16
en>Gal4, UAS-GFP; UAS-Nup98 RNAi
GFP
pMad
Hoechst
GFP
pMad
n=14

Supplemental Figure 3-3 Knockdown of Nup98-96 leads to wing disc overgrowth and patterning defects consistent with apoptosis-induced proliferation.

(A) Expression of *Nup98-96 RNAi* in the dorsal compartment with *UAS-P35* for 5d (using *ap-Gal4, UAS-GFP/ UAS-P35; tub-Gal80^{TS}*) leads to tissue folding, overgrowth and invasion across the D-V boundary as well as ectopic Wg expression.
(B) Expression of *Nup98-96 RNAi* + *P35* in the posterior compartment (with *en-Gal4*, left) or dorsal compartment (with *ap-Gal4*, right) abolishes Cut expression at the D-V boundary.
(C) Expression of *Nup98-96 RNAi* in the posterior compartment with *UAS-P35* for 4d (using *en-Gal4, UAS-GFP/ UAS-P35; tub-Gal80^{TS}*) leads to tissue folding and invasion at the A-P boundary as well as ectopic Ptc expression demonstrating mis-patterning.
(D) Normal pMad staining is shown (top) for *en-Gal4, UAS-GFP; tub-Gal80^{TS}* driving *white* RNAi. (bottom) *Nup98-96 RNAi* expression driven by *en-Gal4, UAS-GFP; tub-Gal80^{TS}* leads to broad pMad staining in the posterior compartment indicating mis-patterning.

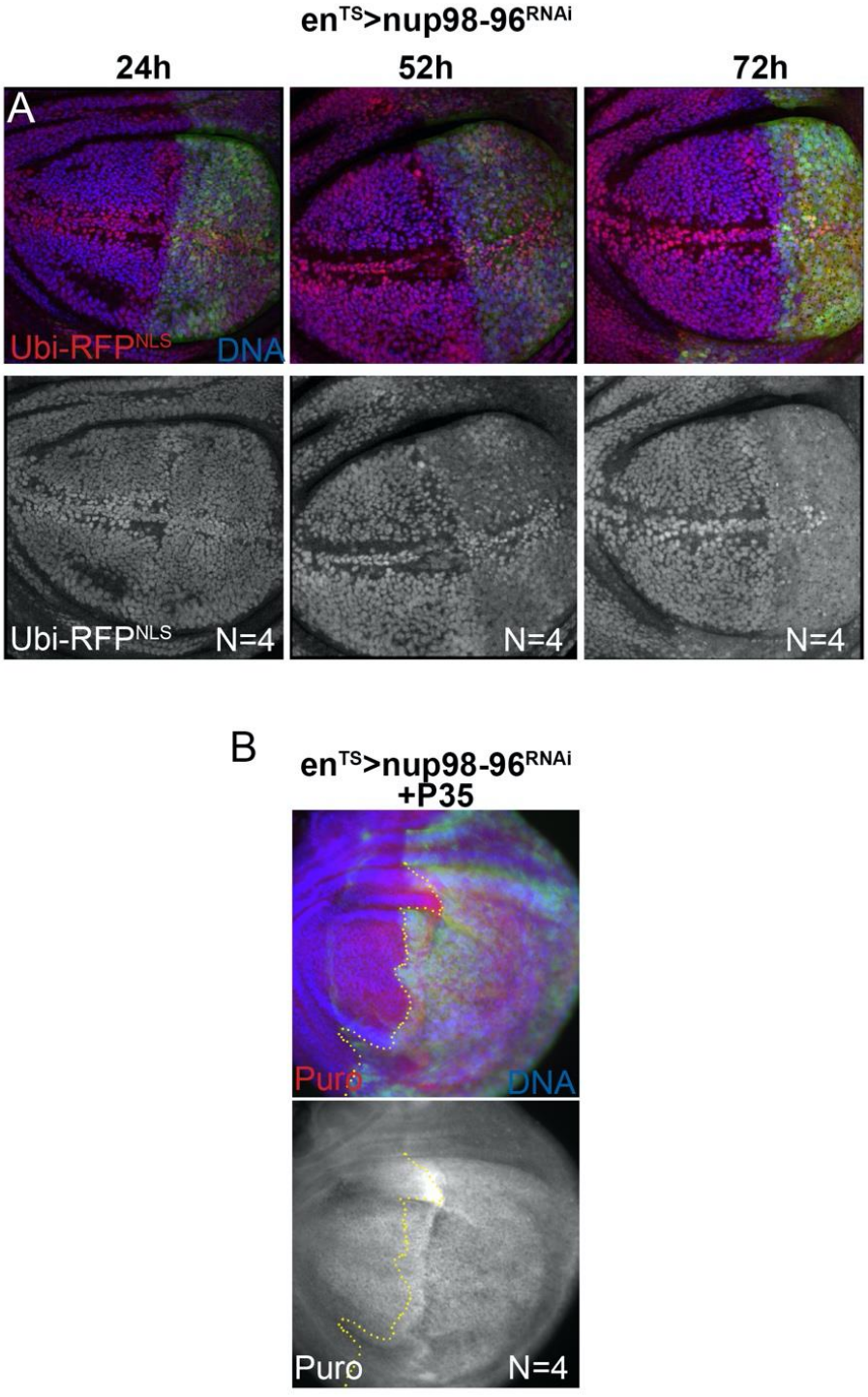

Supplemental Figure 3-4 Knockdown of Nup98-96 disrupts nucleo-cytoplasmic localization and reduces protein synthesis independent of apoptosis.

(A) *Nup 98-96 RNAi* was expressed in the posterior compartment using *en-Gal4, UAS-GFP; tub-Gal80^{TS}* in a background expressing *Ubiquitin* promoter driven-*RFP* with a nuclear localization signal (Ubi-RFP^{NLS}) at 27°C to minimize cell lethality. By 52h of Nup98-96 knockdown, nuclear localization of RFP is visibly disrupted. By 72h of knockdown nuclear localization of Ubi-RFP^{NLS} is nearly abolished.

(B) Co-expression of *UAS-P35* with *Nup 98-96 RNAi* did not rescue the reduction in protein synthesis when Nup98-96 is compromised. This suggests the reduced proteins synthesis is not a consequence of apoptosis.

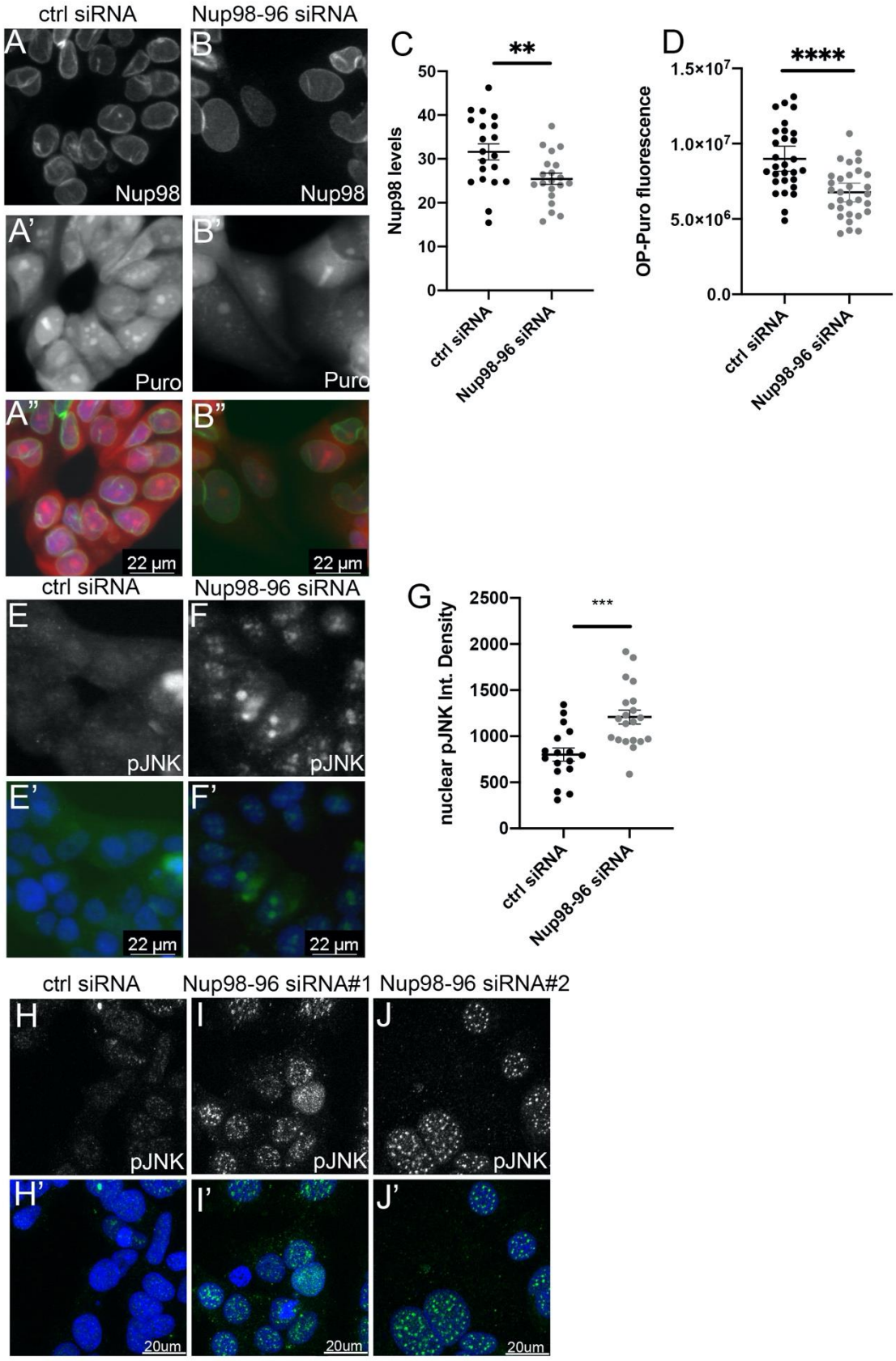
ctrl siRNA
Nup98-96 siRNA
A
B
Nup98
A'
B'
Puro
A"
B"
22 µm
C
**
Nup98 levels
50
40
30
20
10
0
ctrl siRNA
Nup98-96 siRNA
D
****
OP-Puro fluorescence
1.5×10^7
1.0×10^7
5.0×10^6
0.0
ctrl siRNA
Nup98-96 siRNA
ctrl siRNA
Nup98-96 siRNA
E
F
pJNK
E'
F'
22 µm
G
***
nuclear pJNK Int. Density
2500
2000
1500
1000
500
0
ctrl siRNA
Nup98-96 siRNA
ctrl siRNA
Nup98-96 siRNA#1
Nup98-96 siRNA#2
H
I
J
pJNK
H'
I'
J'
20um

Supplemental Figure 3-5 Knockdown of Nup98 in MCF7 cells leads to reduced protein synthesis and JNK phosphorylation.

(A-B, E-F) MCF7 cells were treated with small interfering (si) RNAs for 72h and cells were labeled with Puro(A'-B') or fixed and stained with anti-Nup98 antibody (A-B), or phospho-JNK (E-J). Control siRNA (Ctrl) is a scrambled siRNA. Nup98 siRNA reduces Nup98 levels (C) as well as reduced protein synthesis (D) and increases pJNK labeling (G). Quantifications of fluorescence were performed on individual cells from at least two experiments. ****P<0.0001, ***P<0.001, **P<0.01, *P<0.05 by unpaired t-tests, (G) uses Welch's correction for unequal sample size

3.6 Bibliography

Ahn, J. H., Davis, E. S., Daugird, T. A., Zhao, S., Quiroga, I. Y., Uryu, H., Li, J., Storey, A. J., Tsai, Y. H., Keeley, D. P., et al. (2021). Phase separation drives aberrant chromatin looping and cancer development. *Nature* 595, 591-595.

Akai, N., Ohsawa, S., Sando, Y. and Igaki, T. (2021). Epithelial cell-turnover ensures robust coordination of tissue growth in Drosophila ribosomal protein mutants. *PLoS Genet* 17, e1009300.

Amoyel, M., Anderson, A. M. and Bach, E. A. (2014). JAK/STAT pathway dysregulation in tumors: a Drosophila perspective. *Semin Cell Dev Biol* 28, 96-103.

Bachi, A., Braun, I. C., Rodrigues, J. P., Pante, N., Ribbeck, K., von Kobbe, C., Kutay, U., Wilm, M., Gorlich, D., Carmo-Fonseca, M., et al. (2000). The C-terminal

domain of TAP interacts with the nuclear pore complex and promotes export of specific CTE-bearing RNA substrates. *RNA* 6, 136-158.

Bandura, J. L., Jiang, H., Nickerson, D. W. and Edgar, B. A. (2013). The molecular chaperone Hsp90 is required for cell cycle exit in Drosophila melanogaster. *PLoS Genet* 9, e1003835.

Baonza, A., Roch, F. and Martin-Blanco, E. (2000). DER signaling restricts the boundaries of the wing field during Drosophila development. *Proc Natl Acad Sci U S A* 97, 7331-7335.

Baril, C., Gavory, G., Bidla, G., Knaevelsrud, H., Sauvageau, G. and Therrien, M. (2017). Human NUP98-HOXA9 promotes hyperplastic growth of hematopoietic tissues in Drosophila. *Dev Biol* 421, 16-26.

Baumgartner, M. E., Dinan, M. P., Langton, P. F., Kucinski, I. and Piddini, E. (2021). Proteotoxic stress is a driver of the loser status and cell competition. *Nat Cell Biol* 23, 136-146.

Bergantinos, C., Corominas, M. and Serras, F. (2010). Cell death-induced regeneration in wing imaginal discs requires JNK signalling. *Development* 137, 1169-1179.

Bordonaro, M., Drago, E., Atamna, W. and Lazarova, D. L. (2014). Comprehensive suppression of all apoptosis-induced proliferation pathways as a proposed approach to colorectal cancer prevention and therapy. *PLoS One* 9, e115068.

Braune, E. B. and Lendahl, U. (2016). Notch -- a goldilocks signaling pathway in disease and cancer therapy. *Discov Med* 21, 189-196.

Brodsky, M. H., Nordstrom, W., Tsang, G., Kwan, E., Rubin, G. M. and Abrams, J. M. (2000). Drosophila p53 binds a damage response element at the reaper locus. *Cell* 101, 103-113.

Brown, J. B., Boley, N., Eisman, R., May, G. E., Stoiber, M. H., Duff, M. O., Booth, B. W., Wen, J., Park, S., Suzuki, A. M., et al. (2014). Diversity and dynamics of the Drosophila transcriptome. *Nature* 512, 393-399.

Buttitta, L. A., Katzaroff, A. J. and Edgar, B. A. (2010). A robust cell cycle control mechanism limits E2F-induced proliferation of terminally differentiated cells in vivo. *J Cell Biol* 189, 981-996.

Buttitta, L. A., Katzaroff, A. J., Perez, C. L., de la Cruz, A. and Edgar, B. A. (2007). A double-assurance mechanism controls cell cycle exit upon terminal differentiation in Drosophila. *Dev Cell* 12, 631-643.

Capelson, M., Liang, Y., Schulte, R., Mair, W., Wagner, U. and Hetzer, M. W. (2010). Chromatin-bound nuclear pore components regulate gene expression in higher eukaryotes. *Cell* 140, 372-383.

Chaichanit, N., Wonglapsuwan, M. and Chotigeat, W. (2018). Ribosomal protein L10A and signaling pathway. *Gene* 674, 170-177.

Chakraborty, P., Wang, Y., Wei, J. H., van Deursen, J., Yu, H., Malureanu, L., Dasso, M., Forbes, D. J., Levy, D. E., Seemann, J., et al. (2008). Nucleoporin levels regulate cell cycle progression and phase-specific gene expression. *Dev Cell* 15, 657-667.

Cheng, G., Liu, F., Asai, T., Lai, F., Man, N., Xu, H., Chen, S., Greenblatt, S., Hamard, P. J., Ando, K., et al. (2017). Loss of p300 accelerates MDS-associated leukemogenesis. *Leukemia* 31, 1382-1390.

Choi, C. W., Chung, Y. J., Slape, C. and Aplan, P. D. (2008). Impaired differentiation and apoptosis of hematopoietic precursors in a mouse model of myelodysplastic syndrome. *Haematologica* 93, 1394-1397.

Colombani, J., Andersen, D. S. and Leopold, P. (2012). Secreted peptide Dilp8 coordinates Drosophila tissue growth with developmental timing. *Science* 336, 582-585.

de Celis, J. F., Garcia-Bellido, A. and Bray, S. J. (1996). Activation and function of Notch at the dorsal-ventral boundary of the wing imaginal disc. *Development* 122, 359-369.

Deliu, L. P., Ghosh, A. and Grewal, S. S. (2017). Investigation of protein synthesis in Drosophila larvae using puromycin labelling. *Biol Open* 6, 1229-1234.

Dimova, D. K., Stevaux, O., Frolov, M. V. and Dyson, N. J. (2003). Cell cycle-dependent and cell cycle-independent control of transcription by the Drosophila E2F/RB pathway. *Genes Dev* 17, 2308-2320.

Donato, A. L., Huang, Q., Liu, X., Li, F., Zimmerman, M. A. and Li, C. Y. (2014). Caspase 3 promotes surviving melanoma tumor cell growth after cytotoxic therapy. *J Invest Dermatol* 134, 1686-1692.

Dopie, J., Rajakyla, E. K., Joensuu, M. S., Huet, G., Ferrantelli, E., Xie, T., Jaalinoja, H., Jokitalo, E. and Vartiainen, M. K. (2015). Genome-wide RNAi screen for nuclear actin reveals a network of cofilin regulators. *J Cell Sci* 128, 2388-2400.

Duman-Scheel, M., Johnston, L. A. and Du, W. (2004). Repression of dMyc expression by Wingless promotes Rbf-induced G1 arrest in the presumptive Drosophila wing margin. *Proc Natl Acad Sci U S A* 101, 3857-3862.

Dvorak, H. F. (1986). Tumors: wounds that do not heal. Similarities between tumor stroma generation and wound healing. *N Engl J Med* 315, 1650-1659.

Fahrenkrog, B., Martinelli, V., Nilles, N., Fruhmann, G., Chatel, G., Juge, S., Sauder, U., Di Giacomo, D., Mecucci, C. and Schwaller, J. (2016). Expression of Leukemia-Associated Nup98 Fusion Proteins Generates an Aberrant Nuclear Envelope Phenotype. *PLoS One* 11, e0152321.

Faria, A. M., Levay, A., Wang, Y., Kamphorst, A. O., Rosa, M. L., Nussenzveig, D. R., Balkan, W., Chook, Y. M., Levy, D. E. and Fontoura, B. M. (2006). The nucleoporin Nup96 is required for proper expression of interferon-regulated proteins and functions. *Immunity* 24, 295-304.

Flegel, K., Grushko, O., Bolin, K., Griggs, E. and Buttitta, L. (2016). Roles for the Histone Modifying and Exchange Complex NuA4 in Cell Cycle Progression in Drosophila melanogaster. *Genetics* 203, 1265-1281.

Fogarty, C. E. and Bergmann, A. (2017). Killers creating new life: caspases drive apoptosis-induced proliferation in tissue repair and disease. *Cell Death Differ* 24, 1390-1400.

Fontoura, B. M., Blobel, G. and Matunis, M. J. (1999). A conserved biogenesis pathway for nucleoporins: proteolytic processing of a 186-kilodalton precursor generates Nup98 and the novel nucleoporin, Nup96. *J Cell Biol* 144, 1097-1112.

Forrester, A. M., Grabher, C., McBride, E. R., Boyd, E. R., Vigerstad, M. H., Edgar, A., Kai, F. B., Da'as, S. I., Payne, E., Look, A. T., et al. (2011). NUP98-HOXA9-transgenic zebrafish develop a myeloproliferative neoplasm and provide new insight into mechanisms of myeloid leukaemogenesis. *Br J Haematol* 155, 167-181.

Franks, T. M. and Hetzer, M. W. (2013). The role of Nup98 in transcription regulation in healthy and diseased cells. *Trends Cell Biol* 23, 112-117.

Gabriele, L., Phung, J., Fukumoto, J., Segal, D., Wang, I. M., Giannakakou, P., Giese, N. A., Ozato, K. and Morse, H. C., 3rd (1999). Regulation of apoptosis in myeloid cells by interferon consensus sequence-binding protein. *J Exp Med* 190, 411-421.

Garelli, A., Gontijo, A. M., Miguela, V., Caparros, E. and Dominguez, M. (2012). Imaginal discs secrete insulin-like peptide 8 to mediate plasticity of growth and maturation. *Science* 336, 579-582.

Gleizes, P. E., Noaillac-Depeyre, J., Leger-Silvestre, I., Teulieres, F., Dauxois, J. Y., Pommet, D., Azum-Gelade, M. C. and Gas, N. (2001). Ultrastructural localization of rRNA shows defective nuclear export of preribosomes in mutants of the Nup82p complex. *J Cell Biol* 155, 923-936.

Gough, S. M., Slape, C. I. and Aplan, P. D. (2011). NUP98 gene fusions and hematopoietic malignancies: common themes and new biologic insights. *Blood* 118, 6247-6257.

Grewal, S. S. (2009). Insulin/TOR signaling in growth and homeostasis: a view from the fly world. *Int J Biochem Cell Biol* 41, 1006-1010.

Griffis, E. R., Altan, N., Lippincott-Schwartz, J. and Powers, M. A. (2002). Nup98 is a mobile nucleoporin with transcription-dependent dynamics. *Mol Biol Cell* 13, 1282-1297.

Gurevich, R. M., Rosten, P. M., Schwieger, M., Stocking, C. and Humphries, R. K. (2006). Retroviral integration site analysis identifies ICSBP as a collaborating tumor suppressor gene in NUP98-TOP1-induced leukemia. *Exp Hematol* 34, 1192-1201.

Halder, G., Polaczyk, P., Kraus, M. E., Hudson, A., Kim, J., Laughon, A. and Carroll, S. (1998). The Vestigial and Scalloped proteins act together to directly regulate wing-specific gene expression in Drosophila. *Genes Dev* 12, 3900-3909.

Hay, B. A., Wolff, T. and Rubin, G. M. (1994). Expression of baculovirus P35 prevents cell death in Drosophila. *Development* 120, 2121-2129.

Herranz, H., Perez, L., Martin, F. A. and Milan, M. (2008). A Wingless and Notch double-repression mechanism regulates G1-S transition in the Drosophila wing. *EMBO J* 27, 1633-1645.

Herrera, S. C., Martin, R. and Morata, G. (2013). Tissue homeostasis in the wing disc of Drosophila melanogaster: immediate response to massive damage during development. *PLoS Genet* 9, e1003446.

Hu, L., Huang, W., Hjort, E. E., Bei, L., Platanias, L. C. and Eklund, E. A. (2016). The Interferon Consensus Sequence Binding Protein (Icsbp/Irf8) Is Required for Termination of Emergency Granulopoiesis. *J Biol Chem* 291, 4107-4120.

Jeganathan, K. B., Baker, D. J. and van Deursen, J. M. (2006). Securin associates with APCCdh1 in prometaphase but its destruction is delayed by Rae1 and Nup98 until the metaphase/anaphase transition. *Cell Cycle* 5, 366-370.

Jeganathan, K. B., Malureanu, L. and van Deursen, J. M. (2005). The Rae1-Nup98 complex prevents aneuploidy by inhibiting securin degradation. *Nature* 438, 1036-1039.

Ji, Z., Kiparaki, M., Folgado, V., Kumar, A., Blanco, J., Rimesso, G., Chuen, J., Liu, Y., Zheng, D. and Baker, N. E. (2019). Drosophila RpS12 controls translation, growth, and cell competition through Xrp1. *PLoS Genet* 15, e1008513.

Johnson, A. W., Lund, E. and Dahlberg, J. (2002). Nuclear export of ribosomal subunits. *Trends Biochem Sci* 27, 580-585.

Johnston, L. A. and Edgar, B. A. (1998). Wingless and Notch regulate cell-cycle arrest in the developing Drosophila wing. *Nature* 394, 82-84.

Joyce, J. A. and Schofield, P. N. (1998). Genomic imprinting and cancer. *Mol Pathol* 51, 185-190.

Kalverda, B., Pickersgill, H., Shloma, V. V. and Fornerod, M. (2010). Nucleoporins directly stimulate expression of developmental and cell-cycle genes inside the nucleoplasm. *Cell* 140, 360-371.

Karin, M. and Clevers, H. (2016). Reparative inflammation takes charge of tissue regeneration. *Nature* 529, 307-315.

Katsuyama, T., Comoglio, F., Seimiya, M., Cabuy, E. and Paro, R. (2015). During Drosophila disc regeneration, JAK/STAT coordinates cell proliferation with Dilp8-mediated developmental delay. *Proc Natl Acad Sci U S A* 112, E2327-2336.

Khan, S. J., Abidi, S. N. F., Skinner, A., Tian, Y. and Smith-Bolton, R. K. (2017). The Drosophila Duox maturation factor is a key component of a positive feedback loop that sustains regeneration signaling. *PLoS Genet* 13, e1006937.

Kim, J., Sebring, A., Esch, J. J., Kraus, M. E., Vorwerk, K., Magee, J. and Carroll, S. B. (1996). Integration of positional signals and regulation of wing formation and identity by Drosophila vestigial gene. *Nature* 382, 133-138.

Kristo, I., Bajusz, C., Borsos, B. N., Pankotai, T., Dopie, J., Jankovics, F., Vartiainen, M. K., Erdelyi, M. and Vilmos, P. (2017). The actin binding cytoskeletal protein Moesin is involved in nuclear mRNA export. *Biochim Biophys Acta Mol Cell Res* 1864, 1589-1604.

Kucinski, I., Dinan, M., Kolahgar, G. and Piddini, E. (2017). Chronic activation of JNK JAK/STAT and oxidative stress signalling causes the loser cell status. *Nat Commun* 8, 136.

Kulshammer, E., Mundorf, J., Kilinc, M., Frommolt, P., Wagle, P. and Uhlirova, M. (2015). Interplay among Drosophila transcription factors Ets21c, Fos and Ftz-F1 drives JNK-mediated tumor malignancy. *Dis Model Mech* 8, 1279-1293.

Lam, D. H. and Aplan, P. D. (2001). NUP98 gene fusions in hematologic malignancies. *Leukemia* 15, 1689-1695.

Langton, P. F., Baumgartner, M. E., Logeay, R. and Piddini, E. (2021). Xrp1 and Irbp18 trigger a feed-forward loop of proteotoxic stress to induce the loser status. *PLoS Genet* 17, e1009946.

Lapik, Y. R., Fernandes, C. J., Lau, L. F. and Pestov, D. G. (2004). Physical and functional interaction between Pes1 and Bop1 in mammalian ribosome biogenesis. *Mol Cell* 15, 17-29.

Law, C. W., Chen, Y., Shi, W. and Smyth, G. K. (2014). voom: Precision weights unlock linear model analysis tools for RNA-seq read counts. *Genome Biol* 15, R29.

Lee, C. H., Kiparaki, M., Blanco, J., Folgado, V., Ji, Z., Kumar, A., Rimesso, G. and Baker, N. E. (2018). A Regulatory Response to Ribosomal Protein Mutations Controls Translation, Growth, and Cell Competition. *Dev Cell* 46, 807.

Liao, Y., Smyth, G. K. and Shi, W. (2014). featureCounts: an efficient general purpose program for assigning sequence reads to genomic features. *Bioinformatics* 30, 923-930.

Lin, Y. W., Slape, C., Zhang, Z. and Aplan, P. D. (2005). NUP98-HOXD13 transgenic mice develop a highly penetrant, severe myelodysplastic syndrome that progresses to acute leukemia. *Blood* 106, 287-295.

Lo, K. Y., Li, Z., Bussiere, C., Bresson, S., Marcotte, E. M. and Johnson, A. W. (2010). Defining the pathway of cytoplasmic maturation of the 60S ribosomal subunit. *Mol Cell* 39, 196-208.

Lockhead, S., Moskaleva, A., Kamenz, J., Chen, Y., Kang, M., Reddy, A. R., Santos, S. D. M. and Ferrell, J. E., Jr. (2020). The Apparent Requirement for Protein Synthesis during G2 Phase Is due to Checkpoint Activation. *Cell Rep* 32, 107901.

Ma, C., Wu, S., Li, N., Chen, Y., Yan, K., Li, Z., Zheng, L., Lei, J., Woolford, J. L., Jr. and Gao, N. (2017). Structural snapshot of cytoplasmic pre-60S ribosomal particles bound by Nmd3, Lsg1, Tif6 and Reh1. *Nat Struct Mol Biol* 24, 214-220.

Marygold, S. J., Roote, J., Reuter, G., Lambertsson, A., Ashburner, M., Millburn, G. H., Harrison, P. M., Yu, Z., Kenmochi, N., Kaufman, T. C., et al. (2007). The ribosomal protein genes and Minute loci of Drosophila melanogaster. *Genome Biol* 8, R216.

McEwen, D. G. and Peifer, M. (2005). Puckered, a Drosophila MAPK phosphatase, ensures cell viability by antagonizing JNK-induced apoptosis. *Development* 132, 3935-3946.

Mendes, A., Juhlen, R., Bousbata, S. and Fahrenkrog, B. (2020). Disclosing the Interactome of Leukemogenic NUP98-HOXA9 and SET-NUP214 Fusion Proteins Using a Proteomic Approach. *Cells* 9, 1666.

Mesquita, D., Dekanty, A. and Milan, M. (2010). A dp53-dependent mechanism involved in coordinating tissue growth in Drosophila. *PLoS Biol* 8, e1000566.

Mondal, B. C., Shim, J., Evans, C. J. and Banerjee, U. (2014). Pvr expression regulators in equilibrium signal control and maintenance of Drosophila blood progenitors. *Elife* 3, e03626.

Moroianu, J., Hijikata, M., Blobel, G. and Radu, A. (1995). Mammalian karyopherin alpha 1 beta and alpha 2 beta heterodimers: alpha 1 or alpha 2 subunit binds nuclear localization signal and beta subunit interacts with peptide repeat-containing nucleoporins. *Proc Natl Acad Sci U S A* 92, 6532-6536.

Moy, T. I. and Silver, P. A. (2002). Requirements for the nuclear export of the small ribosomal subunit. *J Cell Sci* 115, 2985-2995.

Musalgaonkar, S., Black, J. J. and Johnson, A. W. (2019). The L1 stalk is required for efficient export of nascent large ribosomal subunits in yeast. *RNA* 25, 1549-1560.

Muzzopappa, M., Murcia, L. and Milan, M. (2017). Feedback amplification loop drives malignant growth in epithelial tissues. *Proc Natl Acad Sci U S A* 114, E7291-E7300.

Narbonne-Reveau, K. and Maurange, C. (2019). Developmental regulation of regenerative potential in Drosophila by ecdysone through a bistable loop of ZBTB transcription factors. *PLoS Biol* 17, e3000149.

Neufeld, T. P., de la Cruz, A. F., Johnston, L. A. and Edgar, B. A. (1998). Coordination of growth and cell division in the Drosophila wing. *Cell* 93, 1183-1193.

Neumann, C. J. and Cohen, S. M. (1997). Long-range action of Wingless organizes the dorsal-ventral axis of the Drosophila wing. *Development* 124, 871-880.

O'Keefe, D. D., Thomas, S. R., Bolin, K., Griggs, E., Edgar, B. A. and Buttitta, L. A. (2012). Combinatorial control of temporal gene expression in the Drosophila wing by enhancers and core promoters. *BMC Genomics* 13, 498.

Oeffinger, M., Dlakic, M. and Tollervey, D. (2004). A pre-ribosome-associated HEAT-repeat protein is required for export of both ribosomal subunits. *Genes Dev* 18, 196-209.

Panda, D., Pascual-Garcia, P., Dunagin, M., Tudor, M., Hopkins, K. C., Xu, J., Gold, B., Raj, A., Capelson, M. and Cherry, S. (2014). Nup98 promotes antiviral gene

expression to restrict RNA viral infection in Drosophila. *Proc Natl Acad Sci U S A* 111, E3890-3899.

Parrott, B. B., Chiang, Y., Hudson, A., Sarkar, A., Guichet, A. and Schulz, C. (2011). Nucleoporin98-96 function is required for transit amplification divisions in the germ line of Drosophila melanogaster. *PLoS One* 6, e25087.

Pascual-Garcia, P., Debo, B., Aleman, J. R., Talamas, J. A., Lan, Y., Nguyen, N. H., Won, K. J. and Capelson, M. (2017). Metazoan Nuclear Pores Provide a Scaffold for Poised Genes and Mediate Induced Enhancer-Promoter Contacts. *Mol Cell* 66, 63-76 e66.

Pascual-Garcia, P., Jeong, J. and Capelson, M. (2014). Nucleoporin Nup98 associates with Trx/MLL and NSL histone-modifying complexes and regulates Hox gene expression. *Cell Rep* 9, 433-442.

Perez-Garijo, A. (2018). When dying is not the end: Apoptotic caspases as drivers of proliferation. *Semin Cell Dev Biol* 82, 86-95.

Perez-Garijo, A., Shlevkov, E. and Morata, G. (2009). The role of Dpp and Wg in compensatory proliferation and in the formation of hyperplastic overgrowths caused by apoptotic cells in the Drosophila wing disc. *Development* 136, 1169-1177.

Pinal, N., Martin, M., Medina, I. and Morata, G. (2018). Short-term activation of the Jun N-terminal kinase pathway in apoptosis-deficient cells of Drosophila induces tumorigenesis. *Nat Commun* 9, 1541.

Presgraves, D. C., Balagopalan, L., Abmayr, S. M. and Orr, H. A. (2003). Adaptive evolution drives divergence of a hybrid inviability gene between two species of Drosophila. *Nature* 423, 715-719.

Reber, A., Lehner, C. F. and Jacobs, H. W. (2006). Terminal mitoses require negative regulation of Fzr/Cdh1 by Cyclin A, preventing premature degradation of mitotic cyclins and String/Cdc25. *Development* 133, 3201-3211.

Romero-Pozuelo, J., Demetriades, C., Schroeder, P. and Teleman, A. A. (2017). CycD/Cdk4 and Discontinuities in Dpp Signaling Activate TORC1 in the Drosophila Wing Disc. *Dev Cell* 42, 376-387 e375.

Romero-Pozuelo, J., Figlia, G., Kaya, O., Martin-Villalba, A. and Teleman, A. A. (2020). Cdk4 and Cdk6 Couple the Cell-Cycle Machinery to Cell Growth via mTORC1. *Cell Rep* 31, 107504.

Rosenblum, J. S. and Blobel, G. (1999). Autoproteolysis in nucleoporin biogenesis. *Proc Natl Acad Sci U S A* 96, 11370-11375.

Roy, A. and Narayan, G. (2019). Oncogenic potential of nucleoporins in non-hematological cancers: recent update beyond chromosome translocation and gene fusion. *J Cancer Res Clin Oncol* 145, 2901-2910.

Ruggiero, R., Kale, A., Thomas, B. and Baker, N. E. (2012). Mitosis in neurons: Roughex and APC/C maintain cell cycle exit to prevent cytokinetic and axonal defects in Drosophila photoreceptor neurons. *PLoS Genet* 8, e1003049.

Sabri, N., Roth, P., Xylourgidis, N., Sadeghifar, F., Adler, J. and Samakovlis, C. (2007). Distinct functions of the Drosophila Nup153 and Nup214 FG domains in nuclear protein transport. *J Cell Biol* 178, 557-565.

Sarov, M., Barz, C., Jambor, H., Hein, M. Y., Schmied, C., Suchold, D., Stender, B., Janosch, S., K, J. V., Krishnan, R. T., et al. (2016). A genome-wide resource for the analysis of protein localisation in Drosophila. *Elife* 5, e12068.

Schmidt, H. B. and Gorlich, D. (2015). Nup98 FG domains from diverse species spontaneously phase-separate into particles with nuclear pore-like permselectivity. *Elife* 4, e04251.

Schuster, K. J. and Smith-Bolton, R. K. (2015). Taranis Protects Regenerating Tissue from Fate Changes Induced by the Wound Response in Drosophila. *Dev Cell* 34, 119-128.

Shi, Z., Fujii, K., Kovary, K. M., Genuth, N. R., Rost, H. L., Teruel, M. N. and Barna, M. (2017). Heterogeneous Ribosomes Preferentially Translate Distinct Subpools of mRNAs Genome-wide. *Mol Cell* 67, 71-83 e77.

Simon, D. N. and Rout, M. P. (2014). Cancer and the nuclear pore complex. *Adv Exp Med Biol* 773, 285-307.

Singer, S., Zhao, R., Barsotti, A. M., Ouwehand, A., Fazollahi, M., Coutavas, E., Breuhahn, K., Neumann, O., Longerich, T., Pusterla, T., et al. (2012). Nuclear pore component Nup98 is a potential tumor suppressor and regulates posttranscriptional expression of select p53 target genes. *Mol Cell* 48, 799-810.

Slape, C., Liu, L. Y., Beachy, S. and Aplan, P. D. (2008). Leukemic transformation in mice expressing a NUP98-HOXD13 transgene is accompanied by spontaneous mutations in Nras, Kras, and Cbl. *Blood* 112, 2017-2019.

Smith-Bolton, R. K., Worley, M. I., Kanda, H. and Hariharan, I. K. (2009). Regenerative growth in Drosophila imaginal discs is regulated by Wingless and Myc. *Dev Cell* 16, 797-809.

Sullivan, W. A., M; Hawley, RS (2000). *Drosophila Protocols*: Cold Spring Harbor Press.

Sun, D. and Buttitta, L. (2015). Protein phosphatase 2A promotes the transition to G0 during terminal differentiation in Drosophila. *Development* 142, 3033-3045.

Takahashi, H., Yumoto, K., Yasuhara, K., Nadres, E. T., Kikuchi, Y., Buttitta, L., Taichman, R. S. and Kuroda, K. (2019). Anticancer polymers designed for killing dormant prostate cancer cells. *Sci Rep* 9, 1096.

Tanaka-Matakatsu, M., Thomas, B. J. and Du, W. (2007). Mutation of the Apc1 homologue shattered disrupts normal eye development by disrupting G1 cell cycle arrest and progression through mitosis. *Dev Biol* 309, 222-235.

Thomas, A., Lee, P. J., Dalton, J. E., Nomie, K. J., Stoica, L., Costa-Mattioli, M., Chang, P., Nuzhdin, S., Arbeitman, M. N. and Dierick, H. A. (2012). A versatile method for cell-specific profiling of translated mRNAs in Drosophila. *PLoS One* 7, e40276.

Toggweiler, J., Willecke, M. and Basler, K. (2016). The transcription factor Ets21C drives tumor growth by cooperating with AP-1. *Sci Rep* 6, 34725.

Uhlirova, M. and Bohmann, D. (2006). JNK- and Fos-regulated Mmp1 expression cooperates with Ras to induce invasive tumors in Drosophila. *EMBO J* 25, 5294-5304.

Verghese, S. and Su, T. T. (2017). STAT, Wingless, and Nurf-38 determine the accuracy of regeneration after radiation damage in Drosophila. *PLoS Genet* 13, e1007055.

Walther, T. C., Alves, A., Pickersgill, H., Loiodice, I., Hetzer, M., Galy, V., Hulsmann, B. B., Kocher, T., Wilm, M., Allen, T., et al. (2003). The conserved Nup107-160 complex is critical for nuclear pore complex assembly. *Cell* 113, 195-206.

Wild, T., Horvath, P., Wyler, E., Widmann, B., Badertscher, L., Zemp, I., Kozak, K., Csucs, G., Lund, E. and Kutay, U. (2010). A protein inventory of human ribosome biogenesis reveals an essential function of exportin 5 in 60S subunit export. *PLoS Biol* 8, e1000522.

Williams, J. A., Bell, J. B. and Carroll, S. B. (1991). Control of Drosophila wing and haltere development by the nuclear vestigial gene product. *Genes Dev* 5, 2481-2495.

Williams, J. A., Paddock, S. W. and Carroll, S. B. (1993). Pattern formation in a secondary field: a hierarchy of regulatory genes subdivides the developing Drosophila wing disc into discrete subregions. *Development* 117, 571-584.

Wonglapsuwan, M., Chotigeat, W., Timmons, A. and McCall, K. (2011). RpL10A regulates oogenesis progression in the banana prawn Fenneropenaeus merguiensis and Drosophila melanogaster. *Gen Comp Endocrinol* 173, 356-363.

Worley, M. I., Alexander, L. A. and Hariharan, I. K. (2018). CtBP impedes JNK- and Upd/STAT-driven cell fate misspecifications in regenerating Drosophila imaginal discs. *Elife* 7.

Wu, X., Kasper, L. H., Mantcheva, R. T., Mantchev, G. T., Springett, M. J. and van Deursen, J. M. (2001). Disruption of the FG nucleoporin NUP98 causes selective changes in nuclear pore complex stoichiometry and function. *Proc Natl Acad Sci U S A* 98, 3191-3196.

Xu, S. and Powers, M. A. (2009). Nuclear pore proteins and cancer. *Semin Cell Dev Biol* 20, 620-630.

Zecca, M. and Struhl, G. (2010). A feed-forward circuit linking wingless, fat-dachsous signaling, and the warts-hippo pathway to Drosophila wing growth. *PLoS Biol* 8, e1000386.

Chapter 4 Conclusions and Future Directions

4.1 Noise in biological systems gives rise to different levels of quiescence

The intrinsic stochasticity of biological pathways can contribute to a range of expression of mRNAs and proteins across a homogenous population of cells (Eling et al., 2019a; Elowitz et al., 2002; Raser & O'Shea, 2004). This 'noise' can have effects on normal development and disease conditions and hence is an area of active research. The noise in biological systems is broadly classified into extrinsic and intrinsic noise. While the intrinsic noise is constituted of genetic and epigenetic features affecting translation of specific genes, extrinsic noise could be caused by the stochasticity in perceiving external signals and integrating them with regulation of the cellular machinery (Eling et al., 2019b). These gives rise to variation in an otherwise homogenous population.

In chapter 2, we looked at a seemingly stochastic proliferation-quiescence decision in a clonal prostate cancer cell line. We show that even under optimal growth conditions a fraction of cells enter quiescence, and that daughters born of the same mitotic event may enter quiescence synchronously or asynchronously. The cells that enter G0 spend widely different amounts of time in G0, suggesting that G0 depth in different cells is also heterogenous.

The expression of G0 reporters in an untransformed mouse cell line (NIH 3T3) and a transformed metastatic prostate cancer cell line (PC3) gives us a unique opportunity to understand the factors determining various levels of heterogeneity in G0. We used the fluorescent markers to sort the cells into distinct G0, G1 and S/G2/M stages of the cell cycle to study changes in protein expression using bulk proteomics. We also serum starved the cells to push them into a well-characterized G0 state induced by serum withdrawal.

Many factors that regulate the cell cycle are regulated at the level of protein abundance. To identify differentially expressed proteins in spontaneous G0 and serum starved G0, we performed global proteomics on cells isolated by FACS in G0 under spontaneous G0 or reduced serum-induced G0 and compared them to cells in G1 or S/G2/M populations. We found that in NIH 3T3 cells, 64 proteins were upregulated in both spontaneous and reduced serum G0, compared to other cell cycle stages. Interestingly, 412 unique proteins were upregulated in serum starved G0, and 76 unique proteins were upregulated during spontaneous G0 (Table 4.1). We found that 87 proteins were downregulated in both kind of G0s. Levels of 119 proteins were low in cells entering G0 in response to serum starvation, and 218 polypeptides were low in cells entering spontaneous G0 compared to other stages of cell (Fig 4.1).

Similar analysis of the G0 protein signature in PC3 cells will help us identify generic protein signatures that are conserved signaling pathways between transformed and untransformed cells lines under normal growth conditions. This data set could then be used in other cell lines and in *in vivo* experiments to verify and study spontaneous G0.

While mass spec analysis gives us a broad overview of protein abundance in different states of G0, it lacks single cell resolution to study the stochasticity in gene expression among cells that enter spontaneous G0. A recent study from the Purvis lab looked at the expression pattern of 48 core cell cycle proteins by immunofluorescence, single cell imaging and machine learning (Stallaert et al., 2021). While this technique gives us a great opportunity to study protein dynamics in a single cell during the cell cycle, it is limited by the set of proteins used for the analysis. To study the dynamics of proteins during spontaneous G0, the differentially expressed proteins identified in distinct G0s from our pooled mass spec data could be used along with this technique.

Single cell RNA seq of NIH3T3 cells and PC3 cells sorted to G0 state will give us a unique insight into various populations of G0 that exist in normal growth conditions. Comparing these datasets would give us a great insight into the protein and gene expression changes associated with different states of G0 that arise in cell culture.

4.2 Cell cycle heterogeneity may contribute to cytotoxic drug resistance in cultured PC3 cells.

Oncogenic transformations of cells are often associated with overproliferation. However, accumulating evidence suggest that cancer cells exhibit cell cycle heterogeneity. This gives rise to populations of cells that are slowly dividing or are quiescent (Dey-Guha et al., 2011; Pulianmackal et al., 2021; Sharma et al., 2010), These cells are thought to evade cytotoxic chemotherapy and *in vivo*, may cause cancer relapse.

Our studies in Chapter 2 show that the prostate cancer cell line, PC3, spontaneously enters G0 despite lacking the p53 tumor suppressor previously shown to

mediate spontaneous quiescence (Yang et al., 2017). To test whether the spontaneous G0 helps these cells evade chemotherapy, we treated them with chemotherapy drugs. Platinum containing drugs such as cisplatin and taxols such as docetaxel are two main chemotherapy drugs used in prostate cancer (Dasari & Bernard Tchounwou, 2014; Huang et al., 2021; Sobue et al., 2016). While cisplatin binds to the purine residue of DNA and activates the DNA damage checkpoint leading to cell death, docetaxel is a microtubule stabilizer that causes cell cycle arrest and cell death by preventing mitotic spindle assembly.

Initial analysis suggests that short term treatment (3-5 days) of PC3 cells with IC50 dosage of the chemotherapy drugs followed by recovery in normal cell culture media killed most of the cells within a week (Fig 4.2 E,F). The cells remaining on the plate continued to increase in cell size and DNA content while still expressing G0/G1 markers (Fig 4.2, A-F). Most of the surviving cells didn't undergo cytokinesis or form clones of cell. Interestingly, rare events of cytokinesis in these cells happened while the cells were still expressing the G0/G1 markers, suggesting that the cells are undergoing non-conventional cell cycles. After two weeks-two months of recovery in normal cell culture media with rare mitotic events, a few of these cells re-enter the normal cell cycle and form clones of cells on the plate (Fig 4.2 G,H).

To analyze whether the resistance to the drug is a result of cells spontaneously entering G0 and whether niche factors can enhance the drug resistance, we cotreated the cells with TGFβ2 and a chemotherapy drug. We saw that TGFβ2 increased the number of cells surviving after the drug treatment and also increased the number of clones formed after cytotoxic drug removal (Fig 4.2 I-K). TGFβ2 treatment also

decreased the time required for cell cycle re-entry from about a month to less than a month. We also observed that cells at high confluency are resistant to the chemotherapy treatment, which induces G0. Together, our data suggest that increased G0 in cancer cells increases resistance to chemotherapeutic agents. *In vivo*, populations of cancer cells in G0 may enhance the probability of cancer relapse.

4.3 Are the drug-selected cells similar to parental PC3 cells?

The cells that survived drug treatment had increased DNA damage as shown by gamma H2Av staining and slower growth rate (Fig 4.3 A-C'). But when they were co-treated with TGFβ2, the cells looked more like normal PC3 cells and had basal levels of DNA damage (Fig 4.3 A-C'). We treated the surviving PC3 cells with the chemotherapy drugs again, to test whether they are resistant or retain some memory from the previous treatment and behave differently from the parental population. Surprisingly, our initial analysis suggests that the cells surviving the first drug treatment are more sensitive to a second chemotherapy treatment compared to cells drug selected cells that were cotreated with TGFβ2 (Fig 4.3 D-F'). We found that TGFβ2 cotreated cells have growth dynamics and cell division very similar to the parental population.

These data suggest that the tumor dormancy factors helped cancer cells be resistant to chemotherapy drugs and enhanced the survival of these cells. Further analysis on how other tumor dormancy factors such as GAS6 would affect the drug resistance in cancer cell would aid in understanding the biology behind drug resistant cancer and how dormancy factors help it. Proteomic or transcriptomic analysis of the drug-selected cell lines under treatment with different tumor dormancy factors would

also help us identify key molecular pathways that are affected by these factors, thus conferring better survival outcomes for the cells.

4.4 Can reduction of spontaneous G0 reduce chemotherapy resistance?

Prostate cancer cells that exit the cell cycle and survive in a resting G0 state can be identified by their stabilization of a P27 degron-containing reporter. This suggests that the cells arrested in G0 are expressing high levels of stabilized CKIs. The gene locus of two of the CKIs known to promote G0, P16 and P21, is known to be epigenetically silenced by DNA methylation in PC3 cells (Bott et al., 2005; Jarrard et al., 1997). But DNA methylation is reversible, and when treated with chemotherapy drugs, we found surviving PC3 cells expressed P16 (Fig 4.4). This suggests that the CKIs could be playing a role in cancer cell chemotherapy resistance.

We can investigate whether the CKIs play a role in inducing spontaneous quiescence and help in drug resistance by knocking down these CKIs in PC3 cells harboring the G0 reporter system and measuring the rate of spontaneous quiescence by live imaging. These cells could then be subjected to chemotherapy drug treatment to analyze whether the knockdown of these CKIs affects the rate at which drug-resistant populations arise. We would expect that if the CKIs are enhancing the survivability of the cancer cells, knock down of these factors will cause fewer drug-selected colonies and will increase the time for cell cycle reentry in these cells.

4.5 Does loss of Nup98-96 affect localization of other ribosomal or cell cycle proteins?

In chapter 3, we show that knockdown of Nup98 and 96 causes mis-localization of the ribosomal protein RPL10A, decreased protein synthesis, activation of JNK signaling, and bypass of G0/G1 arrest. This led us to ask whether there are some ribosomal subunits that are differentially expressed in proliferating and quiescent cell populations. Hence, we looked at the mass spec data set from NIH 3T3 cells to see whether there are some specific ribosomal subunits that are differentially regulated in G0.

We did not find any ribosomal subunits to be upregulated in the G0 state of cell cycle, but we found three ribosomal proteins, RPL19, RPS5 and RPL36A to be downregulated in quiescent cells. Interestingly, heterozygous mutations of these genes are known to be causal for a rare bone marrow failure syndrome called Diamond-Blackfan anemia (DBA) (Hopes et al., 2020; Simkins et al., 2017). DBA affects differentiation into red blood cells and causes bone marrow failure. Interestingly, many cases of DBA also lead to hematological malignancies later in life (Hopes et al., 2020; Simkins et al., 2017). However, how these ribosomal defects affect the proliferation-quiescence decision in DBA is not well known.

In chapter 3, we tested for the localization of 6 different ribosomal proteins but found the mislocalization of only RPL10A. It is likely that some other ribosomal subunits may also be mislocalized when the proliferation-quiescence decision is affected by knocking down Nup98-96. Subcellular fractionation of cells where Nup98-96 is knocked down and proteomic analysis of the proteins in nuclear and cytoplasmic fractions would

give us a better understanding about the nucleo-cytoplasmic localization of other ribosomal and cell cycle proteins.

This could help us elucidate specific types of ribosomes whose assembly is affected with reduced Nup98-96 function. This potential study would shed further light into whether ribosomal heterogeneity plays a role in the proliferation-quiescence decision.

4.6 Do heterogeneous ribosomes contribute to regulate proliferation-quiescence decision?

The notion of specialized ribosomes is not new. In the 1958 paper where he introduced the central dogma of biology, Francis Crick suggested that there are specialized ribosomes to translate specific RNAs into proteins and the specificity is largely due to the rRNA present in the ribosome (Crick 1958, Crick 1970). But later in 1961, Mathew Meselson's group discovered mRNAs and suggested that ribosomes are just bystanders in the central dogma playing no regulatory function (Brenner 1961). This notion is still widely popular, and the ribosomes are thought to be homogenous cellular organelles.

Recent studies in various model organisms ranging from *Arabidopsis* to mammalian cells have shown that ribosomes are heterogenous and could be specialized to regulate translation in different cell types. A eukaryotic ribosome consists of 80-81 ribosomal proteins and 4-5 rRNAs packaged into large and small ribosomal subunits. In *Arabidopsis* all the ribosomal proteins have 2-7 paralogs, whereas flies have 13 and human have 19 paralogs for ribosomal proteins (Martinez-Seidel 2020, Shimsek 2017, Norris 2021). These paralogs are shown to be expressed sub-

stoichiometrically in different cell types in all three model organisms discussed above (Shi 2017, Shimsek 2017, Tayah hopes 2021, Jun Yu, 2016, Dan Li 2020).
Though the role played by heterogenous ribosomes has been studied in different cell types, the role played by distinct pools of ribosomes in the proliferation-quiescence decision is largely unexplored. Proteomics we did in NIH 3T3 cells suggests that some of the ribosomal subunits are differentially expressed in quiescent vs proliferating cell populations. Further careful analysis of stoichiometry of ribosomal subunits would be useful in understanding the heterogeneity in ribosomes during proliferation-quiescence decision. Analysis of mRNAs associated with these specialized ribosomes would add another level to the control of the cell cycle that has not been reported before.

4.7 Cellular quiescence: a double-edged sword in cancer

This thesis provides an outlook into how proliferation and quiescence play an important role in cancer progression. In Chapter 2, we used a reporter system that was previously used to identify quiescent cells under serum starvation to identify and isolate spontaneous quiescent cells in a metastatic prostate cancer cell line. We identified that the amount of time a cell spent in spontaneous quiescence is heterogenous and this is partly due to asynchronous proliferation-quiescence decisions of daughters after mitosis. We found that tumor dormancy signals influence the spontaneous quiescence, and these quiescent cells express high levels of Hippo pathway components and as well as cancer stem cell markers. We saw that the cancer cells that evade cytotoxic drug treatment are enriched quiescence markers. We also found that tumor dormancy signals enhance the percentage of cells surviving after drug treatment, suggesting cellular quiescence help cancer cells evade drug treatment in *in vitro* conditions. Further

studies will help identify whether spontaneous quiescence occurs in tumors *in vivo* and whether this help in cancer relapse.

In Chapter 3, we identified Nup98-96 in a screen done in *Drosophila* to identify factors that affect cellular quiescence. We found that loss of Nup98-96 triggers cell death and compensatory proliferation mediated via JNK, and cells become tumorigenic when apoptosis is inhibited. Unlike previous studies that looked at the tumorigenic phenotype caused by the transcriptional activity of Nup98, we were able to identify a novel mode in which loss of Nup98 causes defects in nucleo-cytoplasmic transport of proteins. We saw that loss of Nup98-96 caused nuclear sequestration of RPL10A, a ribosomal subunit. which in turn caused defects in protein synthesis and JNK activation**.** Paradoxically, a reduced rate of protein synthesis coupled with increased JNK signaling leads to more proliferation with gene expression profile similar to chronic wounding responses.

Altogether, this thesis pushes forward the boundary of our understanding of the factors affecting proliferation or quiescence in cancer.

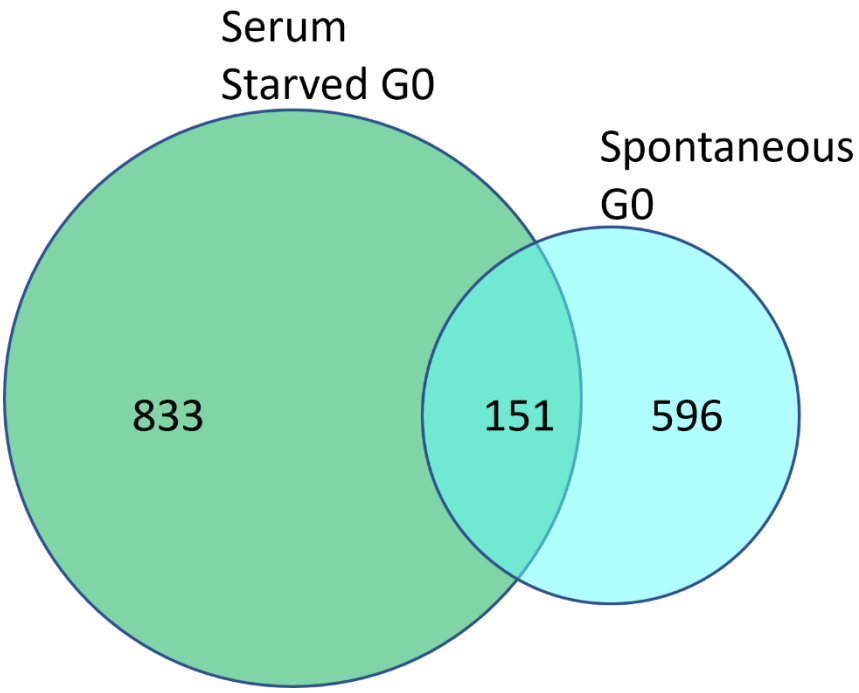

Figure 4-1 Proteins differentially expressed in G0

NIH 3T3 cells were sorted into G0, G1 or S/G2/M and serum starved G0, and mass spec analysis was done to identify peptides expressed in these different populations. Proteins that are differentially expressed in spontaneous and serum starved G0 compared to other cell cycle stages were identified. 833 proteins were differentially regulated in serum starved G0, whereas 596 proteins were differential in spontaneous G0. There were 151 proteins whose expression were differentially regulated in both G0s.

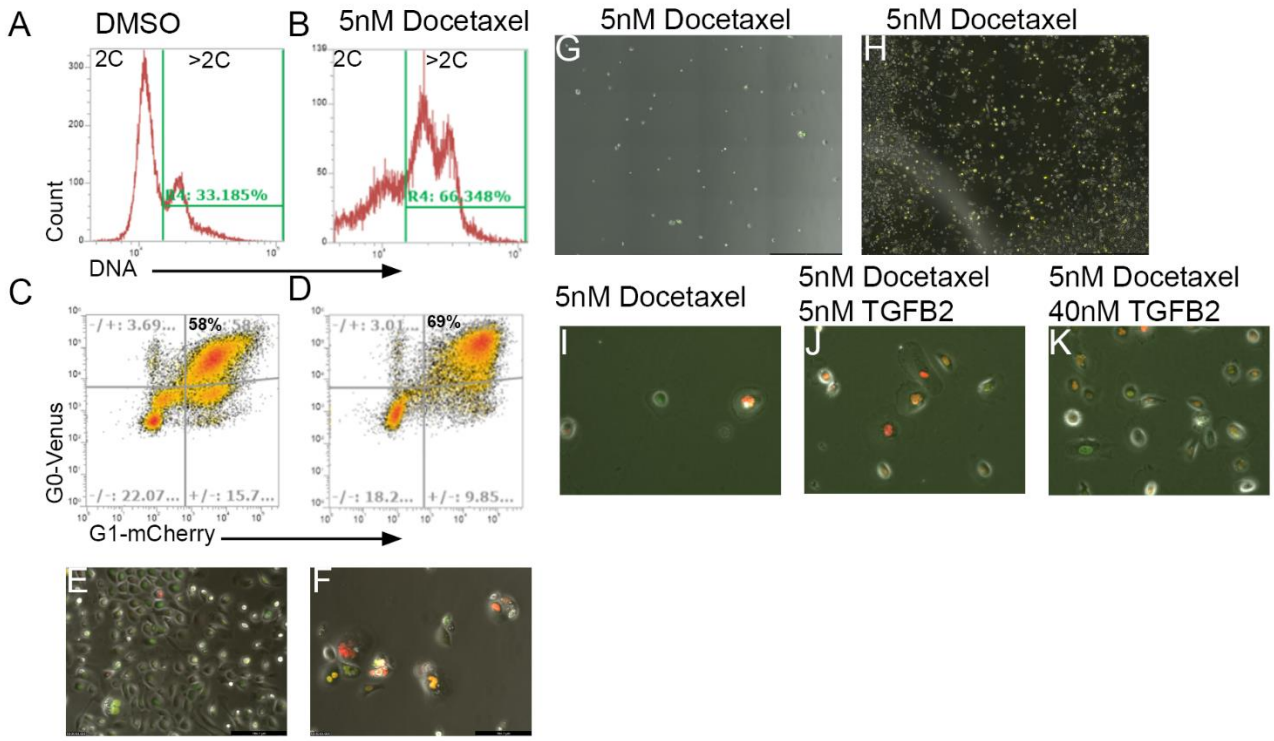

Figure 4-2 Drug tolerant PC3 cells

PC3 cells expressing G0-Venus G1 cherry reporter were treated with docetaxel. The cells treated with docetaxel had increased ploidy (A,B) and an increased number of cells in G0 (C, D). The drug tolerant cells became larger in size and expressed the G0 reporter (E,F). 3 weeks post drug treatment, many cell continue to be in a non-dividing state (G), but some of the cells in normal media re-enter the cell cycle and form clones (H). Co-treatment with TGFβ2 enhanced the survivability of PC3 cells when examined 4 days into recovery (I-K).

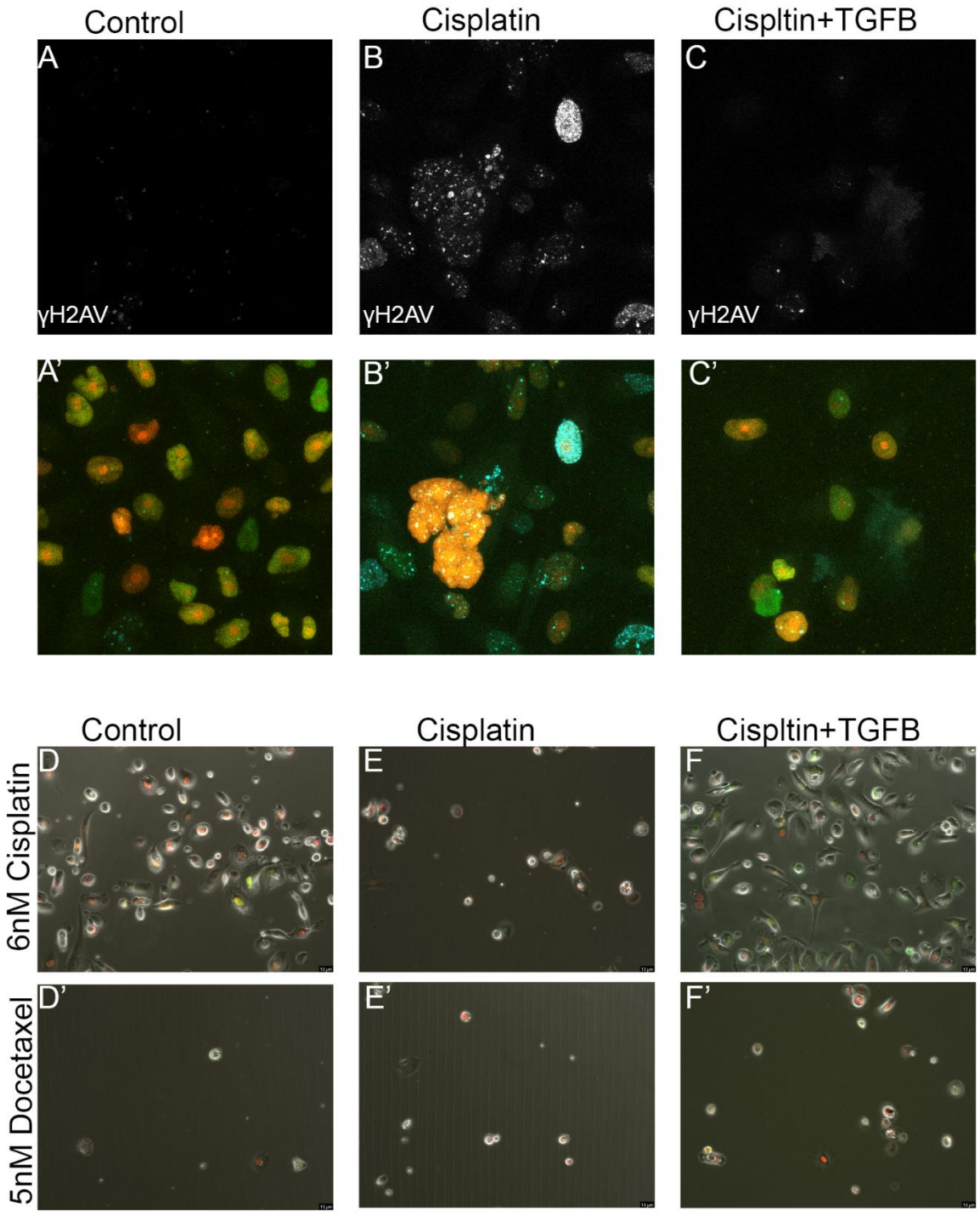

Figure 4-3 TGFβ2 enhances survivability of cells that re-enter the cell cycle after cytotoxic drug treatment

The cells that formed colonies after cisplatin or cisplatin + TGFβ2 treatment were stained for the DNA damage marker γH2Av. Control cells expressed a basal level of γH2Av staining (A,A') whereas cells recovered from cisplatin treatment exhibited a lot of DNA damage (B,B'). This increased DNA damage in recovered cells was reduced when they were co-treated with TGFβ2 (C,C'). The cisplatin recovered cells were more susceptible to docetaxel and cisplatin compared to control or when co-treated with cisplatin+TGFβ2 (D-F').

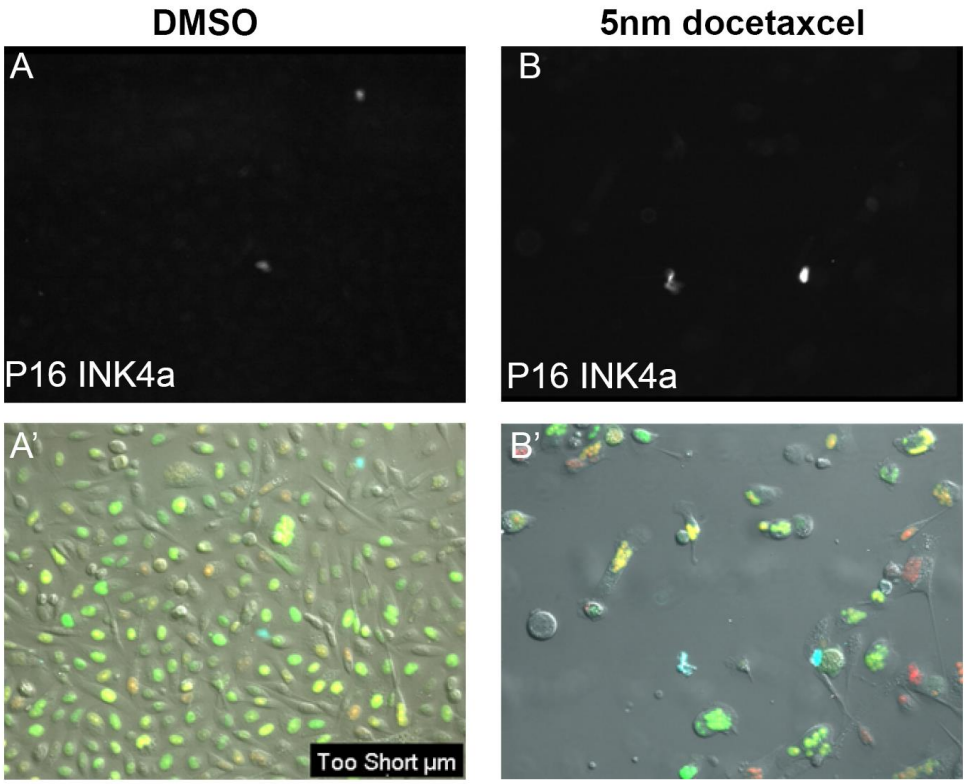

Figure 4-4 p16 expression in PC3 cells

PC3 cells were stained for p16 INK4a 4 days post recovery from docetaxel. The docetaxel treated cells had a higher expression of p16 compared to untreated PC3 cells.

Table 4-1 Differentially expressed proteins in G0

High in spontaneous G0	High in Serum starved	High in Serum starved	High in both G0s		Low in spontaneous G0	Low in Serum starved	Low in Serum starved	Low in both G0s	
Mta1	Rab5b	Rab3gap1	Rab5b		Son	Baz1b	Rpl21	Dnmt1	
Rab5b	Man2b2	Kcmf1	Ppa2		Snrpa	Trove2	Qars	Pdlim7	
Rab5a	Gnao1	Sra1	Rab5a		Nup35	Myadm	Btf3	Nup88	
Krt8	Tln2	Wdtc1	Ank2		Dnmt1	Bckdk	Rpl19	Txnl1	
Cul4b	Ppa2	Enoph1	Rab4b		Nudc	Casp8	Ddx19a	Slfn9	
Rab4b	Man2b1	Zadh2	Acox1		Mthfd2	Il1rl1	Rps9	Thrap3	
Akt1	Pdcd4	Samm50	Cul4b		Tmpo	Csk	Impdh2	Cfdp1	
Smg1	Vps13c	Map4k5	Arl2		Pdlim7	Rpl29	Pnn	Top1	
Rab12	Rab5a	Osgep	Col3a1		Spcs2	Dad1	Eif4b	Uhrf1	
Snrpb2	Acot1	Prepl	Gatd3a		Prpf3	Crnkl1	Pdcd11	Fkbp5	
Scamp1	Nub1	Cwc22	Atp6v1f		Lims1	Polr1b	Thumpd1	Aip	
Cyp20a1	Txnip	Mboat7	Rpia		Nup88	Frg1	Mcm6	Gtpbp4	
Lclat1	Ank2	Fnbp1l	Dnajc11		Nup214	Sec24a	Adk	Lsm3	
Ppa2	Rab4b	Gtf3c1	Ppwd1		Utp20	Trip13	Polr2b	Hist1h1b	
Ank2	Acox1	Hacd3	Scamp1		Txnl1	Prrc1	Nolc1	Nufip2	
Dnajc11	Cul4b	Mepce	Fahd1		Nt5c3b	Tmed1	Rpl26	Poldip3	
Alg2	Sept10	Gfm2	L2hgdh		Snx2	Zbtb8os	Hprt1	Rrm2	
Fbxo22	Gpnmb	Snap47	Alg2		Ccar1	Eif4ebp1	Tra2a	Rras2	
Thoc3	Arl2	Washc1	Sel1l		Pus7	Rad21	Tmsb10	Nol11	
Pip4p2	Ank3	Phip	Col6a2		Slfn9	Eif2b4	Rpl10	Tbc1d15	
Arl2	Fah	Nit1	Fbxo22		Thrap3	Mea1	Got2	Klc1	
Exosc4	Lsm5	Srsf4	Gatd1		Mlkl	Gk	Fkbp5	Gnl2	
Gatd1	Mvk	Pqbp1	Cyp20a1		Cfdp1	Ddx51	Phf5a	Cox6c	
Glrx5	Flot1	Ubl7	Akt1		Prrc2c	Dhx29	Pdlim7	Jun	
Psme2	Scarb2	Spryd4	Bcl2l13		Yap1	Zc3h4	Nup93	Nup43	
Prepl	Ddt	Acy3	Sptlc2		Top1	Nup188	Raly	Aarsd1	
Fahd1	Plin4	Lpgat1	Psme2		Uhrf1	Erbin	Hmox1	Ddx54	
Ak3	Col3a1	Tnfaip8	Thumpd3		Rab8a	Pelo	Col1a2	Rin1	
Enoph1	Agfg2	Dbr1	Micall2		Kpna3	Elac2	Akap2	Srsf9	
Mrps23	Gatd3a	Atad3	Lclat1		Parp1	Tm9sf4	Rpl27	Chaf1b	
Micall2	Atp6v1f	Dhrs1	Mrc2		Atp6v1e1	Elmo2	Gnl1	Trmt112	
Pofut2	Mycbp	Gdpd1	Enoph1		Tbc1d15	Anapc5	Rpl8	Edf1	
Sdad1	Abcc1	Dph5	Samm50		Dcaf13	Vps26b	Nifk	Adnp	
Gon4l	Nnmt	Naxd	Prepl		Rrm2	Ncaph	Mfge8	Pde12	
Washc5	Mt2	Psmg3	Tbcb		Fam114a2	Nelfb	Rangap1	Hells	
Akap12	Rpia	Tbcb	Necap2		M6pr	Pcyox1l	Smarca5	Rpa2	
Thumpd3	Bckdha	Necap2	Ak3		Snx1	Utp6	Rsl1d1	Kyat3	
Golga2	Shc1	Arfgap3	Numbl		Pds5b	Dcp1a	Rbbp4	Csnk1a1	
Mfn1	Plekhf1	Echdc1	Prkcd		Gtpbp4	Acy1	Cluh	Pdhx	
Fam207a	Dnajc11	Nudt3	Ogfod1		Lsm3	Trim16	Rpl18a	Poldip2	
Atp6v0a1	Fkbp15	Ccdc22	Tefm		Adnp	Ncbp2	Rbbp7	Pno1	
Rrp1b	Trmt61a	Mrpl39	Smg1		Ube2v1	Riok2	Srpk1	Tmem33	
Rap2b	Pdk1	Naga	Babam2		Rbpj	Ddx56	Celf1	Degs1	
Nop53	Dglucy	Jmy	Ube2e2		Rras2	Pir	Vbp1	Cox5b	
Col3a1	Snx30	Lypla2	Exosc4		Wdr18	Gpx8	Itga3	Cks1b	
Acox1	Ppwd1	Ak3	Snrpb2		Fxr2	Map3k20	Cnbp	Rala	
Gatd3a	Scamp1	Gipc1	Armc8		Aip	Brd4	Aip	Rpl36a	
Myo6	Gale	Nfs1	Eefsec		Otud4	Rpf2	Prpf31	Epha2	
Ccdc88b	Fahd1	Dhx8	Utp3		Efl1	Timeless	Prrc2a	Gsk3a	

Samm50	Scrn2	Trappc11	Cspg4		Pgrmc1	Fam50b	Rpl7	Mdc1	
Col6a2	L2hgdh	Irf2bp2	Slc4a7		Rin1	Knop1	Rpl13	Inppl1	
Bcl2l13	Hagh	Sec16a	Cdkn1b		Emc8	Tubb4a	Rpl14	Rps19bp1	
Ppwd1	Alg2	Faah	Mavs		Fam98a	Hist1h1e	Rrm1	Atad2	
Fsip2	Palm	Numbl	Gcat		Pno1	Hist1h1d	Dnaja1	Rheb	
Mrpl14	Sel1l	Agpat1	Washc4		Csnk1a1	Rab10	Ddx21	Mrps5	
Dpp9	Grcc10	Adam10	Pmvk		Cks1b	Metap2	Rpl24	Aen	
Atp6v1f	Bet1	Sptlc1	Plod2		Hist1h1b	Slfn9	Ddx18	Rfc5	
Minpp1	Slc1a4	Gamt	Raver1		Ntmt1		Lig1	Rnmt	
Mrc2	Reps1	Nipsnap1	Mecr		Baz1b		Snrpf	Mrpl19	
Sel1l	B2m	Nipsnap2	Stam		Ppp5c		Lrrc40	Rpap3	
Rpia	H2-K1	Smpd2	Pik3c2a		Kyat3		Aaas	Apoo	
L2hgdh	Pdgfra	Mtx2	Letm1		Fkbp5		Thrap3	Higd1a	
Utp3	Vcam1	Sap30	Gnpda1		Bicd2		Rpl6	Gsk3b	
Xirp2	Traf2	Nr3c1	Dennd4c		Gna11		Rps16	Fads2	
Phldb2	Nat2	Prkcd			Poldip3		Zc3hav1	Baz1b	
Sptlc2	Mmp14	Mmp2			Nqo1		Clptm1	Myadm	
Aars2	Ube2g1	Rab23			Pgm2		Snrpe	Il1rl1	
Ehbp1l1	Col6a2	Ptpn12			Exosc8		Nup50	Frg1	
Babam2	Hsdl2	Fbln2			Tmem33		Cebpz	Zbtb8os	
Necap2	Arhgap17	Cdk5			Polr2c		Mcmbp	Mea1	
Prkcd	Cd34	Rida			Nufip2		Gtpbp4	Gk	
Armc8	Isg15	Stom			Dr1		Cfdp1	Dhx29	
Rhot1	Cgnl1	Ube2g2			Nup43		Trim47	Zc3h4	
Nmral1	Fbxo22	Dcaf7			Jun		Wdr3	Erbin	
Tbcb	Gatd1	Nfyb			Dnaja3		Caprin1	Tm9sf4	
Marcks	Ano10	Fer			Banf1		Cdc5l	Anapc5	
Numbl	Cyp20a1	Gclc			Nfib		Tbl3	Nelfb	
Ndufa9	Hook3	Mrpl10			Stt3a		Eif3g	Utp6	
Ube2e2	Ptges2	Alkbh5			Slk		Fau	Trim16	
Tefm	Ufl1	Ogfod1			Mrps36		Pum3	Map3k20	
Galnt2	C1sa	Nol8			Ppp4r2		Ubap2	Brd4	
Thoc5	Otud6b	Eml4			Fkbp11		Sqstm1	Rpf2	
Cd3eap	Svil	Vps51			Mrps22		Tfrc	Timeless	
Thoc1	Dhcr24	Phactr4			Ctr9		Birc6	Fam50b	
Mrps15	Mios	Rilp			Pgrmc2		Iap	Hist1h1e	
Chchd6	Tmlhe	Tefm			Hells		Dnmt1	Hist1h1d	
Tor1aip1	Snx18	Psme4			Rbm12		Csde1		
Eefsec	MArc2	Bloc1s3			Nol11		Cdk1		
Ogfod1	Ndufab1	Sin3a			Cox6c		Hist1h1c		
Ndufaf2	Diablo	Ly75			Rfc5		Top2a		
Atxn3	Lancl2	Stxbp3			Prkra		Kpna2		
Paip1	Acss2	Prpf4b			Rpf2		Uhrf1		
Smarcd3	Add3	Eif2d			Myadm		Lsm3		
Rbm42	Dcun1d1	Ptpmt1			Gnl2		Top1		
Anxa8	Mecp2	Hbs1l			Mdc1		Txlna		
Asf1a	Arfgef2	Ltn1			Rheb		Hist1h1b		
Baiap2l1	Ankrd11	Mob4			Akr7a2		Nufip2		
Rsl24d1	Creg1	Ddx58			Ccdc124		Poldip3		
Pik3r4	Hsd17b7	Fblim1			Chtop		Txnl1		
Mrpl37	Rbbp9	Casd1			Tm9sf4		Ebna1bp2		
Strn4	Src	Impad1			Epha2		Map7d1		
Wiz	Cdh2	Kirrel1			Utp6		Rrm2		
Arih2	Fech	Gopc			Mrpl19		Rras2		
Nedd8	Ppic	Pgs1			Cd2bp2		Cobll1		
Cspg4	Akt1	Elovl5			Rrp7a		Grb10		
Sub1	Nectin2	Cdkn2aip			Erbin		Nol11		

Ppp3r1	Stat5b	Smg1			Apoo		Steap3		
Cox7a2l	Arsb	Nceh1			Aen		Tbc1d15		
Casp6	Dnase2	Col16a1			Aarsd1		Carm1		
Erc1	Bcl2l13	Hsdl1			Fads2		Klc1		
Slc4a7	Cirbp	Mpp7			Chaf1b		H1f0		
Cdkn1b	Gng2	Poglut1			Zc3h4		Impdh1		
Nudt16l1	Nfix	Fam234a			Atad2		Polr1d		
Mavs	Rock2	Heatr5b			Trim16		Cab39		
Lamtor3	Sptlc2	Cfap36			Nln		Prpf38b		
Gcat	Psme2	Parp9			Tmsb4x		Ercc6l		
Pmvk	Thumpd3	Vcpip1			Abi1		Pwp2		
Washc4	Lypla1	Scyl2			Pura		Ythdf3		
Atp6v0d1	Yes1	Gatad2a			Rbpms		Gnl2		
Plod2	Aplp2	Amdhd2			Bcap31		Cox6c		
Raver1	Micall2	Eipr1			Clip1		Ddx20		
Pcmt1	Hectd3	Arhgap18			Ubfd1		Dnajc7		
Exosc2	Aak1	Ints9			Nadk2		Jun		
Mecr	Babam1	Stx5			Lgmn		Srp14		
Keap1	Lclat1	Nek9			Qdpr		Rpl36		
Stam	Rbm27	Os9			Ago2		Nup43		
Pik3c2a	Kif1b	Babam2			Mrpl12		Aarsd1		
Lsm12	Flot2	Wdr33			Nhp2		Scoc		
Tmx3	Dvl2	Suox			Vasp		Ipo8		
Vps26b	Cp	Gga1			Ccdc58		Pdcl3		
Clpp	Dag1	Vps37c			Larp7		Nup88		
Exosc3	Rab34	Bphl			Nudcd1		Cdc73		
Numb	Mrc2	Pank3			Srsf9		Anln		
Glb1	Git1	Cdc16			Poldip2		Ddx54		
Letm1	Bckdhb	Sh3glb2			Ddx54		Slc38a4		
Rsu1	Ppp2r5a	Clybl			Gng12		Rbm19		
Gnpda1	Exoc8	Kri1			Fkbp2		Coa7		
Lmf2	Akap9	Naa40			Map3k20		Rin1		
Dennd4c	Fuk	Pla2g15			Rpap3		Lamtor1		
Myo1b	Cdc42bpb	Ube2e2			Dynlt1		Nip7		
	Tomm34	Ndufs2			Degs1		Srsf9		
	Aldh1l2	Sh3d19			Arl3		Chaf1b		
	Ilvbl	Pip4k2c			Inppl1		Ube2c		
	Rras	Dera			Dhx29		Ndufv2		
	H2afy2	Msi2			Trim33		Trmt112		
	Rragc	Exosc4			Helb		Edf1		
	Apeh	Gmppa			Trmt112		Ncdn		
	Hexim1	Dhrs7b			Tbca		Adnp		
	Rbpms	Cdk9			Pdhx		Obsl1		
	Gns	Gak			Fndc3b		Zw10		
	Nampt	Cdc42ep3			Acsl1		Ubl4a		
	Dcxr	Spg21			Gsk3a		Csrp2		
	Fn1	Snrpb2			Cox5b		Lyar		
	Fkbp1a	Dnajc19			Prrx1		Pde12		
	Acsf2	Ndufaf1			Mrps5		Col5a2		
	Ech1	Ssu72			Nudt9		Esf1		
	Deptor	Pgm3			Higd1a		Hells		
	Rabep2	Mxra7			Mrps30		Rpa2		
	Armc1	Mrpl45			Kif2a		Kyat3		
	Plod2	Pus10			Srek1		Rbm22		
	Pdk3	Atad1			Rnmt		Csnk1a1		
	Plcg1	Ttc33			Anapc5		Pdhx		
	Stam	Paip2			Pex19		Gemin5		

	Ykt6	Lhpp			Yrdc		Anapc2		
	Stk39	Polr2d			Gk		Hgh1		
	Uba6	Iah1			Zbtb8os		Aqr		
	Ethe1	Armc8			Brd4		Rbm28		
	Ctsz	Klc4			Prcp		Setd7		
	Dennd4c	Ndufs7			Rala		Gatad2b		
	Letm1	Xpo7			Fam50b		Poldip2		
	Nudcd2	Stard5			Pde12		Cavin3		
	Nudcd1	Pla2g12a			Dcakd		Rbms1		
	Fkbp10	Aldh6a1			Nelfb		Arfgap2		
	Acaa1a	Stx12			Klhl22		Hspbp1		
	Raver1	Lrba			Timeless		Pno1		
	Nxn	Agk			Rpa2		Denr		
	Eif3i	Eefsec			Frg1		Tmem33		
	Gsn	Utp3			Gsk3b		Dimt1		
	Rcn3	Tlr2			Il1rl1		Akt1s1		
	Mpst	Tbl2			Rps19bp1		Rpl34		
	Plod1	Akap8l			Edf1		Pak1ip1		
	Dync1li1	Mad1l1			Mea1		Senp3		
	Psap	Ccs			Smarca4		Cpsf1		
	Picalm	Entpd5			Rpl36a		Qki		
	Ap3d1	Gstz1			Capn1		Sec14l1		
	Snap23	Sucla2			Sqle		Degs1		
	Atp6v1d	Unc119			Klc1		Polr1a		
	Scaf8	Ampd3			Pcm1		Cpd		
	Sec61a1	C3			Pofut1		Cox5b		
	Hibadh	Eno2			Hspa1l		Cks1b		
	Dnajc10	Selenbp1			Rhoc		Rala		
	Faf1	Ahcyl2			Hist1h1d		Surf6		
	Gba	Actbl2			Hist1h1e		Rpl36a		
	Nol10	Hspg2					Epha2		
	Oasl1	Glrx					Gsk3a		
	F3	Mrpl46					Qrich1		
	Brcc3	Sdf2l1					Mcu		
	Timm10	Pmm2					Fam91a1		
	Pik3c2a	Pacsin3					Dph1		
	Eea1	Erap1					Mdc1		
	Trip10	Cspg4					Bcar1		
	Pmvk	Colec12					Inppl1		
	Mrpl2	Gsta4					Fbxo30		
	Hspb8	Slc9a3r1					Smad3		
	Ptcd3	Map1a					Rps19bp1		
	Herc4	Xdh					Atad2		
	Lbr	Vwa5a					Trmt6		
	Taco1	Cdkn1b					Nudcd3		
	Adgrl2	Opa1					Nudt4		
	Nfkb2	Dpp7					Tut1		
	Nploc4	Lss					Rheb		
	Galk2	Scp2					Kif2c		
	Calu	Slc12a2					Prmt7		
	Mri1	Dazap1					Sf3b5		
	Ccdc58	Mecr					Derl1		
	Tbcc	Pcyox1					Ddx50		
	Mbnl1	Plin2					Mrps5		
	Washc2	Nfkb1					Mettl16		
	Ptpn11	Idh1					Pin4		
	Etfdh	Tomm40					Aen		
	Sod2	Gcat					Rfc5		

	Hsd17b4	Tom1					Rnmt		
	Nhp2	Washc4					Mrpl19		
	Iars2	Slc4a7					Rpap3		
	Acadsb	Abi1					Apmap		
	Mvd	Mavs					Nol7		
	Tp53bp1	Mvp					Rexo2		
	Glg1	Arsa					Apoo		
	Sqor	Grhpr					Jmjd6		
	Gbe1	Cat					Ifi30		
	Nsdhl	Rab11fip 5					Rcl1		
	Gys1	Plcd1					Higd1a		
	Dnm1	Epm2aip 1					Chaf1a		
	Aldh3a2	Cdkn2c					Gsk3b		
	Ctbp2	Adprhl2					Fads2		
	Osbpl3	Gnpda1					Ik		
	Lgmn	Pc							

4.8 Bibliography

Bott, S., Arya, M., Kirby, R. S., & Williamson, & M. (2005). p21 WAF1/CIP1 gene is inactivated in metastatic prostatic cancer cell lines by promoter methylation. *Prostate Cancer and Prostatic Diseases*, *8*, 321–326. https://doi.org/10.1038/sj.pcan.4500822

Dasari, S., & Bernard Tchounwou, P. (2014). Cisplatin in cancer therapy: molecular mechanisms of action. *European Journal of Pharmacology*, *740*, 364. https://doi.org/10.1016/J.EJPHAR.2014.07.025

Dey-Guha, I., Wolfer, A., Yeh, A. C., Albeck, J. G., Darp, R., Leon, E., Wulfkuhle, J., Petricoin, E. F., Wittner, B. S., & Ramaswamy, S. (2011). Asymmetric cancer cell division regulated by AKT. *Proceedings of the National Academy of Sciences of the United States of America*, *108*(31), 12845–12850. https://doi.org/10.1073/PNAS.1109632108/-/DCSUPPLEMENTAL

Eling, N., Morgan, M. D., & Marioni, J. C. (2019a). Challenges in measuring and understanding biological noise. *Nature Reviews Genetics 2019 20:9*, *20*(9), 536–548. https://doi.org/10.1038/s41576-019-0130-6

Eling, N., Morgan, M. D., & Marioni, J. C. (2019b). Challenges in measuring and understanding biological noise. *Nature Reviews Genetics 2019 20:9*, *20*(9), 536–548. https://doi.org/10.1038/s41576-019-0130-6

Elowitz, M. B., Levine, A. J., Siggia, E. D., & Swain, P. S. (2002). Stochastic gene expression in a single cell. *Science (New York, N.Y.)*, *297*(5584), 1183–1186. https://doi.org/10.1126/SCIENCE.1070919

Hopes, T., Agapiou, M., Norris, K., McCarthy, C. G. P., O'Connell, M. J., Fontana, J., & Aspden, J. L. (2020). Ribosome heterogeneity in Drosophila melanogaster gonads through paralog-switching. *BioRxiv*, 2020.01.20.913020. https://doi.org/10.1101/2020.01.20.913020

Huang, H., Li, P., Ye, X., Zhang, F., Lin, Q., Wu, K., & Chen, W. (2021). Isoalantolactone Increases the Sensitivity of Prostate Cancer Cells to Cisplatin Treatment by Inducing

Oxidative Stress. *Frontiers in Cell and Developmental Biology*, *9*, 809. https://doi.org/10.3389/FCELL.2021.632779/BIBTEX

Jarrard, D. F., Steven Bova, G., Ewing, C. M., Pin, S. S., Nguyen, S. H., Baylin, S. B., Cairns, P., Sidransky, D., Herman, J. G., & Isaacs, W. B. (1997). Deletional, Mutational, and Methylation Analyses of CDKN2 (p16/MTS1) in Primary and Metastatic Prostate Cancer. *Genes Chromosom. Cancer*, *19*, 90–96. https://doi.org/10.1002/(SICI)1098-2264(199706)19:2

Pulianmackal, A. J., Sun, D., Yumoto, K., Li, Z., Chen, Y.-C., Patel, M. V, Wang, Y., Yoon, E., Pearson, A., Yang, Q., Taichman, R., Cackowski, F. C., Buttitta, L. A., Yao, G., Wiper-Bergeron, N., De Blander, H., Cackowski cackowskif, F. C., Laura Buttitta, karmanosorg A., & Y-c, C. (2021). Monitoring Spontaneous Quiescence and Asynchronous Proliferation-Quiescence Decisions in Prostate Cancer Cells. *Frontiers in Cell and Developmental Biology*, *9*, 728663–728663. https://doi.org/10.3389/FCELL.2021.728663

Raser, J. M., & O'Shea, E. K. (2004). Control of stochasticity in eukaryotic gene expression. *Science (New York, N.Y.)*, *304*(5678), 1811–1814. https://doi.org/10.1126/SCIENCE.1098641

Sharma, S. V., Lee, D. Y., Li, B., Quinlan, M. P., Takahashi, F., Maheswaran, S., McDermott, U., Azizian, N., Zou, L., Fischbach, M. A., Wong, K. K., Brandstetter, K., Wittner, B., Ramaswamy, S., Classon, M., & Settleman, J. (2010). A Chromatin-Mediated Reversible Drug-Tolerant State in Cancer Cell Subpopulations. *Cell*, *141*(1), 69–80. https://doi.org/10.1016/J.CELL.2010.02.027

Simkins, A., Bannon, S. A., Khoury, J. D., Kanagal-Shamanna, R., Foglesong, J. S., Alvarado, Y., Borthakur, G., & DiNardo, C. D. (2017). Diamond-Blackfan Anemia Predisposing to Myelodysplastic Syndrome in Early Adulthood. *Https://Doi.Org/10.1200/PO.17.00112*, *1*, 1–5. https://doi.org/10.1200/PO.17.00112

Sobue, S., Mizutani, N., Aoyama, Y., Kawamoto, Y., Suzuki, M., Nozawa, Y., Ichihara, M., & Murate, T. (2016). Mechanism of paclitaxel resistance in a human prostate cancer cell line, PC3-PR, and its sensitization by cabazitaxel. *Biochemical and Biophysical Research Communications*, *479*(4), 808–813. https://doi.org/10.1016/J.BBRC.2016.09.128

Stallaert, W., Kedziora, K. M., Taylor, C. D., Zikry, T. M., Ranek, J. S., Sobon, H. K., Taylor, S. R., Young, C. L., Cook, J. G., & Purvis, J. E. (2021). The structure of the human cell cycle. *Cell Systems*, *0*(0). https://doi.org/10.1016/J.CELS.2021.10.007

Yang, H. W., Chung, M., Kudo, T., & Meyer, T. (2017). Competing memories of mitogen and p53 signalling control cell-cycle entry. *Nature 2017 549:7672*, *549*(7672), 404–408. https://doi.org/10.1038/nature23880